

1972

Structure of friable Iowa loess

William Wiley Badger
Iowa State University

Follow this and additional works at: <https://lib.dr.iastate.edu/rtd>



Part of the [Civil Engineering Commons](#)

Recommended Citation

Badger, William Wiley, "Structure of friable Iowa loess " (1972). *Retrospective Theses and Dissertations*. 5236.
<https://lib.dr.iastate.edu/rtd/5236>

This Dissertation is brought to you for free and open access by the Iowa State University Capstones, Theses and Dissertations at Iowa State University Digital Repository. It has been accepted for inclusion in Retrospective Theses and Dissertations by an authorized administrator of Iowa State University Digital Repository. For more information, please contact digirep@iastate.edu.

INFORMATION TO USERS

This dissertation was produced from a microfilm copy of the original document. While the most advanced technological means to photograph and reproduce this document have been used, the quality is heavily dependent upon the quality of the original submitted.

The following explanation of techniques is provided to help you understand markings or patterns which may appear on this reproduction.

1. The sign or "target" for pages apparently lacking from the document photographed is "Missing Page(s)". If it was possible to obtain the missing page(s) or section, they are spliced into the film along with adjacent pages. This may have necessitated cutting thru an image and duplicating adjacent pages to insure you complete continuity.
2. When an image on the film is obliterated with a large round black mark, it is an indication that the photographer suspected that the copy may have moved during exposure and thus cause a blurred image. You will find a good image of the page in the adjacent frame.
3. When a map, drawing or chart, etc., was part of the material being photographed the photographer followed a definite method in "sectioning" the material. It is customary to begin photoing at the upper left hand corner of a large sheet and to continue photoing from left to right in equal sections with a small overlap. If necessary, sectioning is continued again — beginning below the first row and continuing on until complete.
4. The majority of users indicate that the textual content is of greatest value, however, a somewhat higher quality reproduction could be made from "photographs" if essential to the understanding of the dissertation. Silver prints of "photographs" may be ordered at additional charge by writing the Order Department, giving the catalog number, title, author and specific pages you wish reproduced.

University Microfilms

300 North Zeeb Road
Ann Arbor, Michigan 48106

Company

72-26,901

BADGER, William Wiley, 1934-
STRUCTURE OF FRIABLE IOWA LOESS.

Iowa State University, Ph.D., 1972
Engineering, civil

University Microfilms, A XEROX Company, Ann Arbor, Michigan

Structure of friable Iowa loess

by

William Wiley Badger

A Dissertation Submitted to the
Graduate Faculty in Partial Fulfillment of

The Requirements for the Degree of

DOCTOR OF PHILOSOPHY

Department: Civil Engineering

Major: Soil Engineering

Approved:

Signature was redacted for privacy.

In Charge of Major Work

Signature was redacted for privacy.

For the Major Department

Signature was redacted for privacy.

For the Graduate College

Iowa State University
Ames, Iowa

1972

PLEASE NOTE:

Some pages may have
indistinct print.

Filmed as received.

University Microfilms, A Xerox Education Company

TABLE OF CONTENTS

	Page
INTRODUCTION	1
LITERATURE REVIEW AND THEORY	6
MATERIALS	27
COHESIVE FORCES ACTING ON THE SOIL STRUCTURE	33
PERMEABILITY	57
VOID VOLUMES MEASURED BY MERCURY INJECTION	73
STRUCTURE	85
DISCUSSION	98
CONCLUSIONS	105
SUGGESTION FOR FURTHER RESEARCH	108
ACKNOWLEDGMENTS	110
BIBLIOGRAPHY	111
APPENDIX A SOIL FABRIC CLASSIFICATION	116
APPENDIX B: DEVELOPMENT OF THE EQUATION FOR THE VOLUME OF CONTACT WATER	127
APPENDIX C: APPARENT COHESION EQUATION DEVELOPMENT	131
APPENDIX D: PERMEABILITY DATA	141

I. INTRODUCTION

A. General Statement

Many students of soil engineering approach the soil as a system of particles. These particles are weighed and sieved to obtain densities and grain size distribution and sizes are arbitrarily defined as sand, silt and clay; and the way they all go together forms the soil structure. Soil structure, according to Brewer (1964), refers to "the physical constitution of a soil material as expressed by the size, shape and arrangement of the solid particles and voids, including both the primary particles to form compound particles and the compound particles themselves; fabric is the element of structure which deals with arrangement."

Although the method of analysis to describe a soil which emphasizes the particulate approach in soil engineering is widely accepted and appears to satisfy the need, there is good rationale to take the opposite approach and consider soil as a system of voids and void fillers. In most cases when a soil does not possess adequate engineering properties, the cost of removing the inadequate soil particles and replacing them with better particles is prohibitive. Therefore, the normal field solution is to work with the existing particles, rearrange or reduce the voids and limit the void filling water, i.e., densify or chemically stabilize the soil mass.

The Atterberg limits and related indices are based on the concept that fine grained soil can exist in any of four states depending on its water content. Clayey soil can be solid when dry and upon the addition of water it will proceed through semisolid, plastic and finally liquid states. The field engineer attempts to control the soil states by simply controlling the quantity of void filler (water). External drainage ditches and asphaltic seal coats keep some water out of the system while compaction (reduction of void size) may decrease internal drainage in the system. Actually, dry cohesive soil, regardless of the nature of soil particles, seldom causes trouble if kept dry.

Since in practice the soil engineer controls the engineering properties of soil by manipulating the void and void fillers, it is therefore reasonable to reexamine soil engineering and to consider soil as a system of voids. However, the difficulty in analyzing voids is that the natural tendency is to look at particle size, shape and arrangement and not the size, shape and continuity of the void. This is understandable because looking into a hole, it is almost impossible not to look at the sides and bottom of the hole instead of the vacant space. Therefore, to examine a void requires the inspection of the complete soil structure, the particles which form the voids and finally the voids themselves.

B. Background

The purpose of this research was to obtain a better understanding of the structure of soil through a study of the voids of the soil. Initially, many research techniques were used to study the differences between undisturbed and remolded soil structure. The Differential Thermal Analysis (DTA), Transmission Electron Microscope (TEM), and Scanning Electron Microscope (SEM) were used to study tropical soils in the undisturbed and remolded states; however, the results, even though encouraging, were not conclusive enough to spend additional efforts in those areas.

The initial DTA results indicated that the heat of reactions were transferred from the undisturbed specimens before the heat from equivalent remolded specimens. This difference in transfer rates was attributed to the effects of remolding, but the influence of other variables present (specimen density, moisture content, shape, and size) were present. This DTA data was interpreted by Kellogg (1972).

The TEM photographs revealed a structural difference in relation to the degrees of disturbance; however, because of the limitations of the TEM equipment, photographs of undisturbed specimens could not be obtained. The SEM was able to show both undisturbed and remolded soil structure; however, the capabilities of the SEM are best used in conjunction with other research techniques. During the

initial SEM work, a tentative soil fabric classification system was developed which would classify soils from SEM photographs. A copy of this classification system will be included as Appendix A.

At this stage of the research it became apparent that a technique of measuring voids of a soil structure was needed to complement the SEM study. Hydrometer and sieve analyses have been long used to determine particle size distribution. What was missing was a means to determine the void size distribution of a soil system. The quest for a method of measuring pores in soil led to the investigation and the acceptance of the relatively new concept of mercury porosimetry.

To better understand the structure of soil required a knowledge of the cohesive forces which act on that structure. The cohesive forces, particularly in loess, proved to be greatly influenced by the void filler water. The effect of water on the true and apparent cohesion led to the study of clay bonding and surface tension.

The last phase of the study was to relate the mercury porosimetry, cohesion and scanning electron microscopy research techniques to practical engineering applications. Since the major emphasis of this study was directed toward the voids, two major areas of practical applications were available, permeability and/or compaction.

C. Scope

This research has concentrated on the study of the structure of loess using mercury porosimetry, unconfined compression test, falling head permeability test, and SEM. By combining the quantitative capabilities of the porosimeter, compression test, and permeability test with the qualitative SEM photographs, a better understanding of soil structure was gained. To keep the research in manageable boundaries, the following guide lines were established. First, the primary test soil was limited to friable western Iowa loess. This soil was chosen because of its availability and known physical properties. Secondly, the common theme "soil structure" was studied by using as many different research techniques and equipment as practicable. This approach created problems in relating and tying together the final work but provided an abundance of information about the subject. One tangential result derived from the examination of the abundance of data was the development of a simple parameter, which quantitatively defines soil structure. The distribution ratio, or the ratio of void sizes to grain sizes, was developed to describe soil structure.

II. LITERATURE REVIEW AND THEORY

A. General Description of Loess

Krinitzski and Turnbull (1967) have described loess as a well-sorted, slightly indurated, eolian silt which may or may not be calcareous. It has excellent vertical slope stability if well drained and protected from erosion. Sheeler (1968) states that loess is composed primarily of rather loosely-arranged, angular grains of sand, silt, and clay. Silt is usually the dominant size, see Figure 1. Calcite is also generally present in amounts ranging from near zero to more than 10 percent of the total soil. Gibbs and Holland (1960) describe loess as a quartzose, somewhat feldspathic clastic sediment composed of a uniformly sorted mixture of silt, fine sand, and clay particles arranged in an open, cohesive fabric, frequently resulting in a natural dry density of 70-90 pcf. However, materials which are not cohesive and which are composed of silts and fine sand particles are not considered as loess. The term "loess" is of German origin and is derived from the word "LOSEN," meaning to loosen or to dissolve (Holtz and Gibbs 1951).

Loess may be identified primarily by its regional trends in properties. It is believed to be wind-blown silt originating from streams of glacial outwash. Close to the source area the texture is coarse and becomes finer with increasing distance. Density increases and thickness decreases with increased distance from the source. The

structure and the unique ability to stand in vertical cuts are also distinguishing characteristics.

Loess covers approximately 10 percent of the earth's land surface with major loessial deposits located in the central part of several continents of the world. The most extensive loess areas in the Central United States are found in Nebraska, Iowa, Wisconsin, Illinois, Tennessee, and Mississippi.

B. Engineering Properties of Loess

1. Grain size distribution curve

Holtz and Gibbs (1951) established a clayey loess zone, a silty loess zone, and a sandy loess zone for the grain size distribution chart, see Figure 1. Holtz and Gibbs's findings consisted of 148 samples which were geologically described as loess: 76 percent had gradation curves which were in the silty loess range: 18 percent were in the clayey loess range: and 6 percent were in the sandy loess range.

2. Composition of grains

Quartz is the predominant mineral constituent in all of the Vicksburg loess. Krinitzsky and Turnbull (1967) show a decrease in percent feldspars between calcareous and leached loess with a corresponding increase in clay content. The decrease in the content of feldspars is attributed to the weathering of these minerals into clays. Gibbs and Holland (1960) found that Nebraska's loess range at twenty-five to

twenty-seven percent quartz and ten to twenty-two percent feldspars. They also discovered that the clay mineral montmorillonite commonly occurs as thin hulls around the grains, while illite has a tendency to occur as individual crystals. Larionov (1965) designates two divisions with respect to composition, monomineral, the individual quartz and carbonate grains and polymineral, the accumulation of quartz, carbonates, and clays to form aggregates. Warnke (1971) suggests that the fines observed on loess particles represent comminution debris, produced in the formation of loess quartz material by glacial grinding.

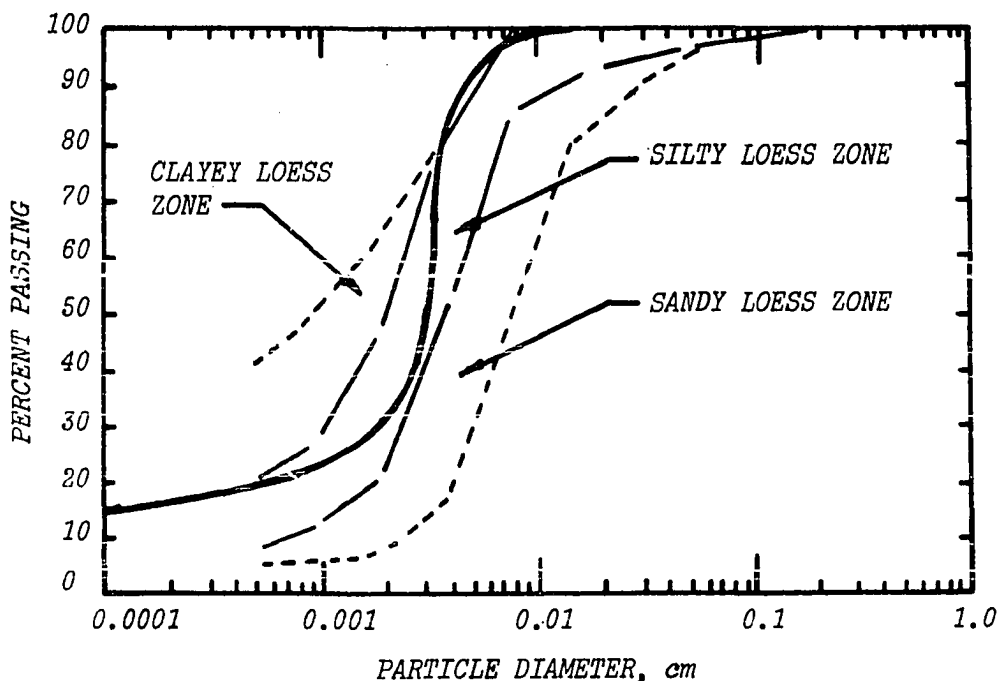


Figure 1. Gradation boundary curves

However, it appears that most authors believe, like Sheeler (1968), that most of the loess grains are coated with thin films of clay, while some of the grains are coated with a mixture of calcite and clay.

3. Specific gravities

Scheidig (1934) determined specific gravity for loess from various locations, Table 1.

Table 1. Specific gravity

LOCATION	SPECIFIC GRAVITY	TEST
Rossbach	2.69	2
Volga-Don Canal	2.64-2.66	12
Collinsville, Illinois	2.69-2.72	2

The amount of quartz which has a specific gravity of 2.65 controls the specific gravity of loess. According to Sheeler (1968) the specific gravity of loess in the United States varies between 2.57 and 2.79. The range for Iowa loess is from 2.68 to 2.79. Gibbs and Holland (1960) found a narrow range of 2.57 to 2.69 for loess in Nebraska.

4. Porosity

Scheidig's (1934) porosity values for loess vary from a high of 65 percent on the Magdeburg Plain to a low of 24 percent in Vienna, Table 2.

Table 2. Undisturbed loess properties

LOCATION	POROSITY %	VOID RATIO	DRY DENSITY pcf
Magdeburg	65.0	1.87	59.0
Lower Austria	55.5	1.25	76.0
Alsace	48.0	0.93	87.5
Central Germany	38.0	0.61	104.0
Vienna	24.0	0.32	128.0
Hungary	39.0	0.64	102.5

Loess generally has a high porosity which is attributed to the uniformity of the grains. Bally (1965) used a mean value of 49.6 percent with a standard deviation of 2.4 percent for the porosity of undisturbed loess from Bucharest, Romania.

5. Atterburg limits

Sheeler (1968) compiled plasticity data from various locations around the United States and concluded that the Atterburg limits are primarily dependent upon the amount of clay present in the loess.

6. Densities

The in-place dry density of loess in Southwestern Iowa varies from 69.4 to 89.5 pcf. Davidson et al. (1953) indicate that in-place density is dependent on the depth and on clay content.

C. Moisture content

Jumikis (1962) categorizes moisture as follows: adsorbed water comprises the hygroscopic soil moisture and soil moisture films. Hygroscopic soil moisture covers all mineral matter with a very thin film of moisture. In the technical literature hygroscopic moisture is also termed "adsorbed moisture," "molecular moisture," "contact moisture" or "surface bound moisture." Film moisture forms in soil upon the condensation of aqueous vapor, or remains there after the removal of the bulk free water.

Capillary moisture exists because of surface tension of the water menisci which act between the grains. A form of capillary moisture is "pore corner or neck moisture," known in German by the term POREWINKELWASSER. The contact moisture is the annular moisture wedge held by the menisci in the

angularities formed at the contact point between grains. Visible evidence of water forming menisci at the contact points of spheres was shown by Smith et al. (1963).

Keen (1924) developed an equation for the volume of water at the contact points of two spheres. The volume of water is defined as the water bound by the meniscus and spheres. The meniscus is taken as the arc of a circle touching the two equal spheres. The volume is expressed in terms of the radius, a , of the spheres and the angle two theta subtended at the center of the soil particle by the radii from the point of contact of the spheres and the edge of the meniscus.

$$V_k = \frac{8\pi a^3 \sin^4 \theta}{\cos^2 2\theta} \left[1 - (\tan 2\theta) \left(\frac{\pi}{2} - 2\theta \right) \right] \quad 1$$

Additional comments about the the Keen equation are included in Appendix B.

Fisher (1926) also developed a volume equation for the water held at the contact point between spheres. Again the assumption that the water-to-air surface of the meniscus is circular was made. The theta angle in the Fisher equation is equal to the two theta angle of the Keen equation, the radius, r , is equal to Keen's radius, a . Initially, the Fisher equation was for the moisture spot on one sphere; however, it is shown below for the total water at one contact point.

$$V_F = \pi r^3 (\sec\theta - 1)^2 [1 - (\tan\theta)(\frac{\pi}{2} - \theta)] \quad 2$$

Additional comments and comparisons about the Fisher equation are included in Appendix B.

Gravitation water was further subdivided by Jumikis (1962) into free water and capillary water. However, it appears that the capillary water should be listed with "pore corner" water since both are closely related to surface tension forces.

Jumikis (1962) and Kane (1969) both define boundaries between the adsorbed and capillary water. Jumikis calls this boundary "critical moisture" and defines it as the moisture content interval corresponding to the transition from maximum molecular moisture capacity to capillary moisture. Kane describes the term "critical water content" as the moisture content at which the clay binder is stable and any increase in moisture causes neither swelling nor shrinkage. A boundary may be established between the capillary and gravity water. Keen (1924), Haines (1925), Fisher (1926) and Haines (1927) all discuss the condition in which the amount of moisture is increased to the point where the menisci coalesce. When all menisci coalesce, the force due to surface tension becomes zero.

In an attempt to simplify the different types of moisture and the related boundaries, a table of moisture

terms was developed, Table 3.

Table 3. Moisture terms¹

CATEGORIES	BOUNDARY CONDITIONS	TERMS
----- (zero moisture) -----		
ADSORBED WATER		
hygroscopic water		(clay bonding)
film moisture		
molecular moisture		
----- (critical moisture) ----- OVERLAP ZONE		
CAPILLARY WATER		
pore corner water		(apparent cohesion)
neck moisture		
porewinkelwasser		
contact moisture		
surface tension moisture		
----- (menisci coalescence) -----		
GRAVITY WATER		
gravitation water		(additional
free water		weight of soil
bulk water		due to gravity
ground water		water)
----- (100 % saturation) -----		

¹The general concept of this table is similar to the Briggs Classification of soil water, Spangler (1960).

D. Cohesion

Jumikis (1962) attributes true cohesion to the intermolecular attraction of the soil particles for each other throughout the soil mass and apparent cohesion to the binding of the soil mass together by the capillary action of the soil moisture.

Lambe and Whitman (1969) define true cohesion as the measurable shear resistance when the normal force is reduced to zero. From many tests true friction is found to be independent of water content, and the true cohesion versus log of the moisture content is a straight line.

When the adsorbed water needs of the clays of a fine grained soil are met, water begins to form menisci at the contact point between grains. The surface tension developed between the water and soil particles causes a grain-to-grain pressure within the soil known as intergranular pressure. This pressure tends to force the grains together with a pressure equal and opposite to the tension through the water. The tension forces act in a circular pattern around the particle at the water-to-solid interface. The y components cancel out and the x components act through the center of the particles.

According to Jumikis (1962) the surface tension force-induced strength of soil is termed "apparent cohesion" after Terzaghi or SAUGFESTIGKEIT after Ohde.

Many researchers have been interested in developing mathematical equations which could be used to calculate apparent cohesion caused by this contact moisture. Haines (1925) defined an equation to measure the force between particles caused by surface tension. Fisher (1926) corrected the Haines force equation by adding a term that Haines left out. The use of a theoretical approach to calculate apparent cohesion requires a simplified concept of the soil system. Both the above researchers used an "ideal soil", a collection of uniform spheres systematically packed and free from colloidal material.

E. Permeability

Scheidig (1934) attempted to express soil structure in terms of permeability. He stated that in cases of soils with simple structures the permeability is often roughly proportional to the pore volume and grain size. Terzaghi (1951) describes the permeability of loess as a very elusive property. This observation is based on the breakdown of loess structure when saturated. The loss of strength due to saturation causes densification and consequent change in permeability. Lambe (1954) presented and discussed the following major factors affecting the permeability of fine-grained soils. The influence of composition on permeability is generally of little importance with silts, sands and gravels. However, the presence of some clays, mica and organic matter

are of major importance: clays because of the potentially high cation exchange capacity; mica for the platey shape; and organic matter for clogging and possible growth action.

Viscosity, density and polarity of the pore fluid must be considered in determining the effect of a permeant on permeability.

The void ratio directly affects permeability. The void-to-solid relationship is the controlling factor: the higher the void ratio the greater the permeability, and, conversely, the smaller the void ratio the lower the permeability.

Permeability depends to a considerable extent on the arrangement of soil particles, or "structure." A change in structure and a following change in permeability are apparent with varying molding water content at compaction, the extent of sample mixing, and the presence of chemical dispersants. A decrease in permeability occurs when the soil is compacted on the wet side of optimum, when the fines are well distributed, and when a chemical dispersant is used. Also if the grains are not dispersed and/or well mixed and are compacted on the dry side of optimum, aggregation may occur causing an increase in permeability.

Voids filled with entrapped air are not serving as channels for water flow. Consequently, the higher the degree of saturation, the greater the permeability.

Lambe and Whitman (1969) modified their initial list of factors which influence permeability to include particle size, void ratio, composition, fabric and degree of saturation. This listing expands the initial heading of structure into two separate headings of particle size and fabric. The smaller the particle size the smaller the voids and thus the lower the permeability. Although fabric is one of the most important soil characteristics influencing permeability, it is hard to isolate because it is so closely interrelated to particle size, void ratio and composition. The particle size establishes a range of void ratios, and the type of fabric controls the void ratio within that range. For an "ideal soil" Graton and Fraser (1935) designated a void ratio range of 0.35 to 0.90. The location of this ideal soil within this range of void ratios was determined by the packing of the spheres.

Childs and Collis-George (1950) account for the uncontrollable variations in permeability as follows: a decrease of permeability with time may occur from flowing water releasing dissolved air into the pores; from the swelling of clays; from the mechanical blocking by movement of fines; from the growth of organisms in the pores; and from the chemical effect of the flowing water upon the porous media. An increase of permeability with time may occur from solution of the initially entrapped air into the flowing water.

Gibbs and Holland (1960) state that the permeability of undisturbed loess is principally related to the density when the basic properties of gradation and plasticity are relatively uniform. This seems reasonable; density, gradation and plasticity are functions of void ratio, particle size and clay content, respectively. Gibbs and Holland (1960) cite root-like voids as a cause for the variation in permeability of undisturbed versus remolded loess.

F. Structure

1. General

The most difficult task of soil structure study is to determine an adequate definition of structure. In fact, Jenny (1941) pointed out that there is no generally accepted definition of soil, and to find a definition which would satisfy all soil workers was practically impossible. The problems inherent in defining soil are basically the same as those encountered in defining structure. With the structure differing profoundly for each soil and with the varying interest of the workers studying the structure, it is no wonder that there are so many different definitions. Soil structure, according to Brewer (1964), refers to "the physical constitution of a soil material as expressed by the size, shape and arrangement of the solid particles and voids, including both the primary particles to form compound particles and the compound particles themselves; fabric is the el-

ement of structure which deals with arrangement." Bayer (1948) defines structure as "the arrangement of sand, silt and clay, and of secondary particles into a particular structural pattern." The U.S.D.A. Soil Survey Manual (1951) states that "soil structure refers to the aggregation of primary soil particles in compound particles, or clusters of primary particles, which are separated from adjoining aggregates by surfaces of weakness." Terzaghi and Peck (1962) say that "the term structure refers to the pattern in which the soil particles are arranged in the aggregate." Lastly, the American Heritage Dictionary defines structure as:

A complex entity.

The configuration of elements, parts, or constituents in such an entity; organization or arrangement.

The interrelationship of parts of a complex entity.

All the above definitions have elements, parts or particles, arranged, aggregated, patterned or configured together to form structures. Since there is little agreement of what a particle is, as well as of how particles go together, the following definition will be used in this study. Sand grains, silt grains and clay plates (clay crystals) are considered the primary soil particles. A composite particle is composed of primary particles which are joined together by some cohesive force. Soil structure is the physical arrangement of primary and/or composite particles. Fabric is the element of structure which deals with a specific arrangement.

2. Voids

An interesting aspect of Brewer's (1964) definition of structure was the reference to the the arrangement of voids.

Table 4. Size classification of voids

Class name	Radius size cm	Mercury injection ¹ pressure, psia
------------	-------------------	--

Macrovoids

coarse	>0.25	<0.043
medium	0.25-0.10	0.043-0.11
fine	0.10-0.05	0.11-0.21
very fine	0.05-0.0037	0.21-2.85

Mesovoids	0.0037-0.0015	2.85-7.12
-----------	---------------	-----------

Microvoids	0.0015-0.00025	7.12-42.7
------------	----------------	-----------

Ultramicrovoids	<0.00025	>42.7
-----------------	----------	-------

Cryptovoids	<0.000005	>2136.0
-------------	-----------	---------

¹Pressure calculated from the Washburn (1921) Equation.

Most writers do not include voids as a part of their definition of structure. The principal identifiable features of voids are size, shape and arrangement. Brewer (1964) classified voids into five size classes for field description of soil material, Table 4.

Shape analyses for particles are based on the concepts of sphericity and roundness originated by Wadell (1932, 1933, and 1935) and as referred to by Brewer (1964). Sphericity concerns the overall form and is a comparison of the degree of conformity of the shape of a particle to that of the shape of a sphere. Roundness concerns only the sharpness of corners irrespective of the form. The shape of individual voids can be described in terms of sphericity by measure of the length of the principal axes. In conjunction with sphericity the variation in the smoothness and conformation of the walls of the voids may be considered as relative characteristics. Lastly, voids were classified by Brewer (1964) according to distribution patterns (random, banded and clustered) and to orientation patterns (parallel and branching). In the morphological classification of voids, the void types (simple packing voids, compound packing voids, vughs, vesicles, chambers, joint planes, skew planes, craze planes, and channels) were listed by Brewer (1964) by specific names. The packing voids were the most commonly observed voids associated with the remolded loess.

3. Measurement of voids by mercury injection

The relatively new technique of mercury injection offers an excellent method of measuring pore size and pore volume. The concept of mercury injection is based on the Washburn (1921) equation which gives the pressure required to force mercury into capillary pores.

$$P = \frac{-2T \cos \theta}{r} \quad \text{where, } P \text{ is pressure} \quad 3$$

T is surface tension
θ is angle of contact
r is radius of pore

After drying and weighing, the sample is placed in the mercury injection chamber where a vacuum pump removes the pore gases. Then the chamber is filled with mercury, and at increments of pressures the volume of mercury intruded into the pores is measured. From the pressures obtained, pore size and volumes may be determined (Rootare, 1968). Purcell (1949) used an apparatus to determine mercury capillary pressures up to 2000 psi which filled all accessible pores with radii larger than 5.33×10^{-6} cm, Table 5. This Shell Oil apparatus is similar to the equipment used by this author at Iowa State University. Winslow and Shapiro's (1959) hydraulic mercury-intrusion porosimeter was capable of pressures of 3000 psi. Diamond (1970) used a modified Aminco-Winslow porosimeter (American Instrument Company,

Silver Spring, Maryland) with a measuring capacity of 15,000 psi.

Table 5. Pressure versus pore radius

Pressure (psi)	Radius (cm)	Radius (angstroms)
1	1.07×10^{-2}	1.07×10^6
50	2.14×10^{-4}	2.14×10^4
100	1.07×10^{-4}	1.07×10^4
500	2.14×10^{-5}	2.14×10^3
2000	5.33×10^{-6}	533
5000	2.14×10^{-6}	214
10,000	1.07×10^{-6}	107
15,000	7.11×10^{-7}	71

The mercury injection technique of measuring porosities and pore size distribution is only an approximation method. Sridharan et al. (1971) points out that only those pores are intruded which are open to the outside of the sample, and then only at the pressure corresponding to their largest continuous opening. Consequently, the measured pore sizes

are not exact descriptions of the pores of the sample, but are adequate parameters for comparative purposes. The following is a listing of possible sources of error which may occur using the mercury injection technique:

- a. Deviation from the assumed circular cross section in applying the Washburn equation, (Mayer and Stowe, 1966).
- b. The selection of correct contact angle between the mercury and sample, (Ritter and Drake, 1945).
- c. The selection of a value for surface tension of mercury, (Diamond, 1970).
- d. The incomplete emptying of the pores of water or any other fluids before the start of the test, (Diamond, 1970).
- e. Completely isolated pores inaccessible to the exterior of the sample cannot be measured, (Diamond, 1970).
- f. The effect of the compressibility of mercury during testing, (Rootare, 1968).
- g. Compressibility of the sample during testing, (Rootare, 1968).
- h. Kinetic hysteresis effect, where a time lag enters into reading of the mercury penetration before equilibrium has been reached, (Rootare, 1968).
- i. Pores accessible only through entryways of smaller diameter will not be intruded until sufficient

pressure is applied to intrude the entryway or "necks"; hence, all of the volume of such pores will be allocated to the diameter class of the neck, (Diamond, 1970).

j. The voids classed as macrovoids and mesovoids are so sensitive to low pressures that they can not be measured by mercury injection.

Diamond (1970) found that the mercury injection technique of determining pore-size distribution of microscopically homogeneous samples of kaolinite produced identical curves. Rootare (1968) states that the reliability of measuring pore-size by mercury intrusion was proven satisfactory when compared with results from nitrogen adsorption pore-size measurements.

III. MATERIALS

The primary material used in this research was friable western Iowa loess and was obtained from Prospect Hill in Sioux City, Iowa. The site was located near the intersection of Bluff and Prospect Streets on a large bluff adjacent to and overlooking the Missouri River floodplain. This site is normally referred to as the Prospect Hill Site. Figures 2, 3, 4 and 5 are SEM photographs of undisturbed loess.

This loess has the physical property of being able to stand in nearly vertical cuts. It is predominately a silty to sandy loess with approximately 14 percent clay. The engineering properties of the loess used throughout this research are shown in Table 6. Two techniques of obtaining undisturbed¹ samples were employed. The Shelby tube method, in which a thin-walled steel tube is forced into the soil by jacking and the hand carved method, which requires only a cutting knife and patience, were used to obtain undisturbed samples. After sampling, Shelby tubes were capped, marked, sealed and shipped to the laboratory. The hand carved samples were placed in a container, marked, sealed and shipped. All samples were stored in a 100 percent

¹The term undisturbed is only relative because it is impossible to remove, transport and store a soil sample without some degree of disturbance, Spangler (1960).

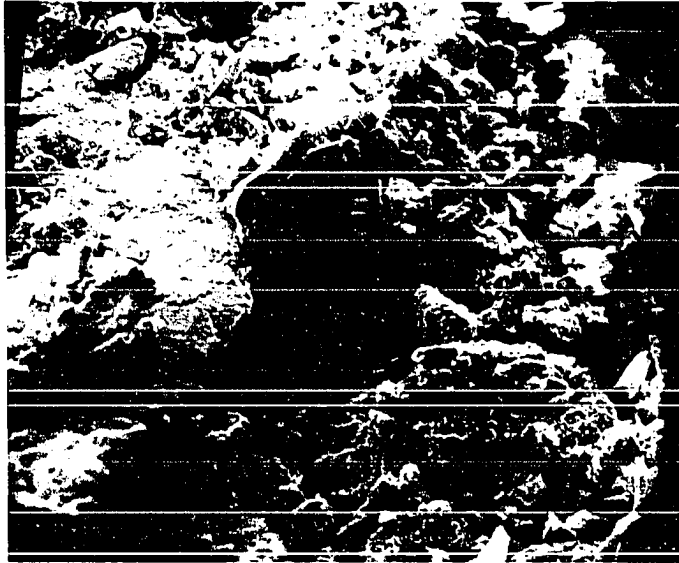


Figure 2 SEM photograph of UND loess at 200x.

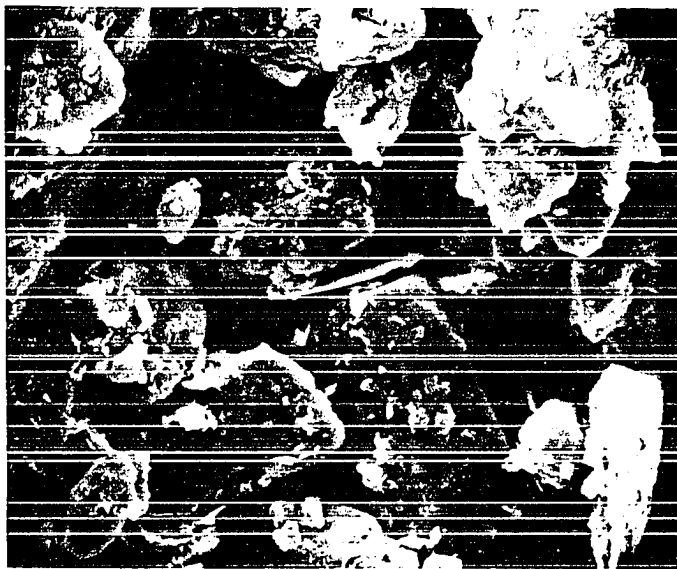


Figure 3 SEM photograph of UND loess at 1000x.

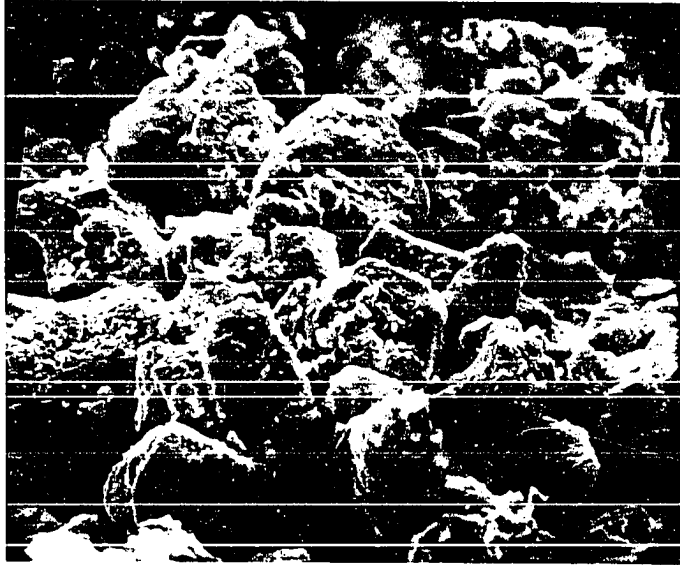


Figure 4 SEM photograph of UND loess at 500x.

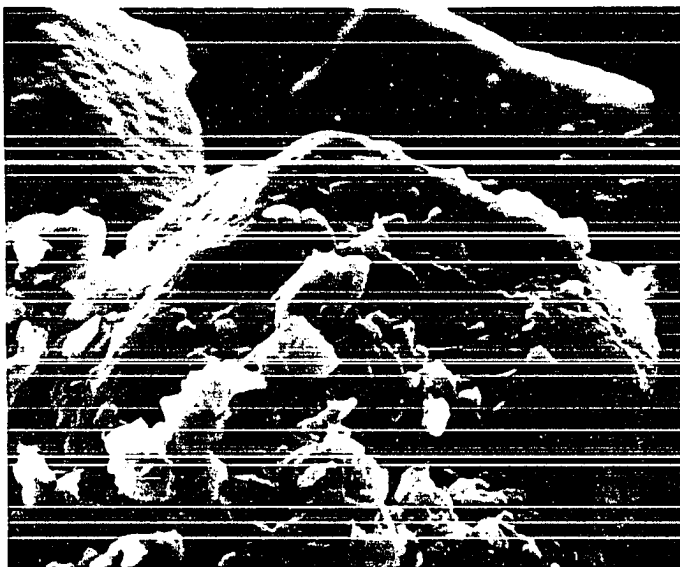


Figure 5 SEM photograph of UND loess at 2000x.

Table 6. Engineering properties of friable western Iowa bluff loess

Properties	Remarks
Grain Size Distribution	See Figure 12
Specific Gravity	2.70 (average of 9 tests)
Dry Density of Hand Carved	88.2 pcf
Porosity of Hand Carved	46%
Liquid & Plastic limits ¹	30 & 26 % respectively
Standard Proctor Compaction optimum moisture maximum Dry Density	16.5 % 109.4 pcf
AASHO Classification ¹	A-4(8)
Field Moisture	7-10%
Strengths ²	$\phi=32.2^\circ, c=1.0$ psi
Minerals Present ³ (X-ray Analysis)	Quartz Montmorillinite & illite Calcium Carbonate Dolomite & Feldspar

¹Handy, (1956).

²Badger, Fox and Johnson unpublished triaxial report of drained test written for Dr. Lohnes.

³Badger, Fish and Klockow unpublished X-ray analysis report written for Dr. Demirel.

humidity room until testing. Table 7 shows the samples use and size.

Table 7. Remolded loess sample use and size

Use	Size and Remarks
Mercury Injection Test	Cylinder with 1/2 inch diameter and 1 inch length, statically molded
Unconfined Compression Test	1.32 inch diameter with 2.8 inch length statically & dynamically molded.
Permeability Test	Harvard miniature cylinders.
Permeability Test	Cylinder with 2.8 inch diameter & 5.6 inch length, statically molded.
SEM Photographs	Segment from the center of a 1/2 inch diameter cylinder, statically molded.

The definition of the terms "undisturbed," "hand carved" and "remolded" are given in Table 8. The undisturbed and hand carved specimens were trimmed to Harvard Miniature and Triaxial sample size. The SEM and Mercury Injection samples of undisturbed and hand carved were small pedis broken from

Table 8. Sample types and designations

Designation	Full Name	Remarks
UND loess	undisturbed loess	samples from Shelby tube
HC loess	hand carved loess	considered in the undisturbed category
REM loess	remolded loess	loess taken from the UND & HC specimen, hand pulverized, sieved through a number 10 sieve and oven dried.
Silt	loess derived silt	loess was processed through 14 sedimentation cycles and boiled in a solution of hydrogen peroxide to separate the clay and organic matter from the silt.

the larger samples. For the SEM work, the specimens were broken to approximately 1/8 inch by 1/4 inch by 1/4 inch size. And for Mercury Injection samples, the UND and HC specimens were broken to a 3/4 inch cube size.

IV. COHESIVE FORCES ACTING ON THE SOIL STRUCTURE

A. General

To complete the study of soil structure requires an understanding of the cohesive forces which hold the mineral skeleton together. These forces are usually divided into true cohesive forces, which are attributed to carbonates, salts and clay bonding cementation, and apparent cohesion, which is attributed to surface tension. The true cohesion was determined by removing the effect of the apparent cohesion forces from the total cohesion of the soil.

B. Theoretical Apparent Cohesion

In fine grained soils capillary water in a form known as "contact moisture" collects at the points where grains touch or nearly touch forming menisci. The surface tension of the water in the menisci provides a force which pulls the grains together giving the soil apparent cohesion. Figure 6 shows a typical contact point between spheres and the volume of contact water formed by the spheres and meniscus.

The equation for the volume of water at a contact point was developed in terms of meniscus angle theta and sphere radius, (Appendix B).

$$V_T = \frac{2}{3}\pi a^3 (1 - \cos\theta) \left[(\sin^2\theta + \tan^2\theta + \sin\theta \tan\theta) - (1 - \cos\theta)(2 + \cos\theta) + \frac{3(1 - \cos\theta)}{\cos^2\theta} \left(\frac{2}{3}(1 - \cos\theta) - \left(\frac{\pi}{2} - \theta\right) \tan\theta \right) \right] \quad 4$$

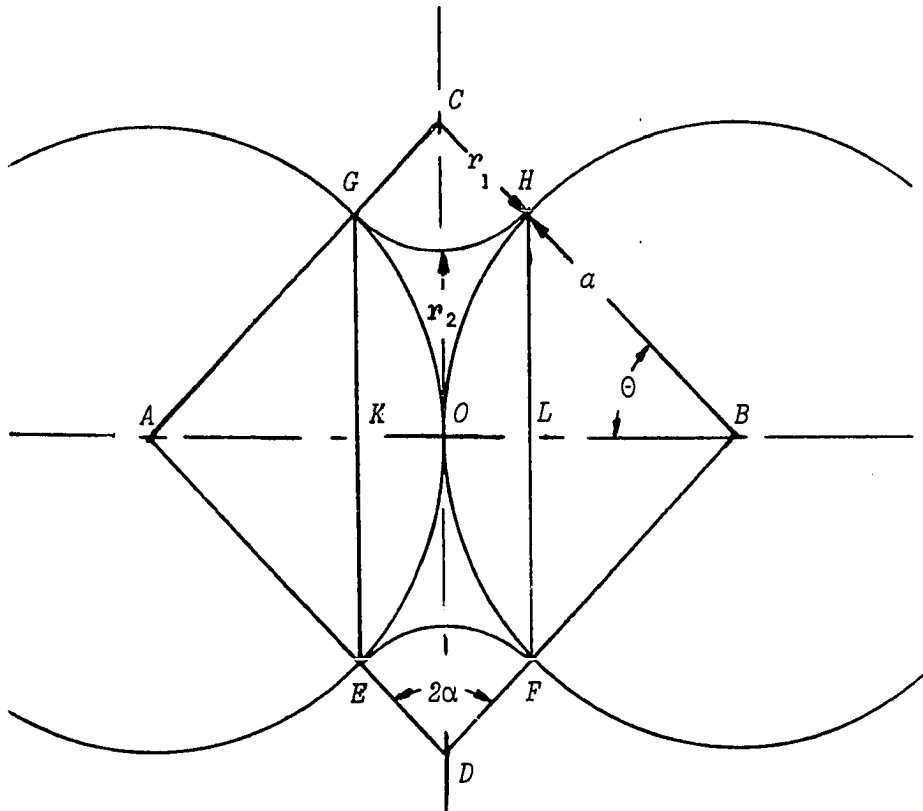


Figure 6 Volume water at contact point.

To develop a theoretical means of calculating apparent cohesion, the selection of a model soil was made. The first model selected was that of uniform spheres in square layers in a cubic arrangement. Figure 7 shows a unit cell in the cubic arrangement. This arrangement is designated case one and has a porosity of 47.64 percent. The volumes of solids, voids and total were all derived from this geometrical arrangement shown in the unit cell.

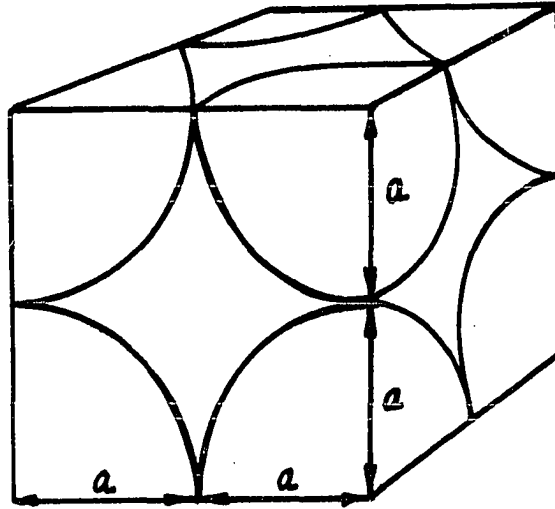


Figure 7 Unit cell in the cubic arrangement.

By combining the contact water volume equation and the volume of void equation with the degree of saturation equation, an equation for the meniscus angle as a function of saturation was obtained.

$$S = \frac{V_{wmc}}{V_V} \times 100 = \frac{2\pi a^3 100 \cdot f(\theta)}{\frac{4}{3}(6 - \pi)a^3} = 164.85 \cdot f(\theta) \quad 5$$

$$\theta = 164.85 f^{-1}(S) \quad 6$$

By combining the meniscus angle equation with the Fisher equation, which was rearranged into terms of meniscus angle and sphere radius, the desired apparent cohesion equation for open packing as developed in Appendix C becomes:

$$C = \frac{\pi T}{2a[1 + \tan(2.3 \ln S + 10.59)]} \quad \text{For } S = 0 \text{ to } 10\% \quad 7.A$$

$$C = \frac{\pi T}{2a[1 + \tan(7.8 \ln S - 0.11)]} \quad \text{For } S = 10 \text{ to } 90\% \quad 7.B$$

In the above apparent cohesion equation, "C" is cohesion, "a" is the sphere radius, "S" is the degree of saturation and "T" is the surface tension of water. Since case one was limited to a sphere arrangement of 47.64 percent porosity, a refinement of the apparent cohesion equation was required to include all porosities. Four types of sphere arrangement were selected over the range of loosest to closest packing (Table 9). Figure 8 indicates the different meniscus angles obtained for varying saturations and porosities. Figure 9 indicates the density correction factor which adjusts for the changing number of contact points and the decreasing cross-sectional area. To determine the apparent cohesions for soil of any porosity, the meniscus angle obtained from Figure 8 and the density factor from Figure 9 are substituted into the modified cohesion equation:

$$C = \frac{16.4 \times 10^{-4} Df}{a[1 + \tan \frac{\theta}{2}]} \quad 8$$

In the modified apparent cohesion equation, "C" is cohesion, "a" is sphere radius, "theta" is the meniscus angle and "Df" is the density factor (Appendix C).

Table 9. Ideal soil systems of uniformed spheres¹

Case numbers	1	2	3	4
Arrangement	Cubic	Ortho- rhombic	Tetra- gonal	Rhomb- hedral
volume voids	$3.81a^3$	$2.74a^3$	$1.81a^3$	$1.47a^3$
volume total	$8.00a^3$	$6.93a^3$	$6.00a^3$	$5.66a^3$
porosity	47.64	39.54	30.19	25.95
density	88.23	101.87	117.63	124.77
void ratio	0.910	0.654	0.431	0.350
contact points	3	4	5	6
area of side	$4a^2$	$2\sqrt{3} a^2$	$2\sqrt{3}a^2$	$2\sqrt{2} a^2$

¹Graton and Fraser (1935).

The theoretical apparent cohesion equation provided a basis to compare the experimental results to theoretical calculations. However, as in the case of most theoretical concepts, the results are only as good as the conditions and assumptions made during development. The conditions were:

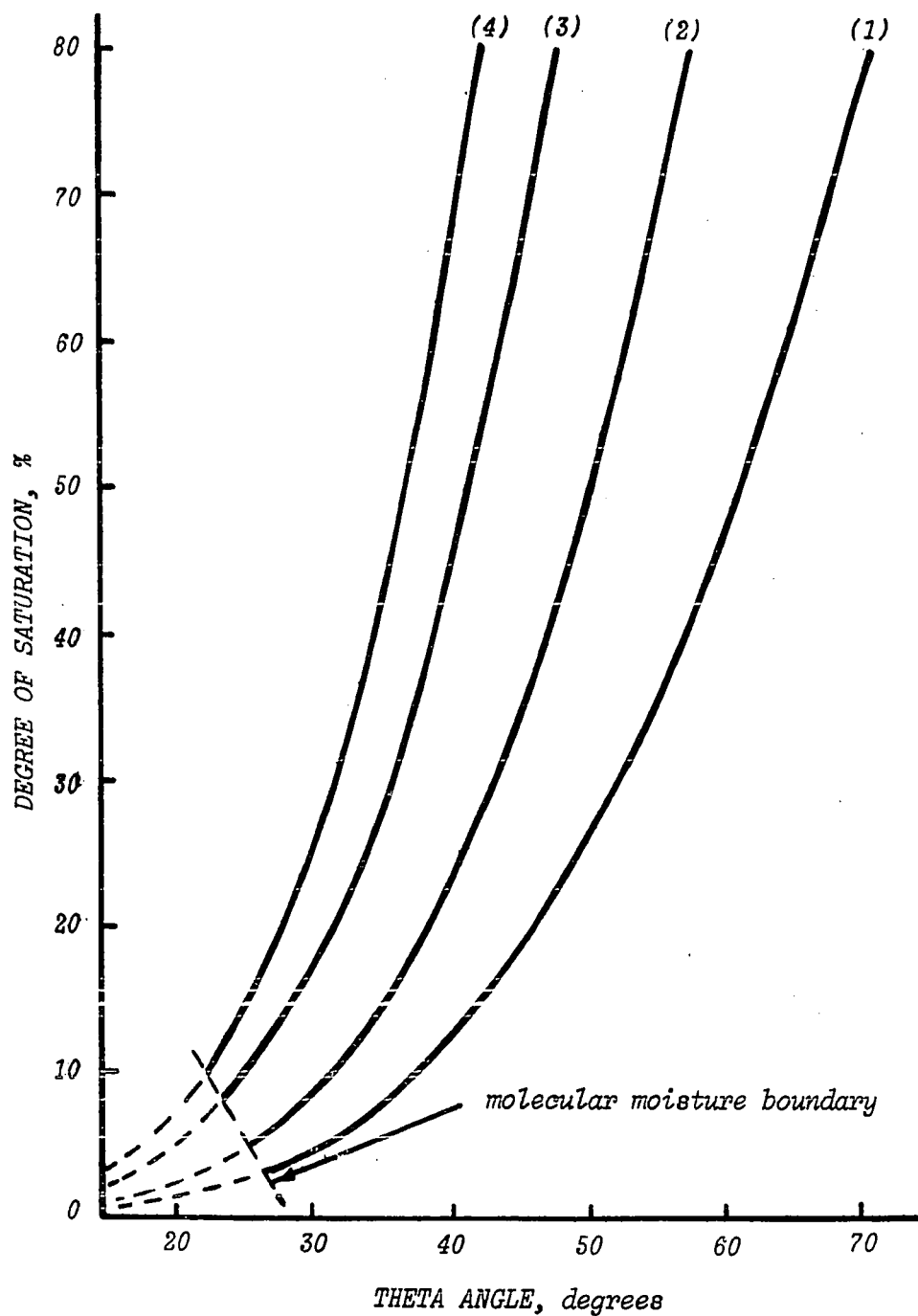


Figure 8 Porosity curves for meniscus angle and saturations.
 Curve 1 is for a porosity of 47.65 percent.
 Curve 2 is for a porosity of 39.54 percent.
 Curve 3 is for a porosity of 30.19 percent.
 Curve 4 is for a porosity of 25.95 percent.

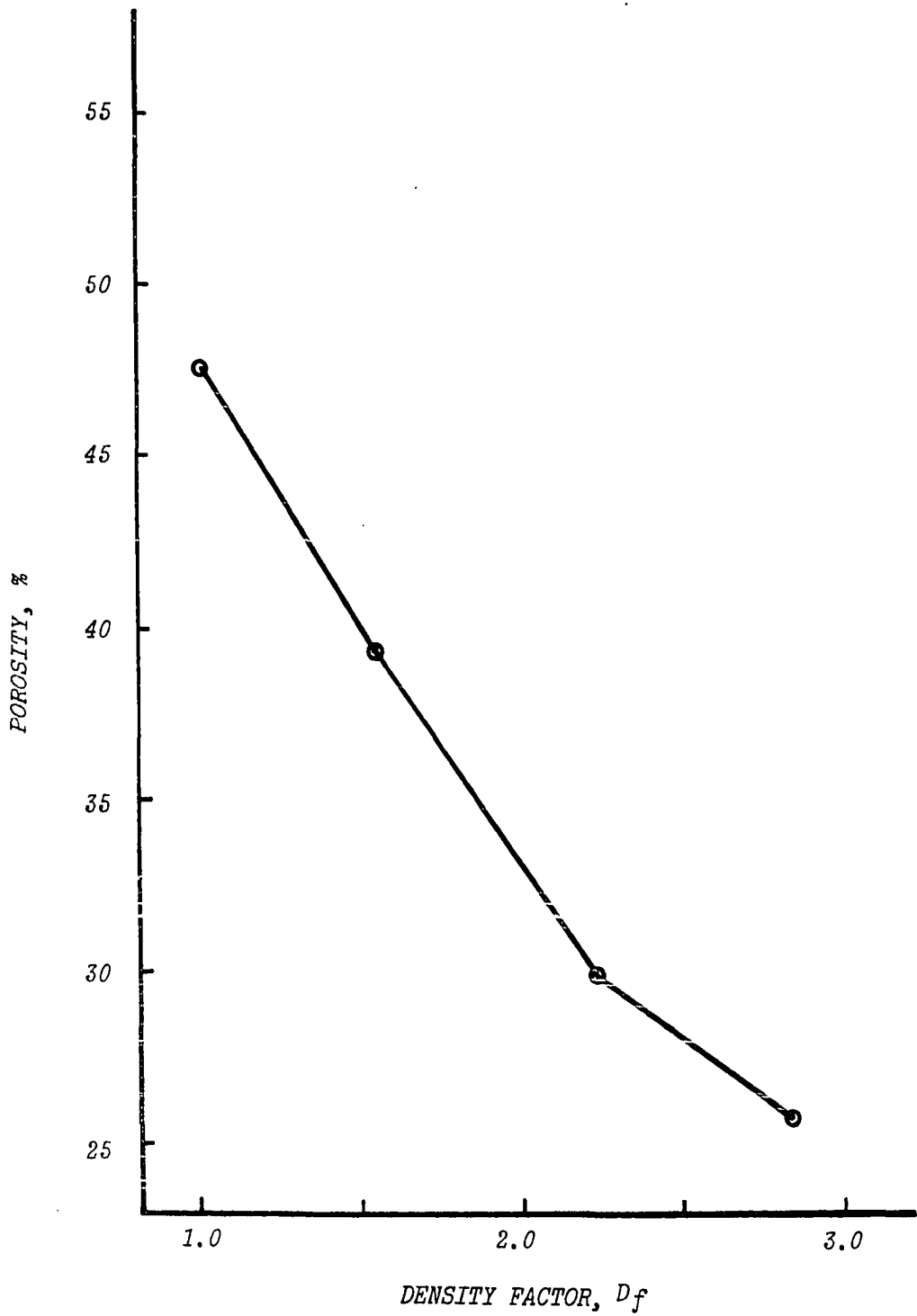


Figure 9 Density correction factor for the apparent cohesion equation.

Soil composed of uniform spheres.

Wetting fluid is water.

The menisci are circular.

No colloidal particles present to adsorb moisture.

C. Experimental Apparent Cohesion

The true test for any theoretical concept is experimental verification. Conveniently, the loess used for testing probably more closely matched the case one model soil than any other soil available. The friable Iowa loess was an extremely uniform soil, low in clay content, high in porosity with a sphericity of 0.76 (Handy et al. 1955). The "Soiltest" apparatus (Chicago, AP-170-1) was used for all unconfined compression tests. The procedure used followed the outline for the unconfined compression test listed in Lambe (1951).

D. Results and Discussion

A series of unconfined compression tests on undisturbed loess were conducted. The tests were made at various degrees of saturation and are plotted in Figure 10. It was apparent that the unconfined compressive strength, q_u , did decrease with increased moisture; however, other properties of loess probably contributed to this q_u strength in addition to contact water surface tension.

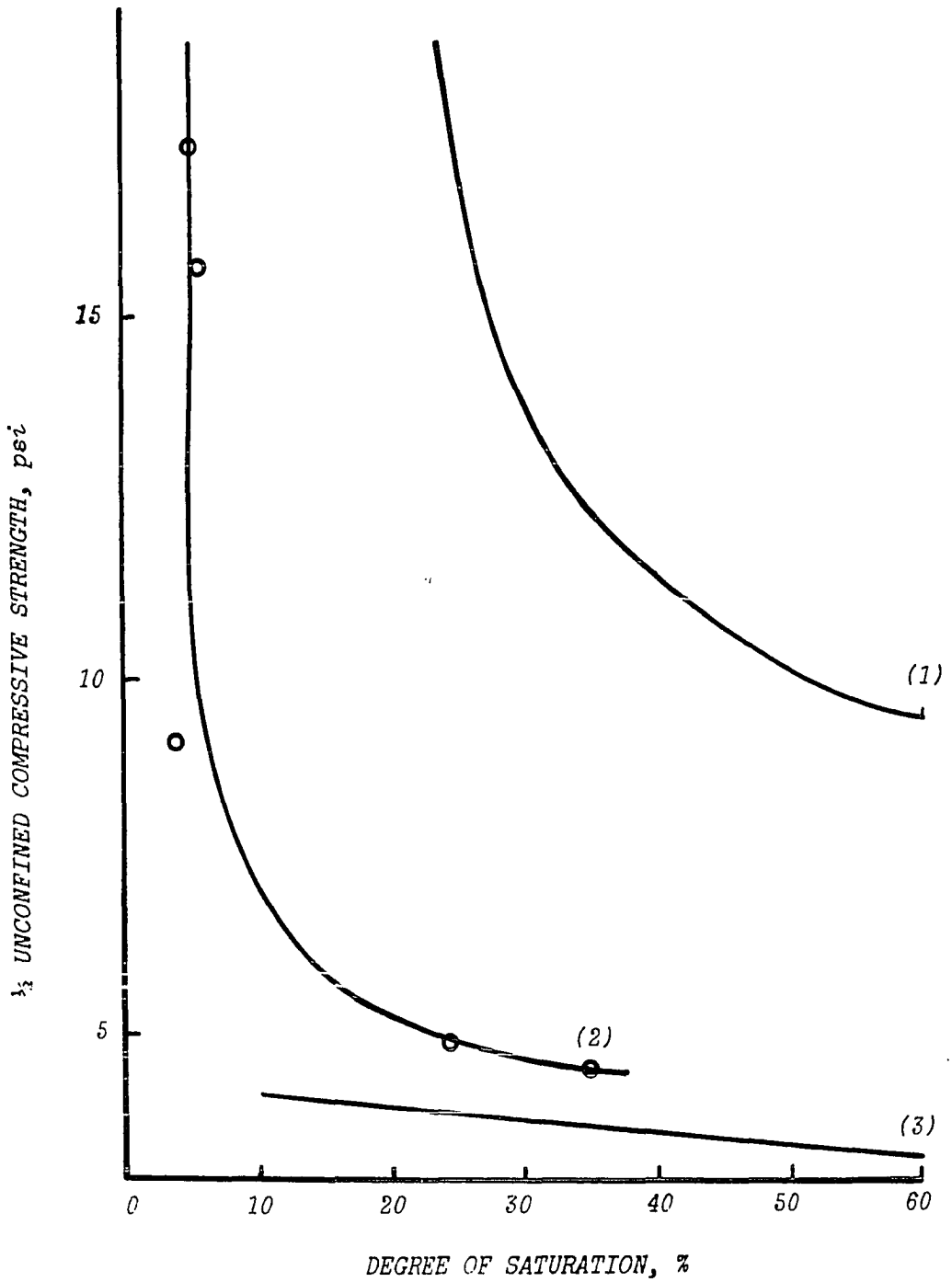


Figure 10 Unconfined compressive strength of UND loess.
 Curve 1 is UND Vicksburg Loess at 90.0 pcf dry density. Lutton (1969)
 Curve 2 is UND Iowa Loess at 88.3 pcf dry density.
 Curve 3 is REM Iowa Loess at 85.5 pcf dry density.

To eliminate any influence of calcium carbonate or other forms of cementation that may have been present in UND loess, the cohesion for remolded loess was determined.

A series of unconfined compression tests for loess remolded to 85 pcf was conducted, Figure 11. The strength of the undisturbed loess was found to be greater than remolded loess of equivalent densities. The differences in strength may be attributed to thixotropic effects, cohesion from calcium carbonate, or to particle stacking and interlocking. Although an attempt was made to rework the remolded samples back to approximately the same density as the undisturbed loess, there was no way to restack the particles in the same order as the particles were stacked during deposition of the loess. There was little indication that calcium carbonate cementation was present. An attempt to increase the strength of loess by numerous wetting and drying cycles with a solution of calcium bicarbonate failed.

To separate the effect of contact water surface tension from clay bonding¹, the loess was processed through numerous sedimentation cycles and treated with a solution of hydrogen peroxide. This washed silt had most of its colloidal

¹Clay bonding is defined as the cohesion obtained when the experimental apparent cohesion is subtracted from the total experimental cohesion.

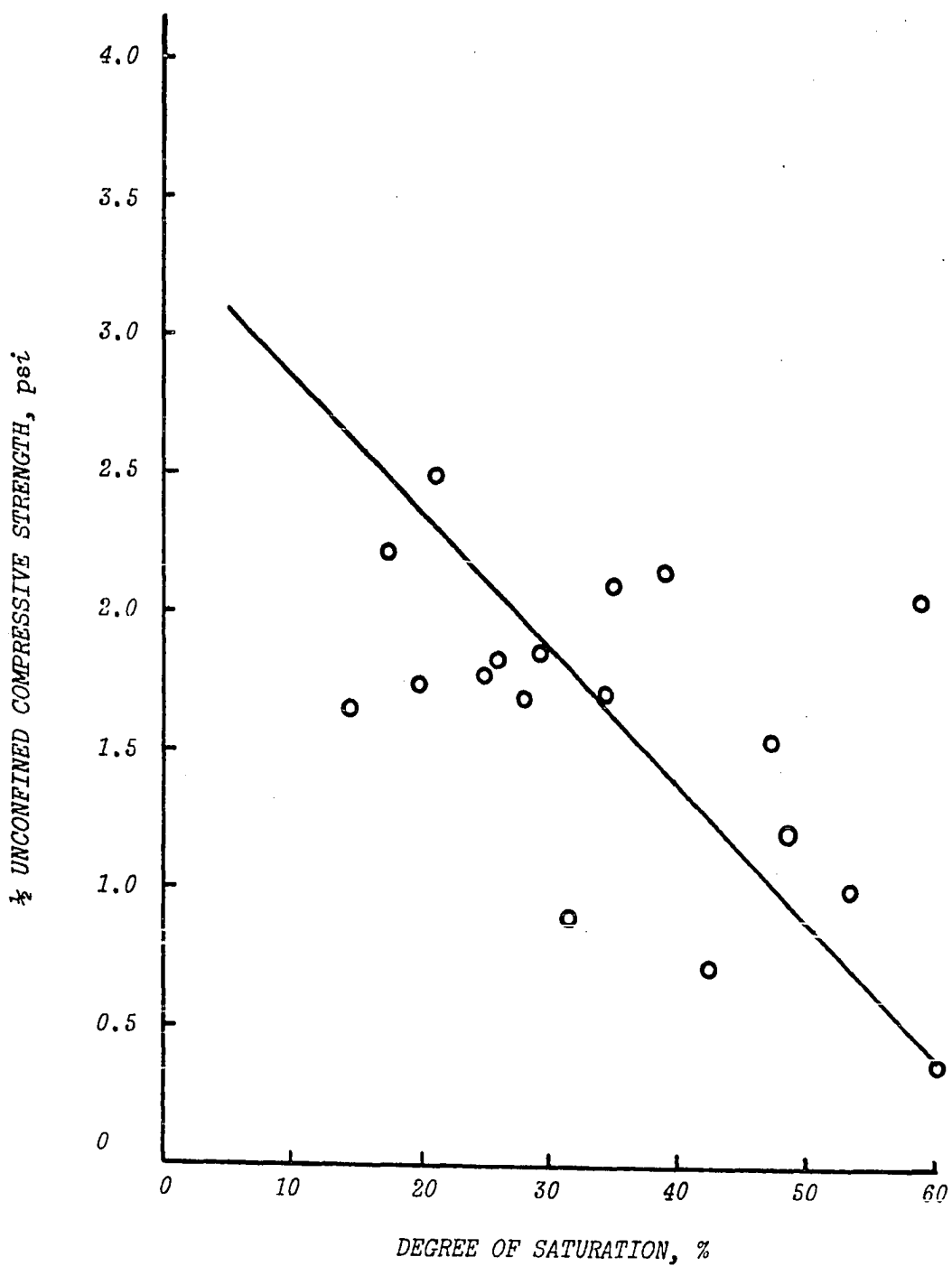


Figure 11 Unconfined compressive strength of REM loess at 85 pcf density.

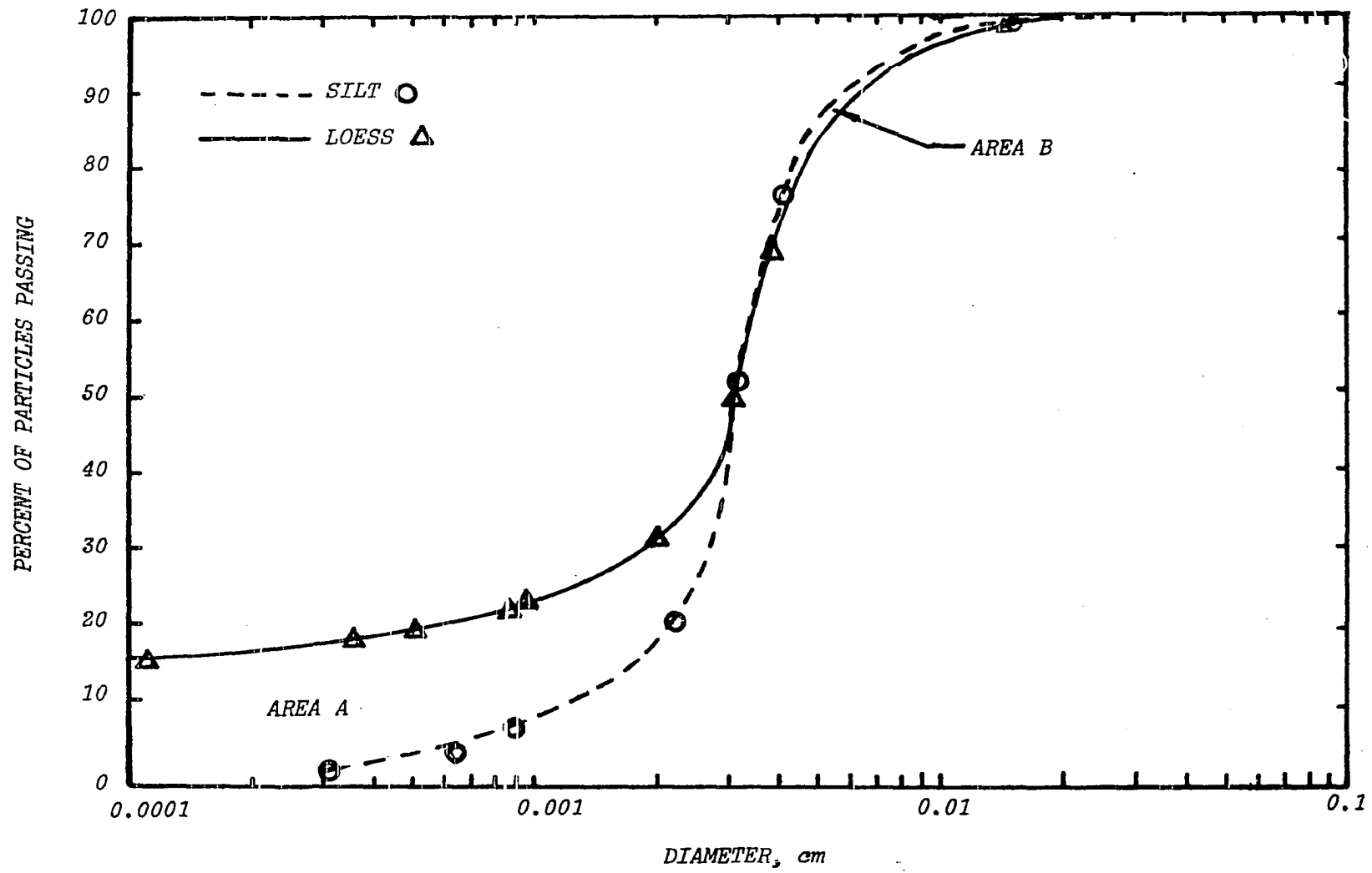


Figure 12 Grain size distribution of loess and silt.

particles removed, Figure 12. The clay in the loess was reduced from 14 percent to less than 1 percent, represented by Area A of Figure 12. Some large particles of organic matter were removed in the hydrogen peroxide bath as indicated by Area B; however, this area may also represent a change in size of quartz grains when the clay specks and skins were removed.

A series of unconfined compression tests on washed silt was conducted to determine the cohesion of a soil without the influence of clay, Figure 13. It appears that the unconfined compressive strength of remolded loess (Figure 11) is in approximately the same range as that of the silt (curve 1, Figure 13), and that the cohesion developed from clay bonding does not become a significant contributing factor in cohesive strength until higher densities are reached.

In Figure 13, the experimental cohesion of silt is plotted as curve 1. Curves 2, 3, 4 and 5 are theoretical values calculated from the apparent cohesion equation case one for spheres of 0.0003 cm, 0.0005 cm, 0.001 cm and 0.003 cm radii respectively.

Curve 1, experimental values, were obtained graphically by extending the Mohr-Coulomb failure envelope ($\phi=32^\circ$) to the left of the origin to the intersection with the horizontal axis. The distance on the horizontal axis from the intersection to the origin may be thought of as an internal

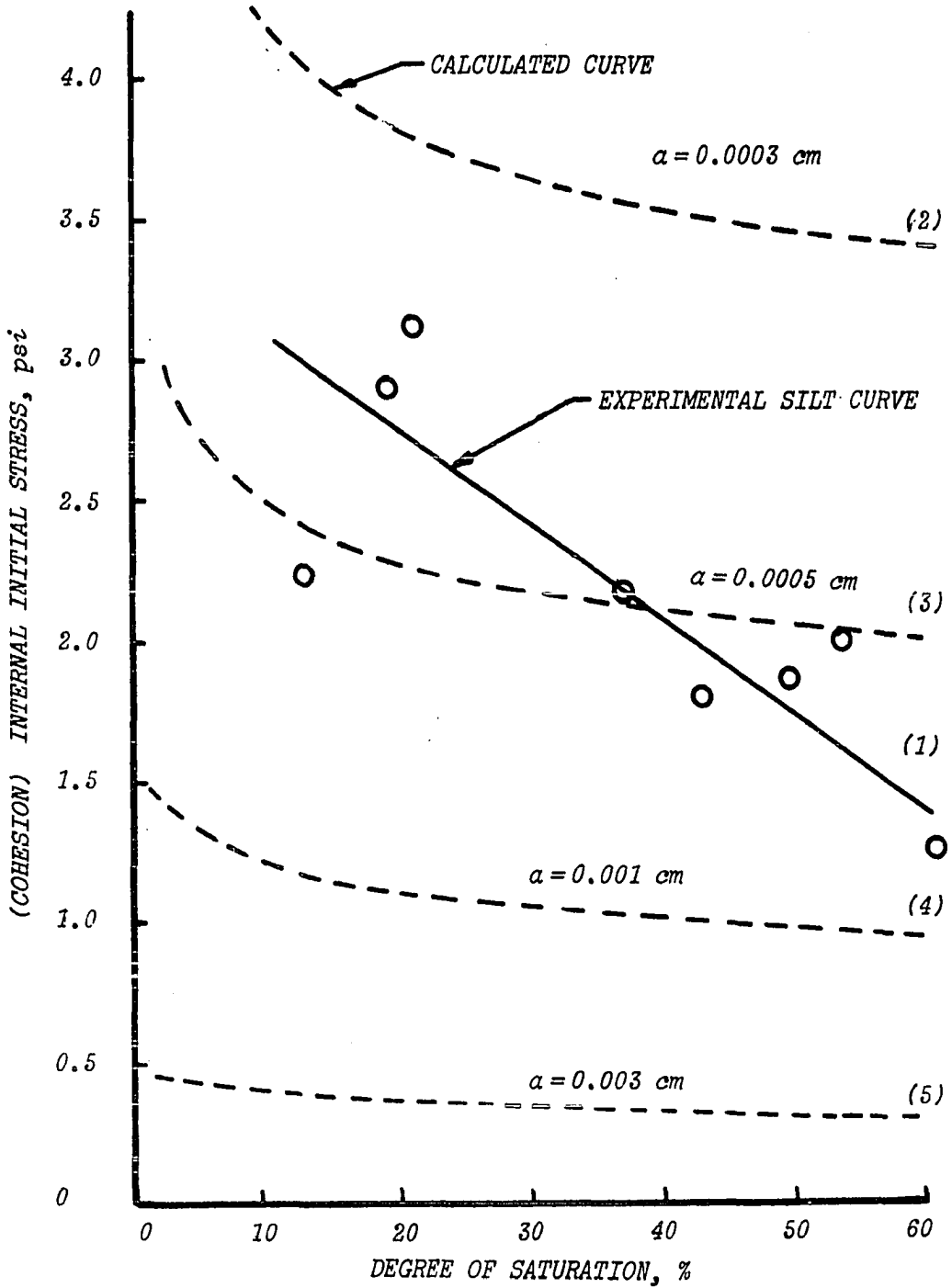


Figure 13 Curve 1, internal initial stress (cohesion) obtained from q_u tests at 85 pcf dry density, curves 2, 3, 4 and 5 are theoretical apparent cohesion curves for uniform spheres.

initial stress which is inherent in the material and is associated with the cohesion property, Spangler (1960). The term cohesion is applied to the theoretical apparent cohesive stress (tensile stress) which is also represented by the horizontal distance between the intersection of the failure envelope and horizontal axis and the origin. By using the above convention the experiment results were compared to the theoretical calculations.

The experimental values obtained in testing silt at different saturation disclose a sensitivity to any variation in densities as well as moisture. With lower densities the apparent cohesion decreases; and conversely, with higher densities the cohesion increases. This experimental behavior of density sensitivity is in agreement with the concepts inherent in the development of the apparent cohesion equation. In the model soil system the open packing produces three contact points per sphere. Since more contact points occur in a more dense packing, there are more and smaller menisci formed at the same degree of saturation. Therefore, a change in density changes the apparent cohesion, Figure 14.

Since the loess particles are not all the same size, the number of contact points generated by the smaller particles is unknown. However, the number is obviously more than the

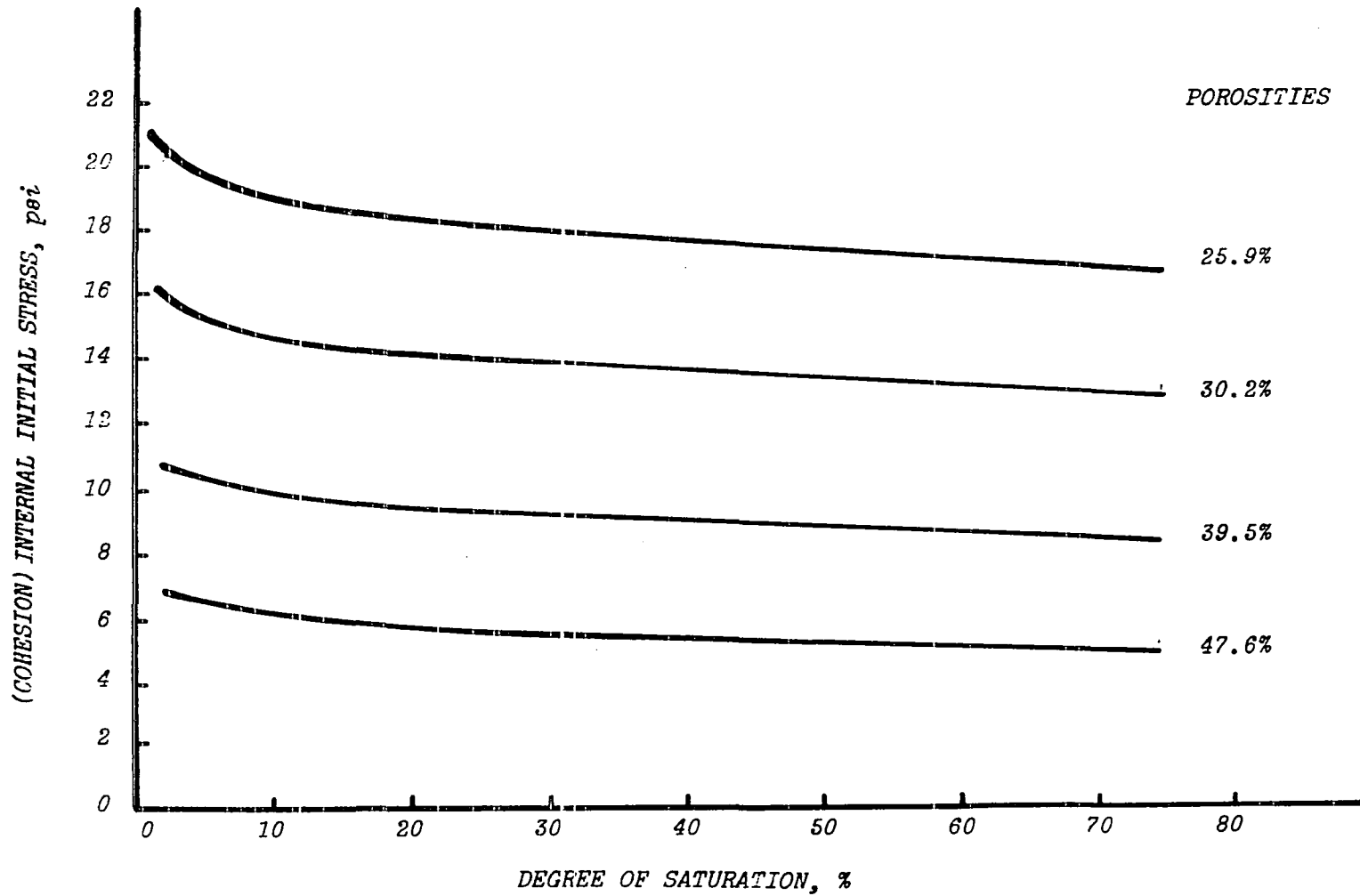


Figure 14 Apparent cohesion values for a particle of 0.0002 cm radius.

six contact points which are shown in Table 9. Also with the additional number of contact points and with the 14 percent clay in the loess consuming moisture, the degree of saturation for coalescence of menisci will be much greater than the 13.21 or 24.3 percent listed by Fisher (1926). It is estimated that the theoretical apparent cohesion equation is valid up to 80 percent saturation when used for calculation in loess type soils. Lutton (1969) shows an experimental curve of q_u strength versus saturation for UND Vicksburg loess. At 80 percent saturation there seems to be a break in his curve which appears to be the boundary between the apparent cohesion zone and the gravitation water zone.

Some criteria for selecting the effective radius of particles for use in the apparent cohesion equation for loess type soils was needed. The determination of the radius of the spheres in the model soil was obviously easy. However, when applying the apparent cohesion equation to loess, the size selection of the effective radius became more complex. Since the smaller grains generate higher cohesive values at equivalent saturation than the larger grains, the influence of these smaller grains is greater than the influence of the large grains. Working from this hypothesis, the effective grain size radius should not be an average radius at 50 percent passing by weight or volume but should be the radius of the mean particle size. The number of particles in each

of the 10 percent by weight passing increment was determined. The average radius for the 10 different weight increment classes were taken from the grain size distribution curve for silt. For example, the average radius in the first class was taken at the 95 percent passing size as 3.75×10^{-3} . This radius was selected as the reference base. The volume of a sphere for the reference radius was determined and equated to the volume of number of spheres for the average radius of the remaining classes. One reference sphere volume in the 90-100 percent class is equal to 1000 spheres calculated from 0-10 percent increments average radius. The most identifiable point near the centroid of the area under the curve generated by plotting the number of grains per class was the 10 percent passing size, Figure 15. By using this value as the effective radius, the effective radius determined from the grain size distribution curve for silt was 0.00065 cm. By modifying the apparent cohesion equation for uniform spheres, the equation for silts and loess was obtained.

$$c = \frac{16.4 \times 10^{-4} D_f}{r_e \left[1 + \tan \frac{\theta}{2} \right]} \quad 9$$

In the above equation, "C" is the cohesion in psi, "theta" is the meniscus angle, "Df" is the density factor and "re" is the effective radius. The surface tension value is reduced to a constant by assuming the water is at 25°C.

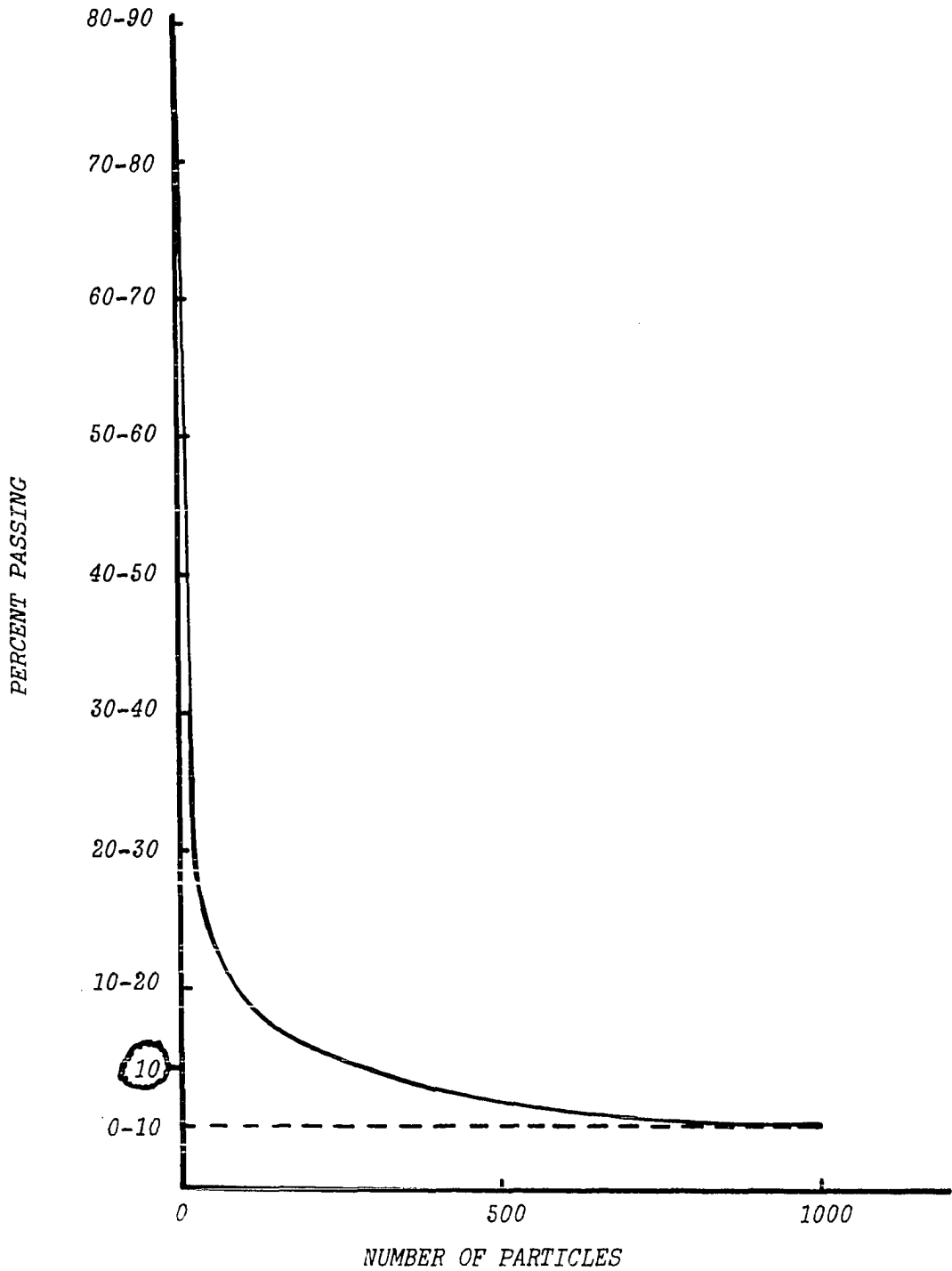


Figure 15 Equivalent particles distribution curve for determining effective radius.

Using this equation with an effective radius of 0.00065 cm, the calculated cohesion values plot just below curve 3 in Figure 13.

The calculated value was slightly lower than the experimental value, but by using effective radius instead of the equivalent sphere radius for the theoretical equation, the apparent cohesion for silt or loess may be realistically calculated. Some of the reasons why the values were lower are the effect of the lack of sphericity of the loess and silt particles, the sensitivity of the experimental data to density/porosity, and the coalescence of the menisci associated with the smaller particles before the coalescence of menisci associated with the larger particles.

Due to the lack of sphericity, menisci may form at the corners of grains which would provide smaller radii and consequently higher cohesive forces than an equivalent sphere radius. The equivalent sphere radius is the radius of the smallest circle that circumscribes a given loess particle. However, menisci are probably forming where the corners are in contact. To account for the effect of these corners, a reduction factor was developed which would reduce the equivalent radius by approximately 1/3. The reduction factor was obtained by dividing the average corner radius by the equivalent radius. The average corner radius was determined by scaling the length of radii from SEM photographs. The reduc-

tion factor of $1/3$ is the average of five randomly chosen loess and silt particle calculations. However in the smaller grain size range, the menisci are large compared to the grains and even larger compared to the corners. At this scale the menisci probably bridge over any corner, negating any effect the corner may have. Since the smaller grain provides the majority of the cohesive force, and since the reduction is probably effective only in the larger particle range, it was not considered sufficiently significant to be included in the equation.

The sensitivity of the apparent cohesion is probably due to the degree of saturation which is directly affected by any change in density or porosity. This effect may be corrected by applying the exact porosity of the test soil to the proper curves in Figures 8 and 9.

Lastly, the coalescence of the menisci associated with the small grains occurs before the coalescence of the larger grain menisci. With a small change in moisture in the lower saturation levels, a large number of small menisci may coalesce, while in upper saturation levels, a small change of moisture may not coalesce any large menisci. In the model soil all coalescence would occur at the same time, whereas in loess the smaller grain menisci coalesce first. This variation in coalescence rate probably caused the difference in slope of the theoretical and experimental curves in Figure 13.

E. True Cohesion

Figure 16 shows the rapid increase of q_u strength with density after the 90-100 pcf range. This rapid increase can not be attributed to apparent cohesion in either the theoretical analysis or the experimental results. By comparing the magnitudes of the q_u strengths in Figure 17 for REM loess, it seems that a change in density greatly outweighs a change in moisture. It is realized that an increase in density increases apparent cohesion. However it appears that clay bonding is the significant contributing factor, although apparent cohesion is dependent on density and does contribute some of this strength. It seems reasonable that density is important in clay bonding because the closer one primary clay covered silt particle is to another particle, the better the chance of clay bonding. As in apparent cohesion, an increase of moisture decreases the cohesive strength of the clay bonding, Figure 17.

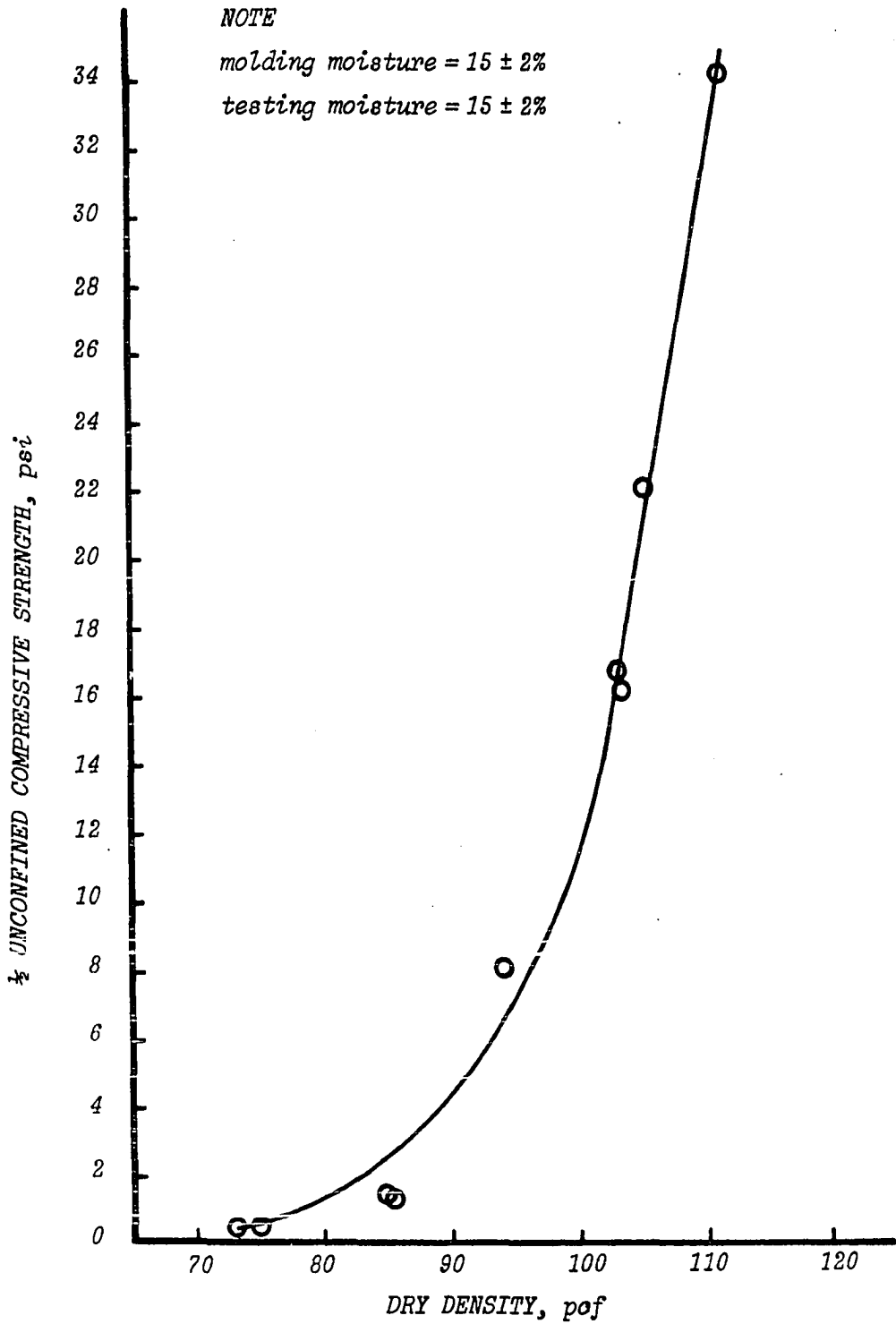


Figure 16 Unconfined compressive strength for loess molded at optimum moisture content versus dry density.

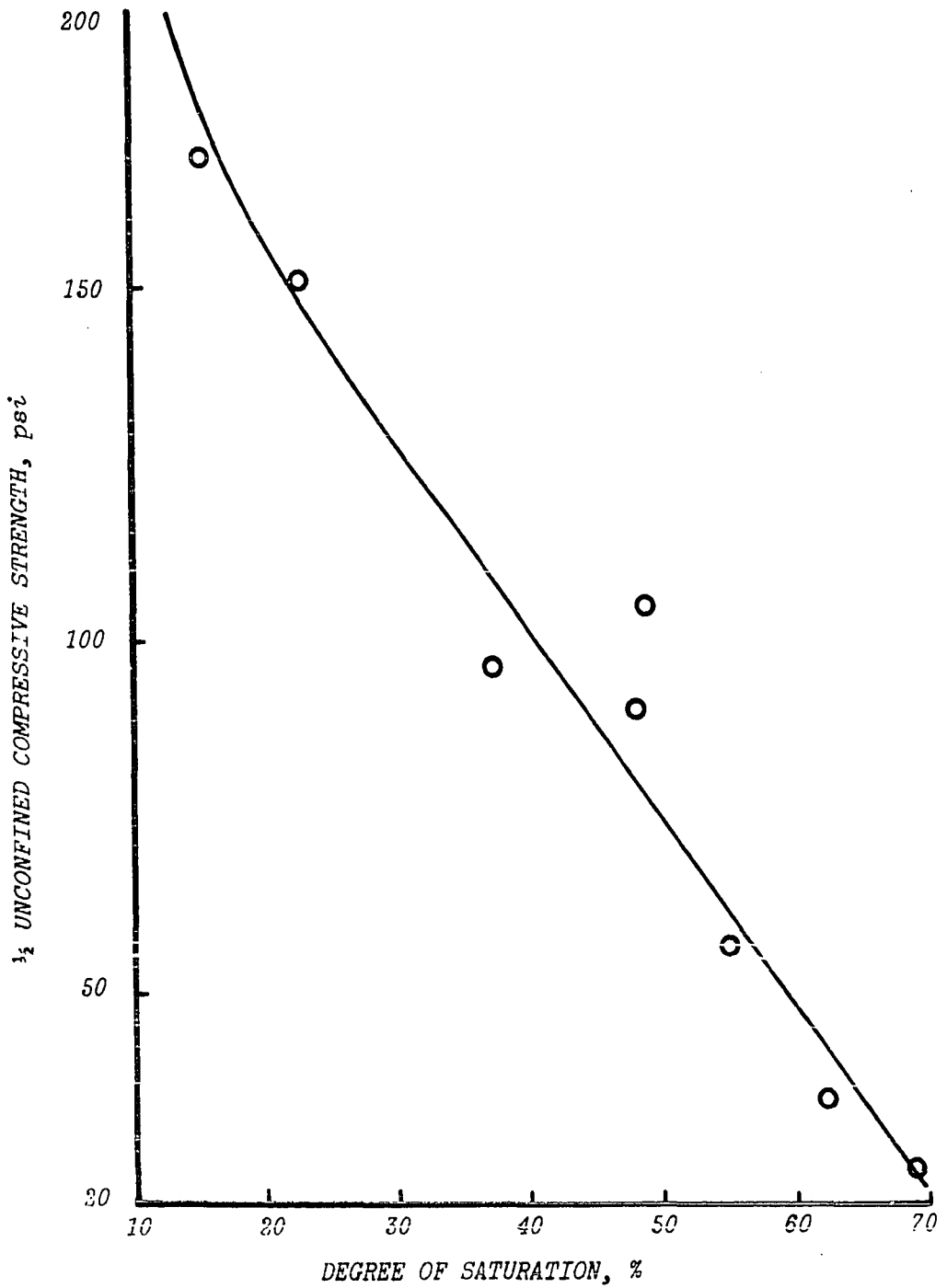


Figure 17 Unconfined compressive strength for a REM loess at 104 pcf dry density with varying degree of saturation at testing.

V. PERMEABILITY

A. General

There is an extreme shortage of permeability information about loessial soils. Some of the available permeability data are shown in Table 10.

Table 10. Summation of loess permeability data

References	Remarks	Type	Density pcf	Permeability cm/sec
(Good Drainage)				
Fenton	C hor	und	77	6×10^{-2}
Terzaghi	---	und	---	10^{-3}
Scheidig	---	und	---	10^{-3}
Holtz	Neb	und	75	10^{-3}
(Poor Drainage)				
Balley	Europe	und	84	10^{-4}
Fenton	C hor	und	92.7	4×10^{-4}
Tuthill	Iowa	und	---	$>1.4 \times 10^{-4}$
Gibbs	Neb	rem	100	10^{-5}
(Practically Impermeable)				
Handy	plastic	und	---	6.3×10^{-6}
Holtz	Neb	und	111	10^{-7}
Gibbs	Neb	rem	111	10^{-7}
Scheidig	Europe	rem	---	10^{-8}
Lambe	---	---	95	10^{-9}

In order to obtain more data and to evaluate the effect of molding moisture, density, type of compaction and soil composition on permeability, a series of permeability tests was conducted.

B. Apparatus

The apparatus known as the variable head permeameter or, more commonly, the falling head permeameter was used, see Lambe (1951). Most of the tests were run in the Harvard Miniature Molds, but a few tests were conducted while the samples were in the Triaxial Testing Machine.

C. Procedure

The majority of the samples were statically compacted under measured loads into the Harvard Miniature cylinder and immediately placed into the falling head apparatus. Then the samples were saturated from the bottom up to reduce the possibility of entrapping air bubbles in the pores. The samples were placed under a head of 44 to 56 inches of distilled water. The permeant was allowed to flow through the samples for approximately one-half hour before the change in head was recorded. For high density samples additional flow time was needed, and because of the long duration of these tests, corrections for evaporation of the permeant were made. Permeability data for the different test series conducted are listed in Appendix D.

D. Calculations and Discussion

During the entire series of permeability tests, constant temperature distilled water was used on 100 percent saturated samples. All the loess used was taken from the Prospect Hill Site from within a 10 foot radius. Therefore, the soil composition of the loess samples probably remained unchanged. The three major variables tested were density, compactive effort and molding moisture, shown in Figures 18, 19, 20 and 21, respectively.

Test series one and two, shown in Figure 18, indicate that the dynamically compacted samples produce higher permeability values at equal densities than the statically compacted samples. The dynamic compaction procedure closely resembles the AASHTO compaction method. However, for the purpose of studying various densities, the procedure was slightly modified.¹

In order to obtain the desired densities the statically compacted samples were compacted to a predetermined sample height on the unconfined compression apparatus. The static compactive load for loess and silt of different densities and moistures are shown in Figure 19. It is interesting to note that the same points that deviate from the compactive effort

¹See dynamic compaction data in Appendix D, test series two.

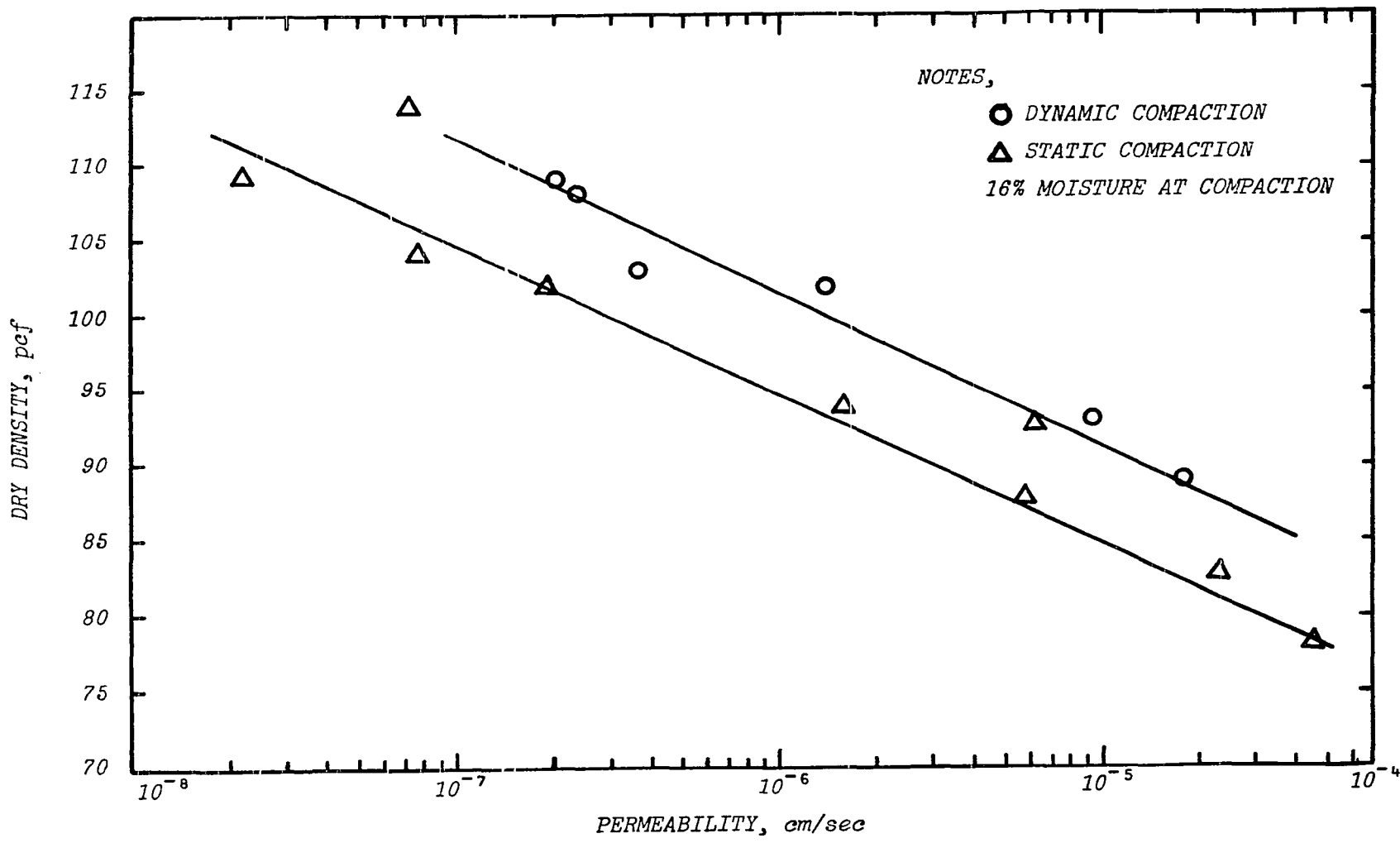


Figure 18 Density-Permeability curves for dynamically and statically compacted loess.

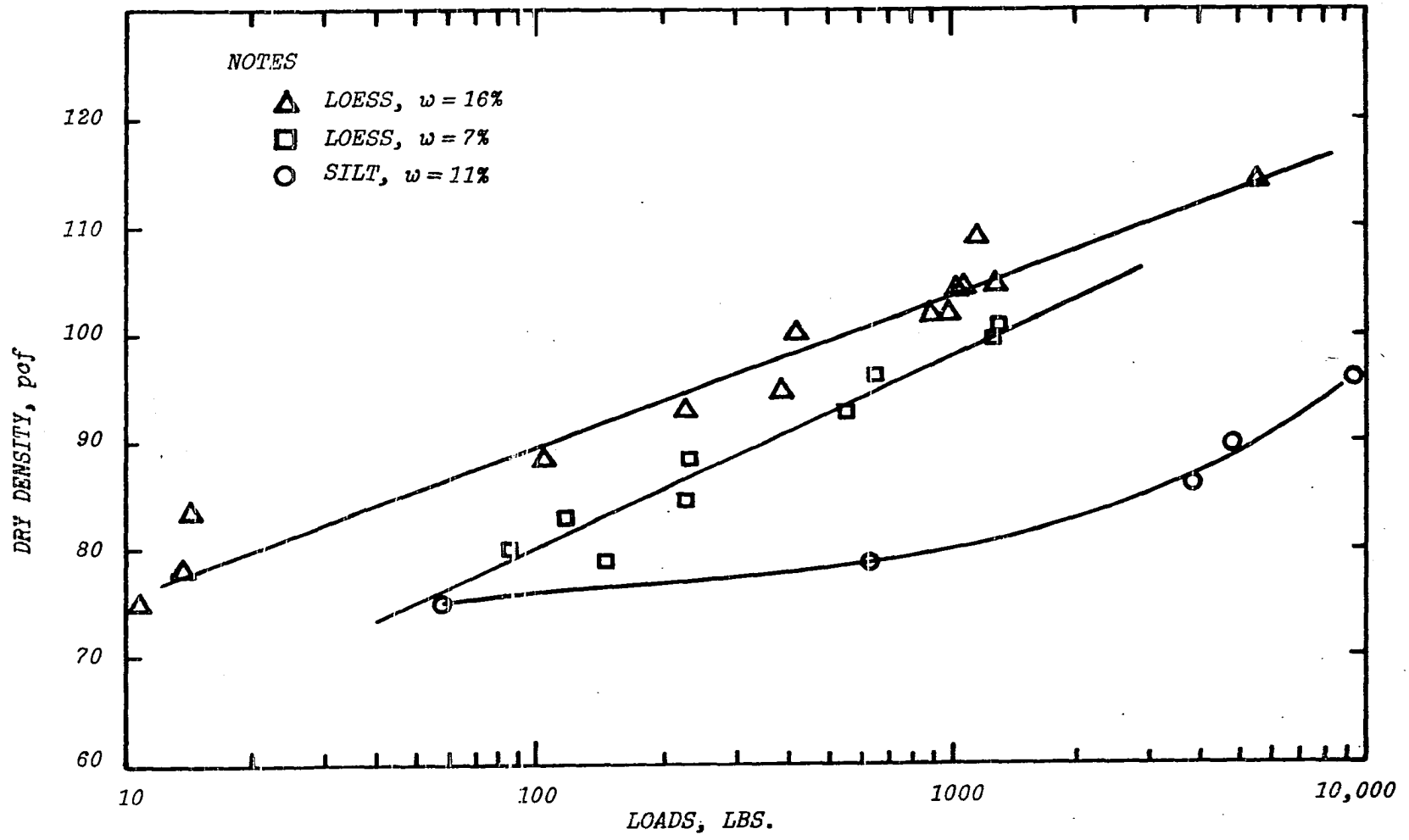


Figure 19 Static compactive effort for loess and silt.

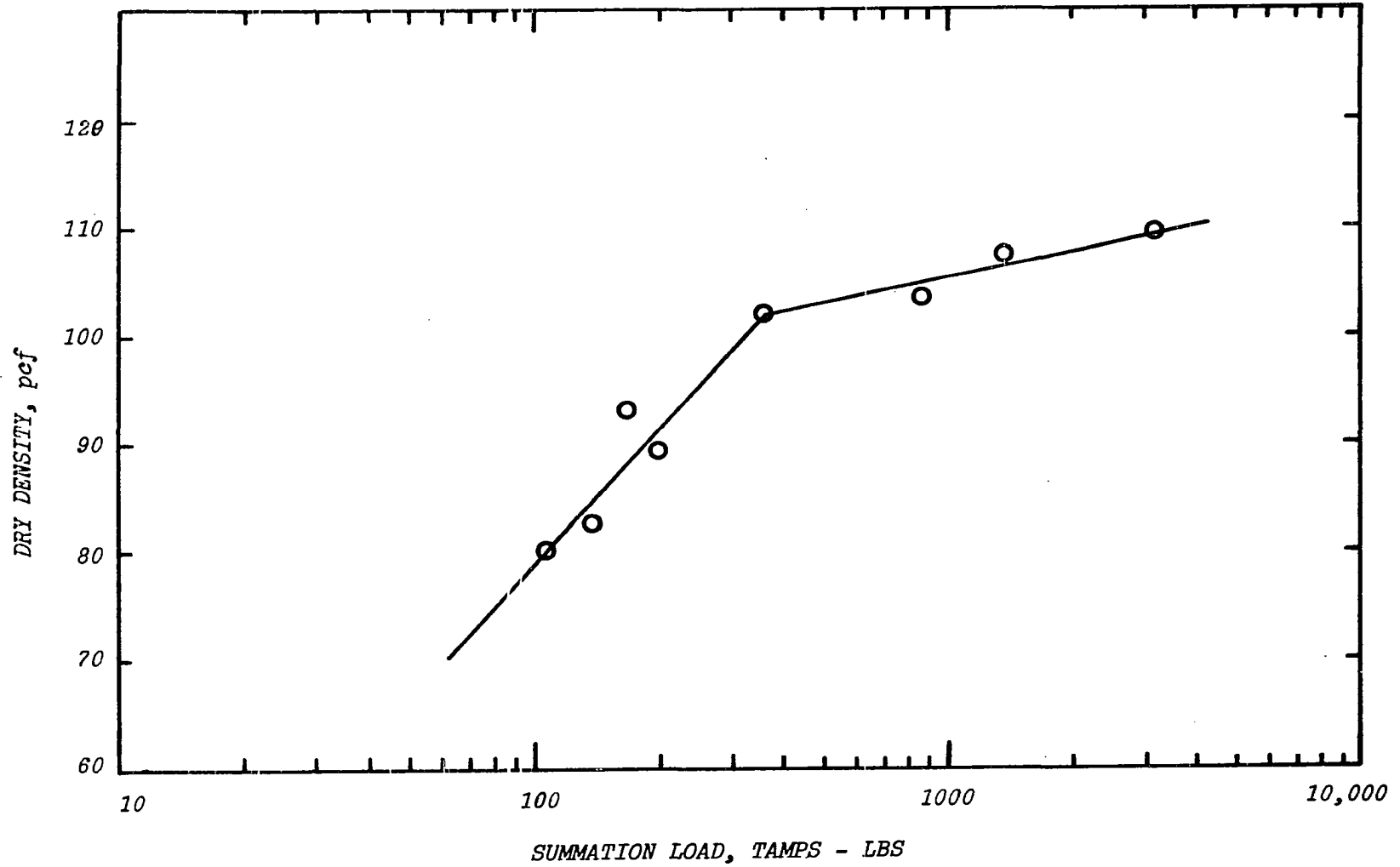


Figure 20 Dynamic compactive effort for loess.

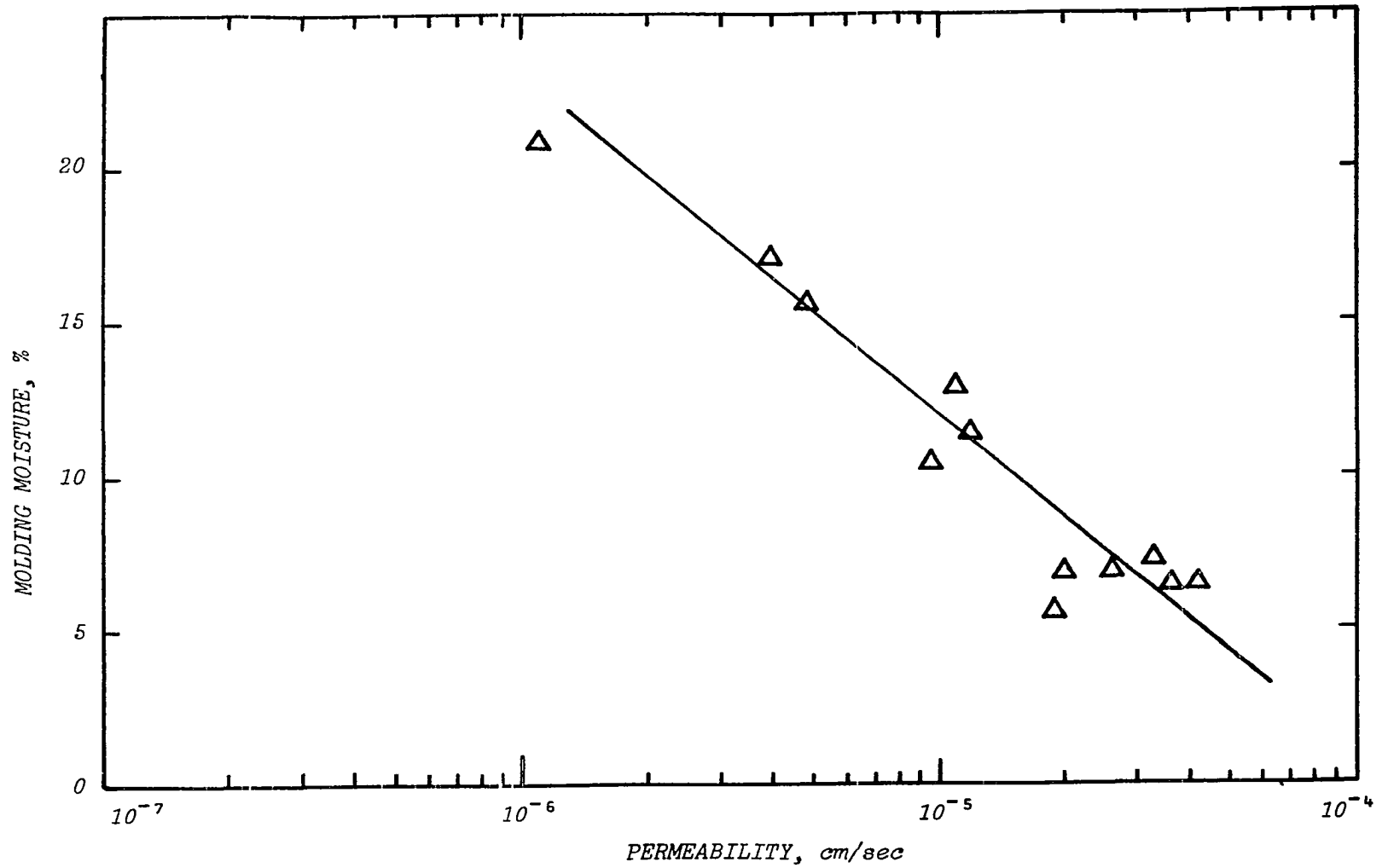


Figure 21 Molding moisture-permeability curve for loess at 85 pcf.

curve also deviate from the permeability-density curve. This is probably due to a moisture difference or a lack of homogeneity within those samples.

The relationship between the permeability and the molding moisture content is clearly shown in Figure 21, where the permeability decreases with increased moisture. A probable explanation for this variation in permeability is that the molding moisture content influences the type structure formed by the loess. A more dispersed structure formed at the higher moistures produces lower permeability values.

The effect of molding moisture is independent of density, as seen in Figure 22 where the relationship of higher moistures, lower permeabilities holds over a range of densities from 75 to 110 pcf. Curve 1, the 7 percent molding moisture, indicates a higher permeability than Curve 2, the 16 percent molding moisture, over the entire density range.

The permeability values for the low density, remolded loess samples were plotted in Figure 23. The scatter noted in this permeability data is significant when compared to the good reproducibility of permeability data obtained at the higher densities. It indicates the wide variation in pore configurations available when remolding loess at low densities and when varying moisture contents.

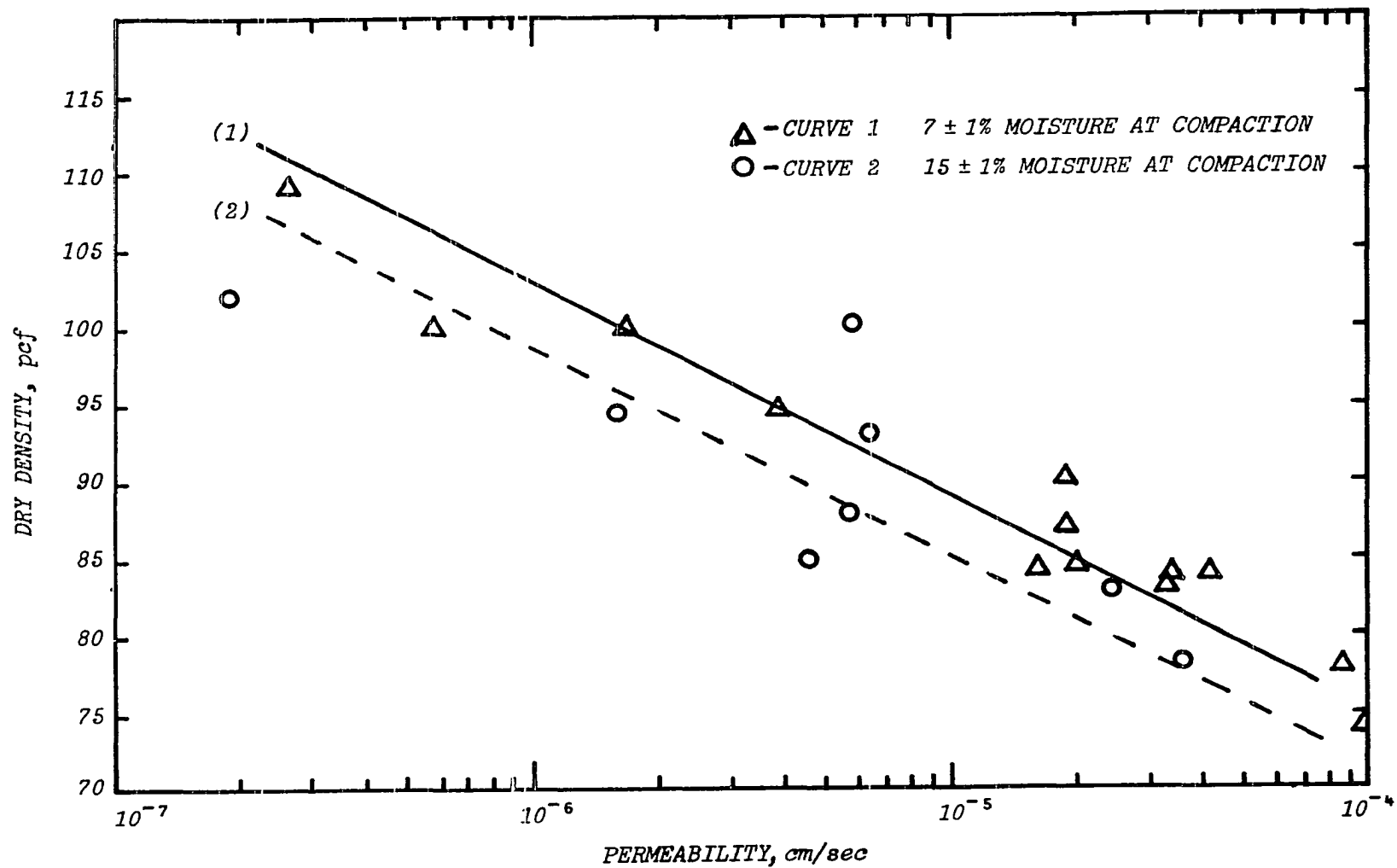


Figure 22 Density-Permeability curves for loess at 7 and 16 percent molding moisture.

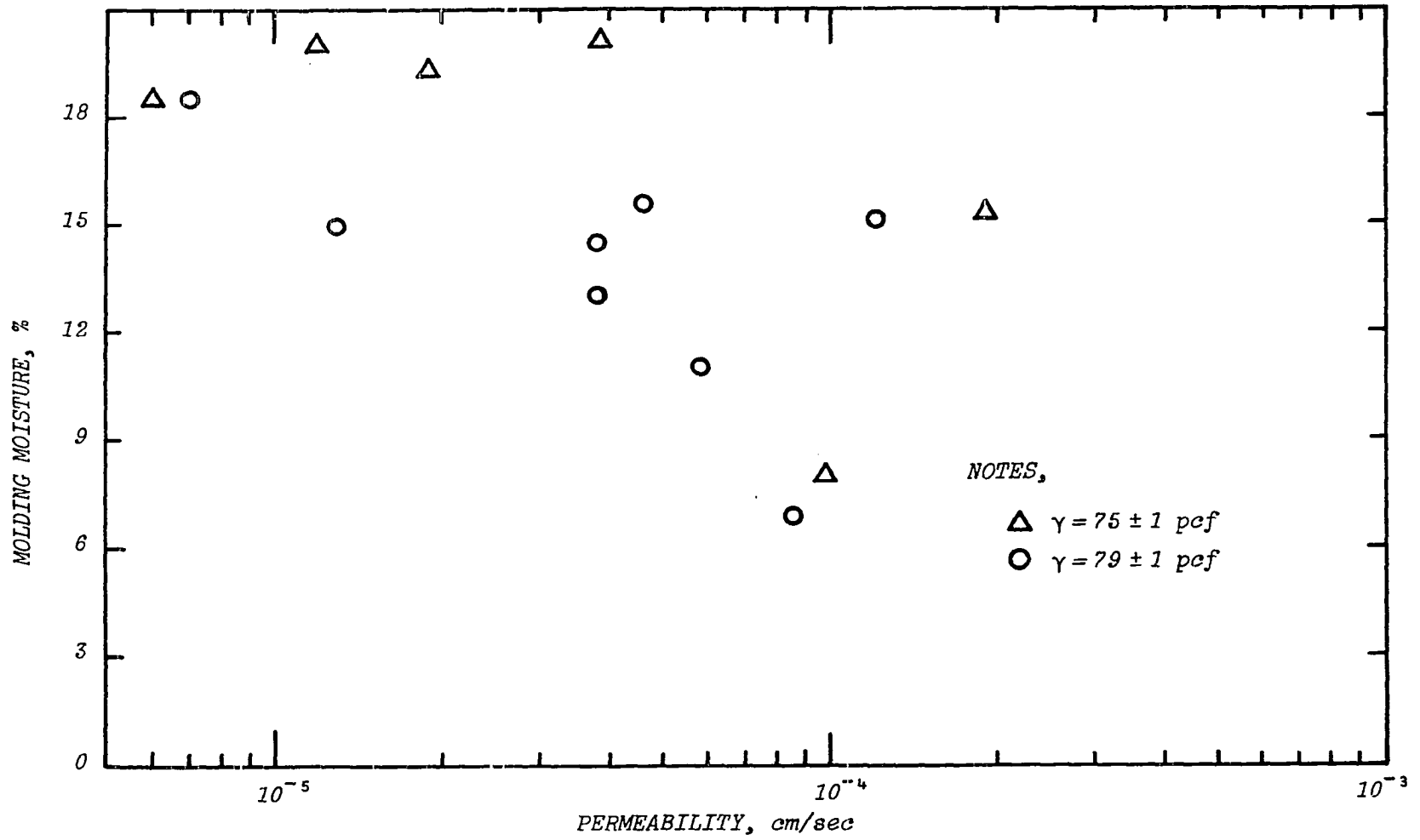


Figure 23 Molding moisture-permeability data for loess.

One of the reasons cited by Terzaghi (1951) for the difficulty in determining permeability of loess is that saturation causes structure collapse and densification. Although this seems reasonable, the densification was not directly measurable. However, a decrease of permeability with time within the same sample was noted (Figure 24). A possible interpretation would be the movement of fines within the loess structure to critical points in the flow channels which could reduce permeability. On the other hand, no movement of fines was observed. Another possible explanation would be the growth of organisms in the pores. However, distilled water was used on REM loess which had been oven-dried at 105° C. And lastly perhaps the fines were coating the porous stone filters causing a decrease in permeability. In the final analysis, probably some or a combination of all the above mentioned reasons contributed to the permeability decrease.

Figure 25 shows the comparison of loess and silt molded at equal moisture contents. From this graph it appears that loess and silt have the same permeabilities, indicating that the 14 percent clay present in the loess has little influence on permeability. However, the clay does have significant influence in determining the load required to mold loess, compared to the load required to mold the silt. A possibility which may have caused the similarity in the loess and silt

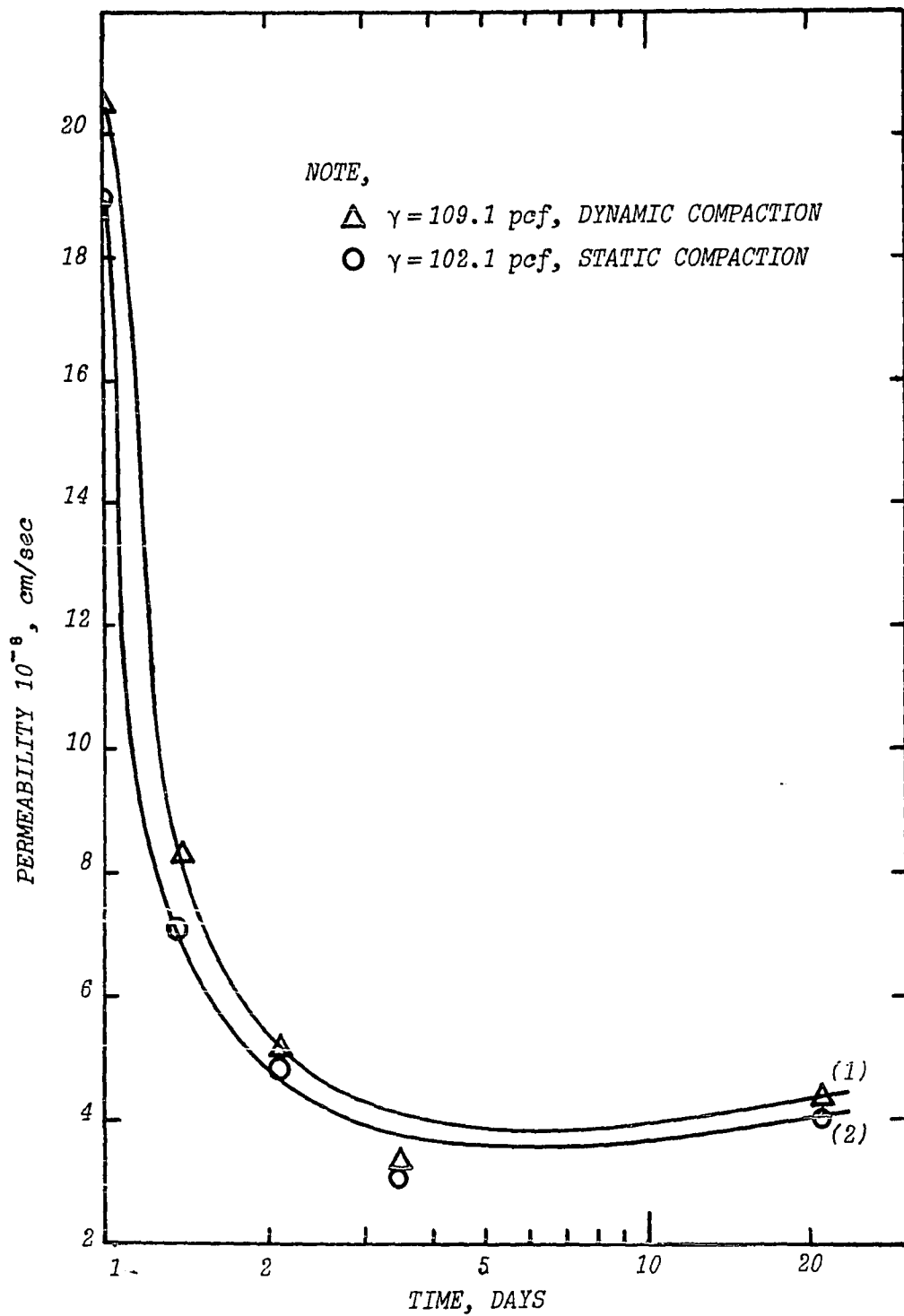


Figure 24 Permeability-Time curve for loess.

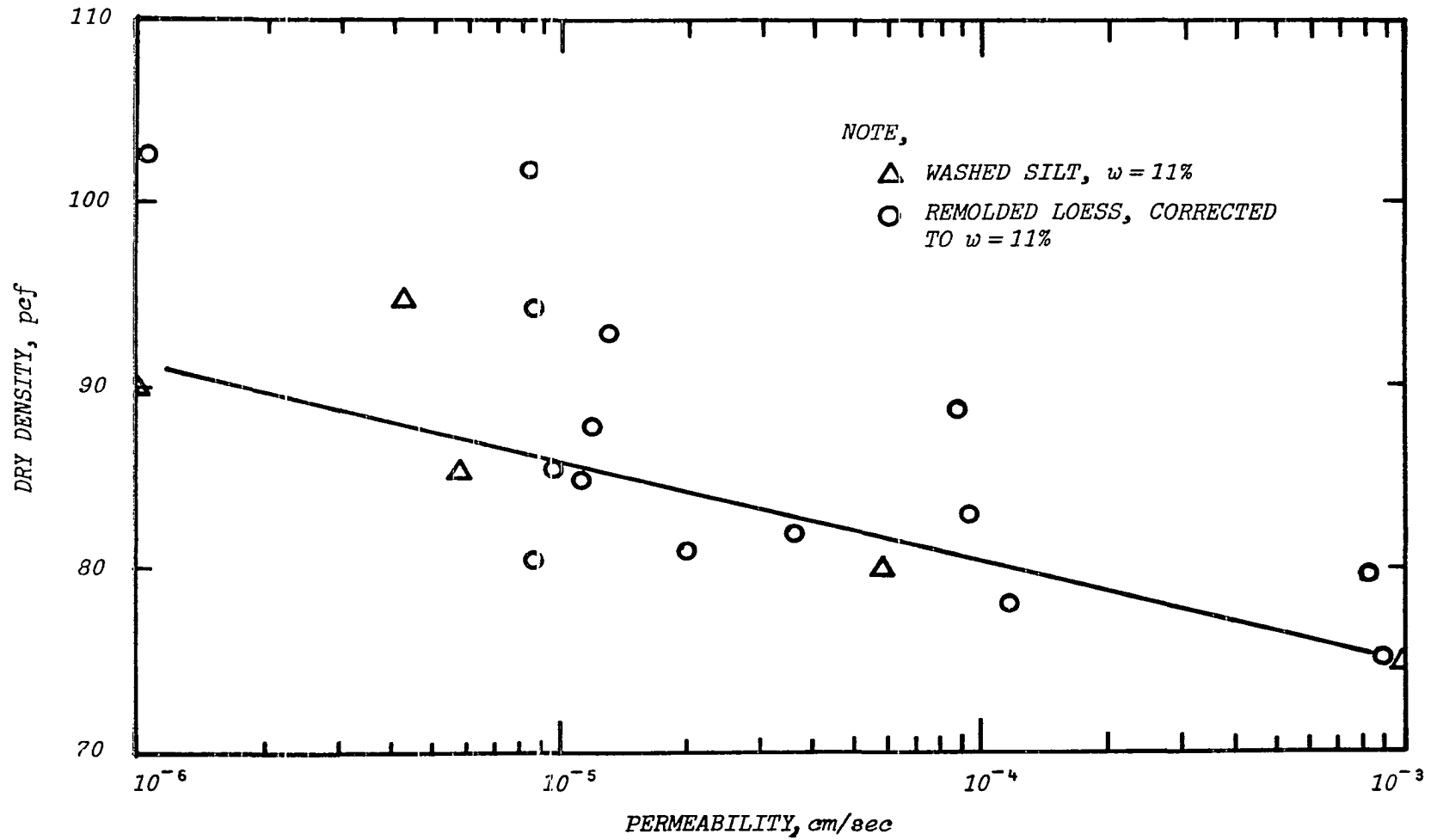


Figure 25 Density-Permeability for loess and silt.

permeability data is a crushing of silt grains during remolding. The estimated crushing stress for silt compacted to 89.2 pcf dry density is over 4,000,000 psi¹ which is high enough to crush the quartz of the silt. The silt with smaller grains would provide lower permeability values.

Permeability values from each of the various type tests were plotted in Figure 26 as dry density versus permeability. The boundaries shown are those defined originally by Holtz and Gibbs (1951). They classify samples which fell above boundary curve 1 as sandy loess, those below boundary curve 2 as clayey loess or reworked loess, and those in between the boundary lines as silty loess. All their permeability tests were for undisturbed natural loess and were conducted in a one-dimensional consolidation apparatus. When the friable Iowa loess permeability values were plotted in relation to the Holtz and Gibbs boundaries, most of the values were in the reworked zone with two exceptions. First the values for the undisturbed and hand carved samples fell within the undisturbed silty loess boundaries. Secondly, the dynamically compacted samples molded at low moisture contents fell within the boundary lines. This is as it should be.

¹Lambe and Whitman (1969) give a value for the actual contact area for sand as 0.0003 square inches per inch and the crushing strength of quartz as 200,000 psi.

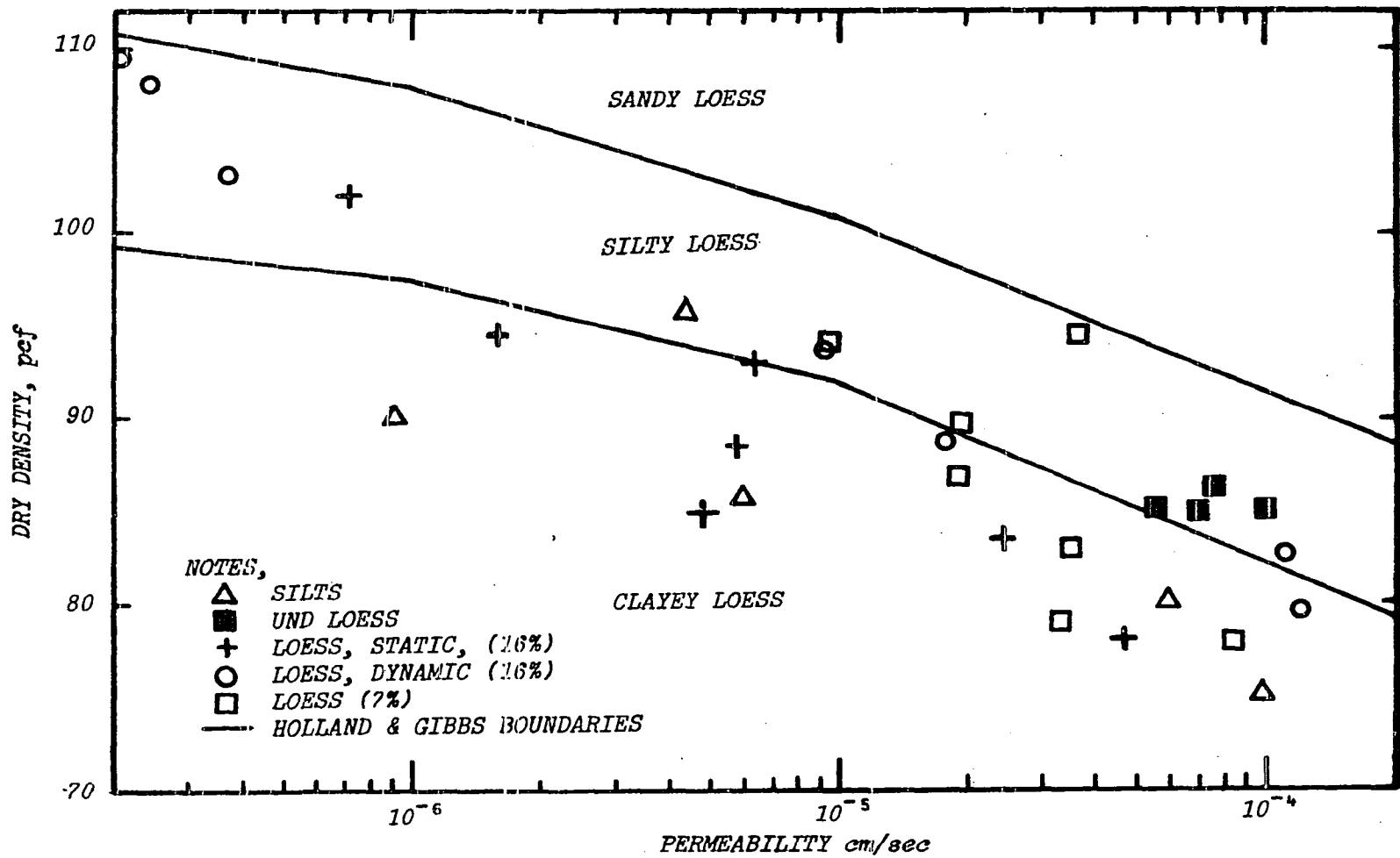


Figure 26 Density Permeability data with Holtz and Gibbs Boundaries.

"Remolded" loess values should fall in the "reworked" classification whereas undisturbed friable loess values should coincide with undisturbed values. One may conclude, however, that dynamically compacted samples result in permeability values which approximate those of undisturbed loess.

VI. VOID VOLUMES MEASURED BY MERCURY INJECTION

A. General

The mercury injection technique to determine the pore volume of undisturbed and remolded loess of different densities provides a means of comparing the change in pore volume caused by remolding. From this comparison a better understanding of the structure of loess, the influence of compaction and the relationship of void sizes to density was obtained.

B. Apparatus

The Mercury Injection apparatus is composed of essentially three components: the mercury displacement pump, the sample chamber, and the pressure manifold system. These components are shown schematically in Figure 27. For a more detailed treatment of the Shell Development Company Porosimeter see Purcell's (1949) article.

C. Procedure

The oven dried specimen is placed in a porosimeter chamber where a vacuum of 30 microns is then obtained. Twenty minutes is usually required to remove most of the entrapped air and moisture from the loess samples.

Mercury is introduced into the chamber completely surrounding the specimen. With the mercury level at the upper reference mark, and the chamber under 30 microns pressure,

the zero psia reading is taken. At this point the vacuum pump is stopped and 5 psia of nitrogen is applied to mercury in the chamber.

At predetermined increments of pressure, the nitrogen forces mercury into the loess sample. The volume of mercury forced into the specimen is recorded at these pressures up to the 2000 psia, the limit of this apparatus.

Upon removal of the loess sample each specimen was visually inspected. In no case was any sample crushed or damaged, however, the samples shrunk 0.8 percent by volume and each sample appeared to be completely saturated with mercury when broken apart.

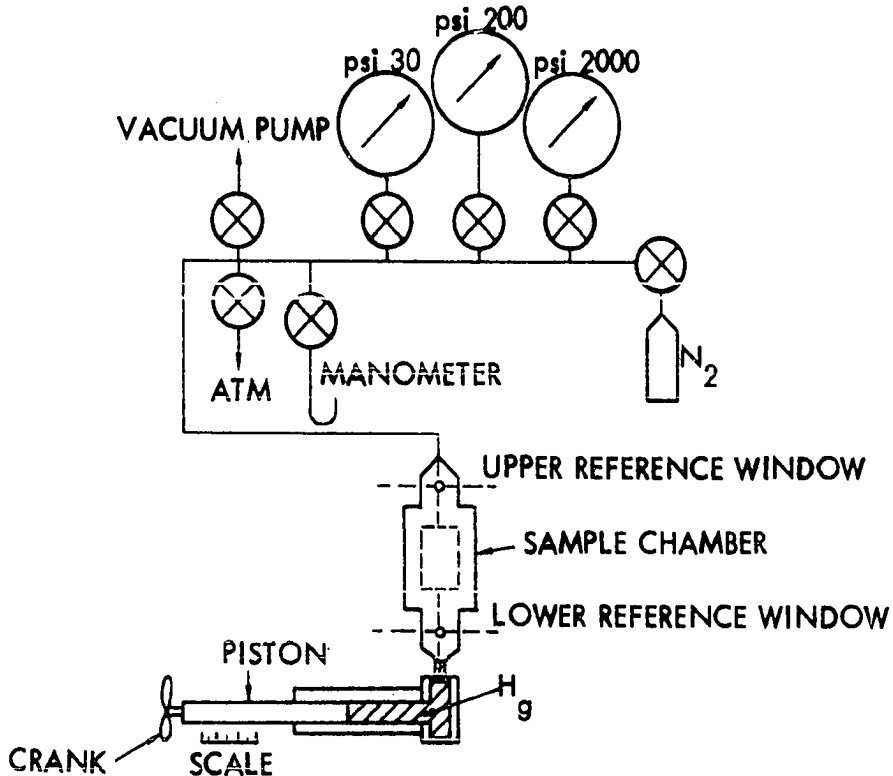


Figure 27 Schematic of shell type porosimeter.

D. Calculations

The loess specimens were weighed before and after drying to determine the molding moisture. The remolded cylinder specimens were measured and the total volume calculated. With the dry weight and total volume, a dry density for each specimen was determined.

For undisturbed samples of irregular shapes, the total volume of the specimen was determined by subtracting the volume of mercury introduced to the chamber, when the specimen was in it, from the total volume of the chamber. This initial reading was taken with a chamber pressure of 5 psia. It is assumed that at that pressure the mercury completely surrounds the specimen, filling all large surface voids but not filling the internal voids. Thus 5 psia was used as the zero datum for all tests.

The mercury volumes corresponding to the different pressures were corrected for mercury compressibility.

The 2000 psia pressure was used as the upper limit in the majority of the tests. However, a few tests were conducted at 1600 to 1800 psia and are so noted. The volume of mercury which filled the voids between 5 to 2000 psia was designated the total volume of voids.

The pressures were then converted to radius of pores by use of the Washburn Equation.

The volume of mercury injected into the sample per pressure/radius increments was divided by the total void volume and multiplied by 100 to obtain percent void volume per total void volume. This percent volume was plotted in incremental or accumulative volumes versus pressures or radius of voids.

E. Discussion of the Experimental Technique

To eliminate as many sources of possible error as practical, the following selections, corrections and techniques were used:

The selection of a contact angle and surface tension value was made after an extensive literature search. The values of 140° and 480 dynes/cm appear realistic values for loess. The values for sands and clays from Table 11 were averaged, and these values were used for loess.

By waiting 20 minutes for the pump down of the 30 micron vacuum and by oven drying for days at 105°C , most of the moisture and air were removed from the sample. The shrinkage due to oven drying of the loess was less than 1 percent by volume.

The effect of compressibility of the mercury was reduced by corrections.

A correction for the kinetic hysteresis effect was made by waiting until the mercury level stabilized before taking a reading.

Table 11. Contact angle and surface tension values¹

Authors	θ (degrees)	T (dynes/cm)	Materials tested
Ritter & Drake (1945)	140°	480	glass earth
Purcell (1949)	140°	480	sand
Winslow & Shapiro (1959)	130°	473	glass iron
Klock et al. (1968)	130°	473	sand
Diamond (1970)	139° 147°	484 484	clays
Sridharan et al. (1971)	137°	454	kaolin grundite blue clay

¹This Author used values of $\theta=140^\circ$ and $T=480$ dynes/cm, Diamond used 139° for kaolinite & illite.

There seems to be no solution to the problem of the inaccessible pore or the neck phenomenon. However, for loess with its near spherical and blocky grains, inaccessible pores may not be too significant. It is difficult to calculate the exact number of inaccessible pores in the cryptovoid range because of the variation in measuring the macrovoids and mesovoids, but it is probably less than 2 percent of the total void volume.

The selection of an appropriate lower reference datum caused considerable consternation. The normal reference for mercury injection of rocks is 5 psia pressure. However for loess with its larger voids, a notable difference in void, solid and total volumes were determined at a 0 psia datum as compared to the 5 psia datum. Calculations at the 0 psia datum reveal a large volume of surface voids (10 to 20 percent of total volume) in the 0 to 5 psia range. Figure 28 shows the porosities plotted versus density for data calculated from the 0 and 5 psia reference as well as data based on gross weight and volume measurements made on cylindrical samples. From this plot it appears that the 0 psia reference provides better porosity, density and volume values. However, the 5 psia reference, which does not seem to have as much initial variation as 0 psia, provides a more stable base. In either case, the general shape of the curves do not change. The 5 psia reference was used in this study.

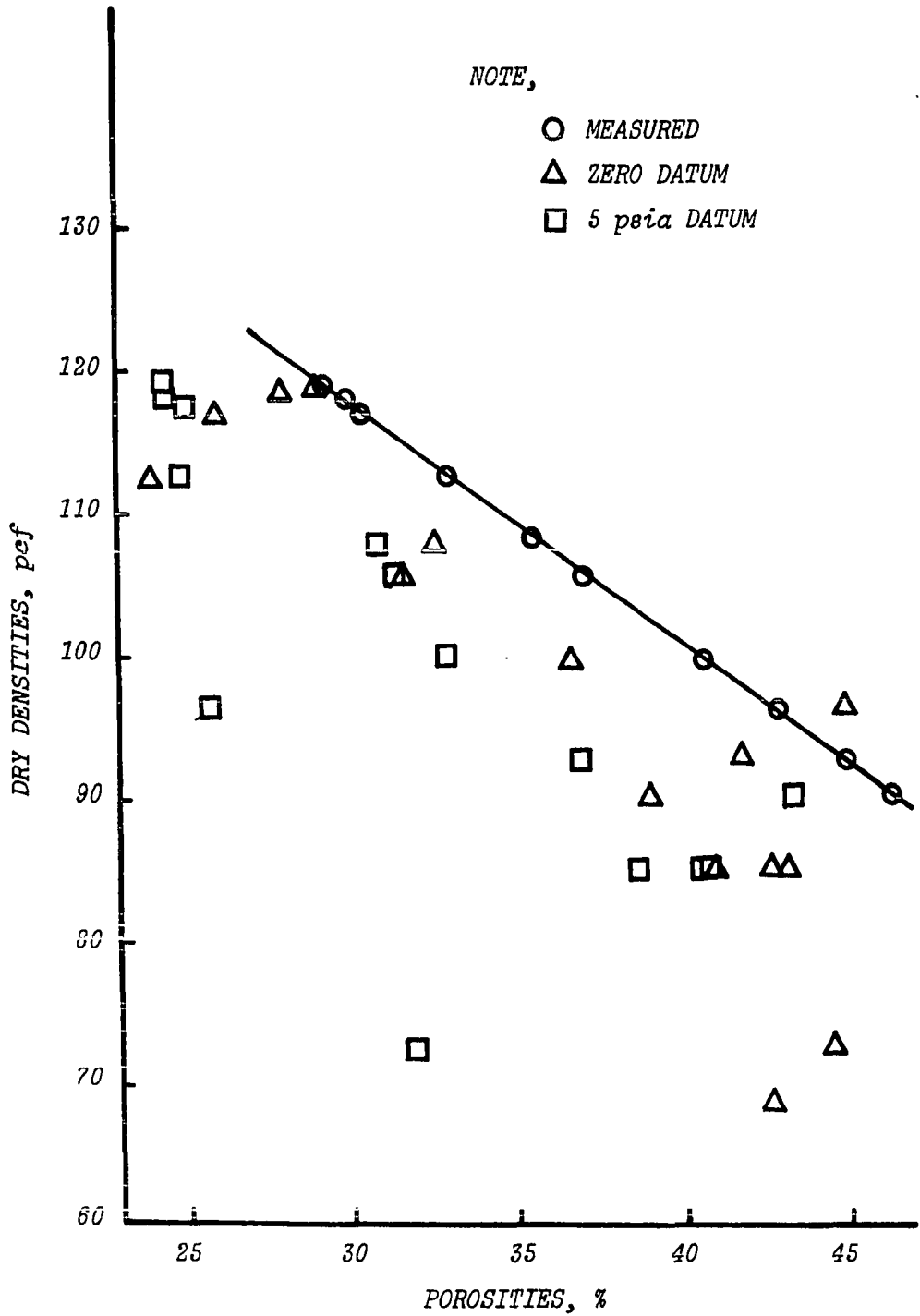


Figure 28 Comparison of 0 psia and 5 psia datum reference.

F. Discussion of Results

The comparison of the void volume of undisturbed loess with remolded loess at the same densities is shown in Figure 29. This comparison reveals a number of significant differences. First, the very fine macrovoids found in the undisturbed loess are partly eliminated by remolding. Secondly, a rearrangement of pore volume distribution caused by remolding is evident. The dominant peak for the remolded loess represents 50 percent of the pore volume, whereas the dominant peak for the undisturbed loess represents only 30 percent of the pore volume. Lastly, the maximum pore volume peak of the loess is increased from 13 to 20 percent in volume and the pore radius from 2.7×10^{-4} to 5.3×10^{-4} by remolding. In general, the undisturbed loess has a more uniform distribution of pore volume. The engineering significances of the redistribution of voids caused by remolding is an increase in permeability.

A comparison of incremental void volumes for a series of remolded loess samples of various densities also shows patterns of eliminating larger voids first. However this comparison indicates a lack of dramatic change in the lower density range even though there is a significant change in the higher density range, Figure 30.

NOTE,

UPPER LIMIT 1800 psia

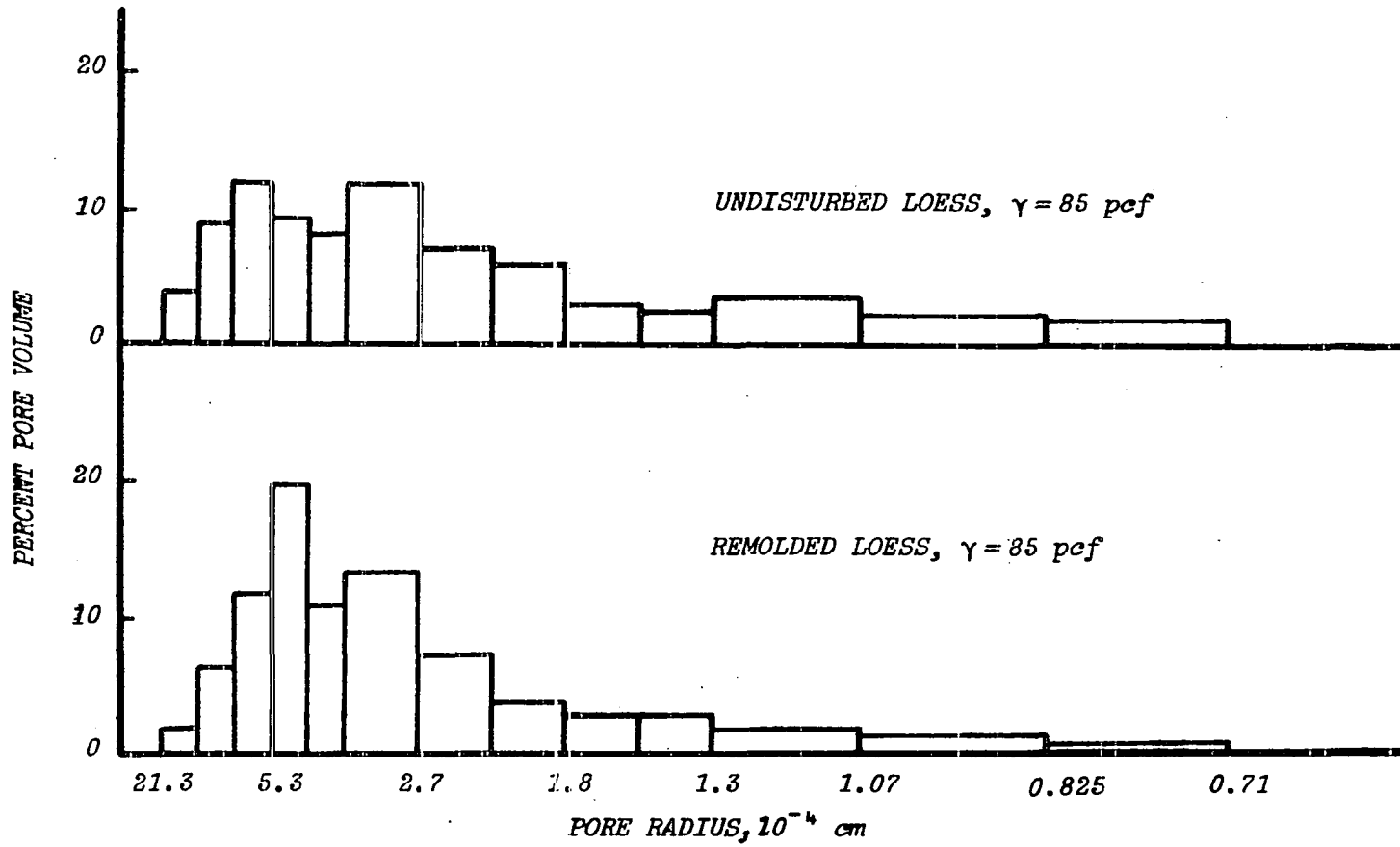


Figure 29 Pore volume distribution comparison of UND and REM loess.

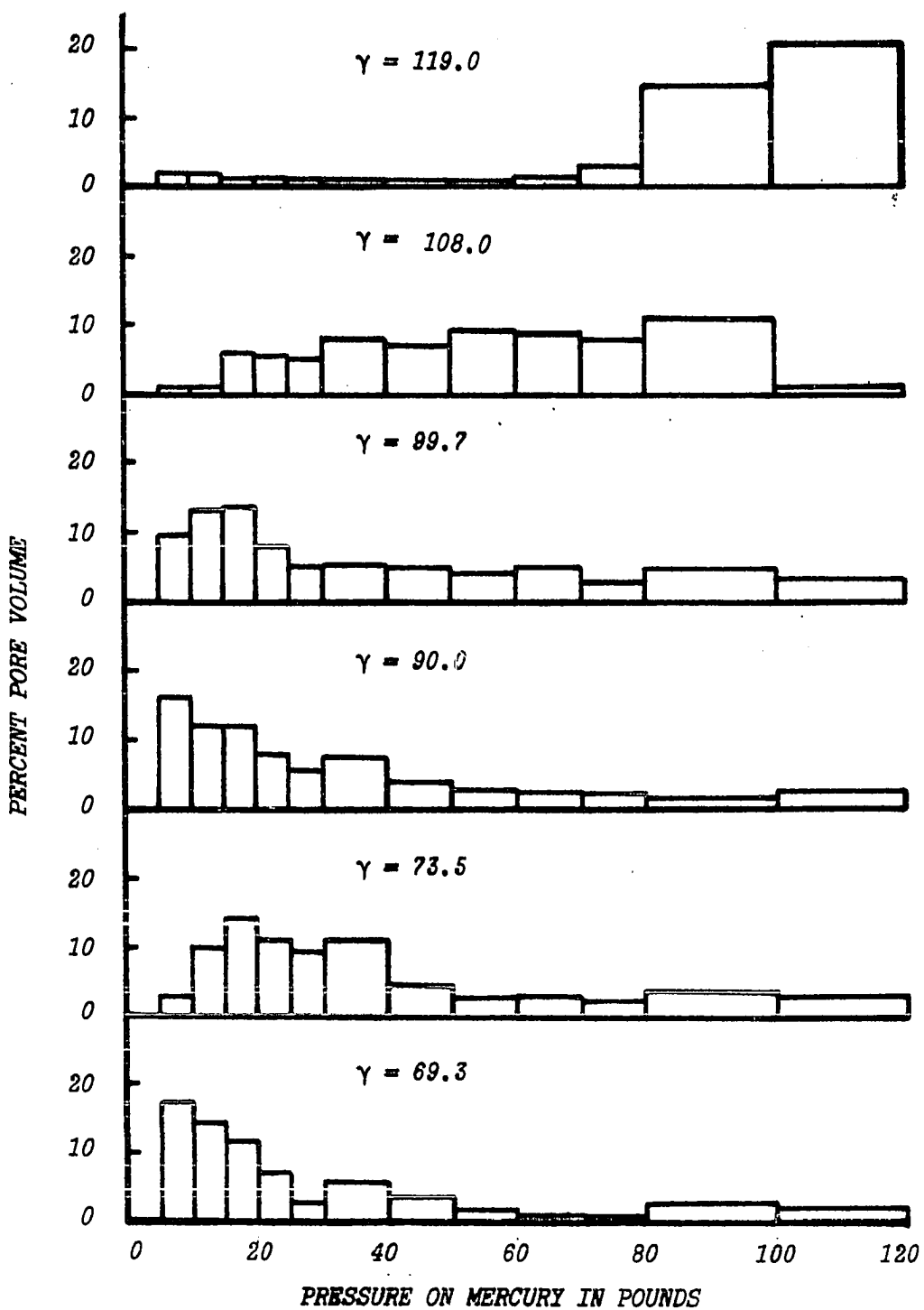


Figure 30 Pore volume distribution of loess remolded to different densities.

A comparison of cumulative void volume for a series of remolded loess samples of various densities shows an interesting change in void distribution. Figure 31 clearly discloses a pattern in which the voids are eliminated in order of largest to smallest as the density is increased. This is reasonable since the larger voids formed by the arching of individual grains would be the weakest structural link of the soil system. This is seen from rudimentary considerations of the larger moments developed in larger arches.

For low density range, the remolded loess samples disclose relatively little differences in void distributions to density changes, (Figure 30). In the high density ranges a small change in density generates a relatively large void distribution change. This behavior is attributed to the limitation of mercury injection to measure the mesovoids and macrovoids and to the variable nature of the loess structure at low densities.

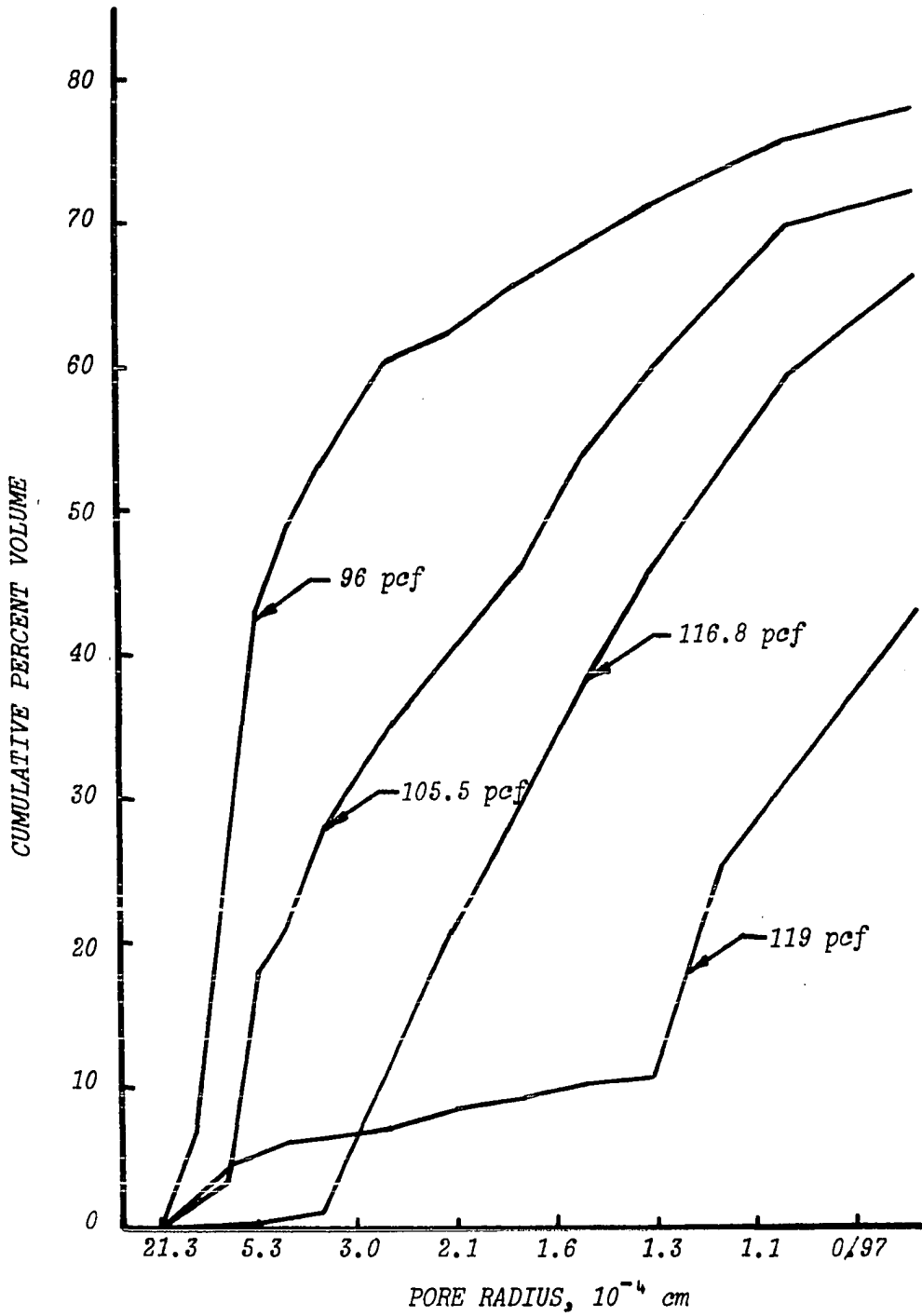


Figure 31 Cumulative pore volumes of loess remolded to different densities.

VII. STRUCTURE

A common method of describing a soil for engineering purposes is the grain size distribution curve obtained from sieve and hydrometer analyses. This data compared to void size distribution data provides an excellent way to quantitatively describe the soil structure. By converting the amount of mercury injected into the voids into equivalent diameters and accumulating the volume filled, the void size distribution curve can be compared to the grain size distribution curve on a volume basis, Figure 32. However, to make this comparison, one assumes the specific gravity of the loess particles are constant in all size ranges. It is realized that this assumption probably does not hold in the clay size range and the lower portion of curve 3 in Figure 32 should shift. However, the upper portion and center of the curve will probably move very little.

Figure 32 shows the void size distribution curves for remolded and undisturbed loess plotted with the grain size distribution curve for loess. The similarity of shapes of the three curves is clear. Evidently the particle size and shape has a significant influence on the size of the voids.

Although the void volume distributions are difficult to obtain, they should serve as excellent indicators of any change in structure or fabric when compared to their respective grain size distributions.

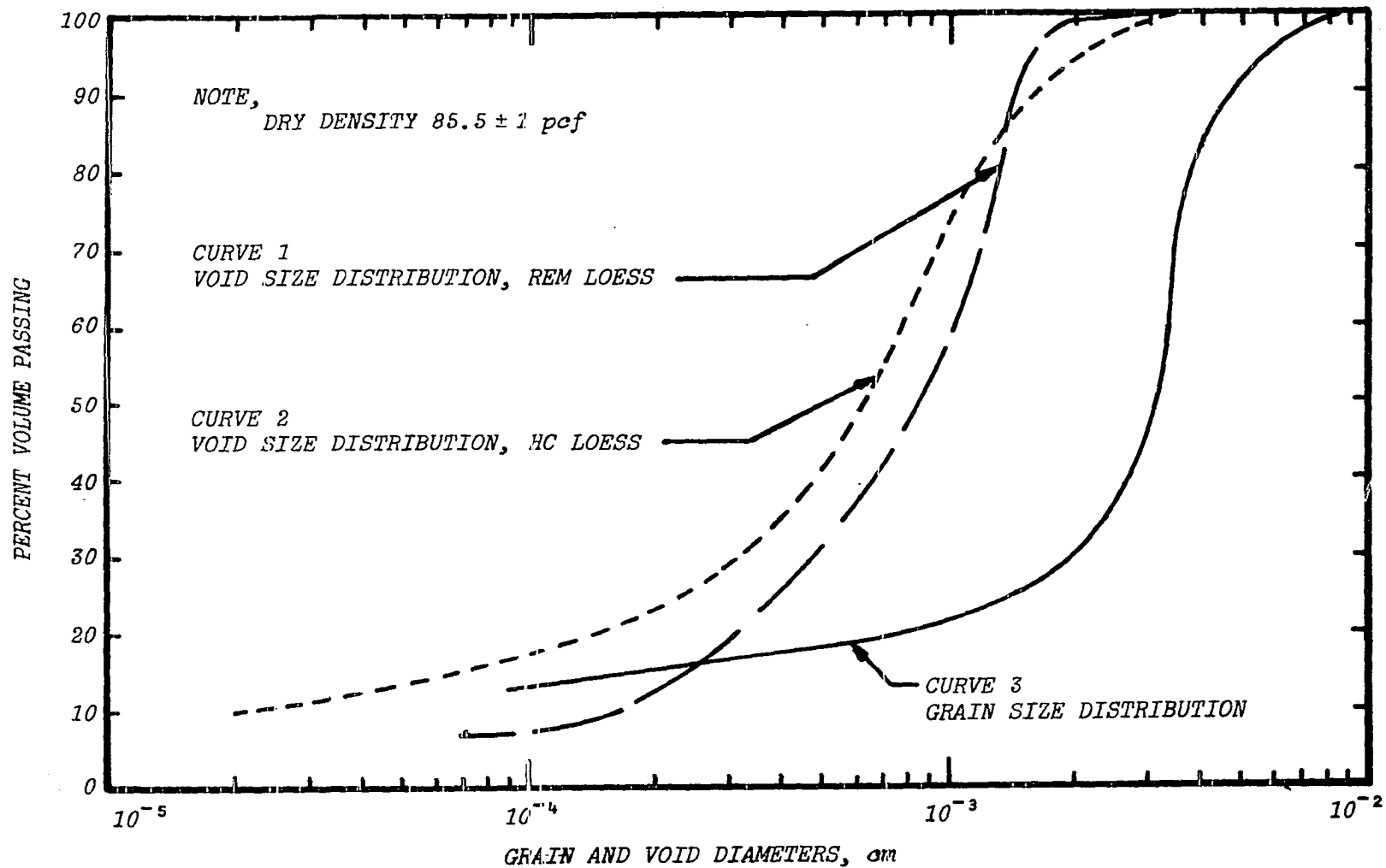


Figure 32 Comparison of grain size and void size distribution curves.

A conceptual approach to describe soil structure is to use the distribution curves in Figure 33 as boundaries and to establish structural zones, Table 12. The boundaries are based on physical features of loess, the first boundary is the void size distribution curve obtained for maximum laboratory density without crushing the primary particles. The second boundary is the void size distribution curve for UND loess. The third boundary is the grain size distribution curve for loess. Zone A represents an area above the maximum laboratory density for loess. To attempt higher densities will probably cause crushing of primary particles. Any void size distribution curve falling in this zone will be classed as an altered particle structure. Zone B represents an area of relatively dense loess (normally higher than the undisturbed field density) in which primary particles are in contact with each other. Any void size distribution curve falling in Zone B will be designated a particulate structure. Zone C represents an area in which many of the primary particles are joined together forming composite particles and two classes of voids. The composite void formed between composite particles, and the particulate void formed between primary particles forms the different void classes. The large composite voids characterize the structure in this zone.

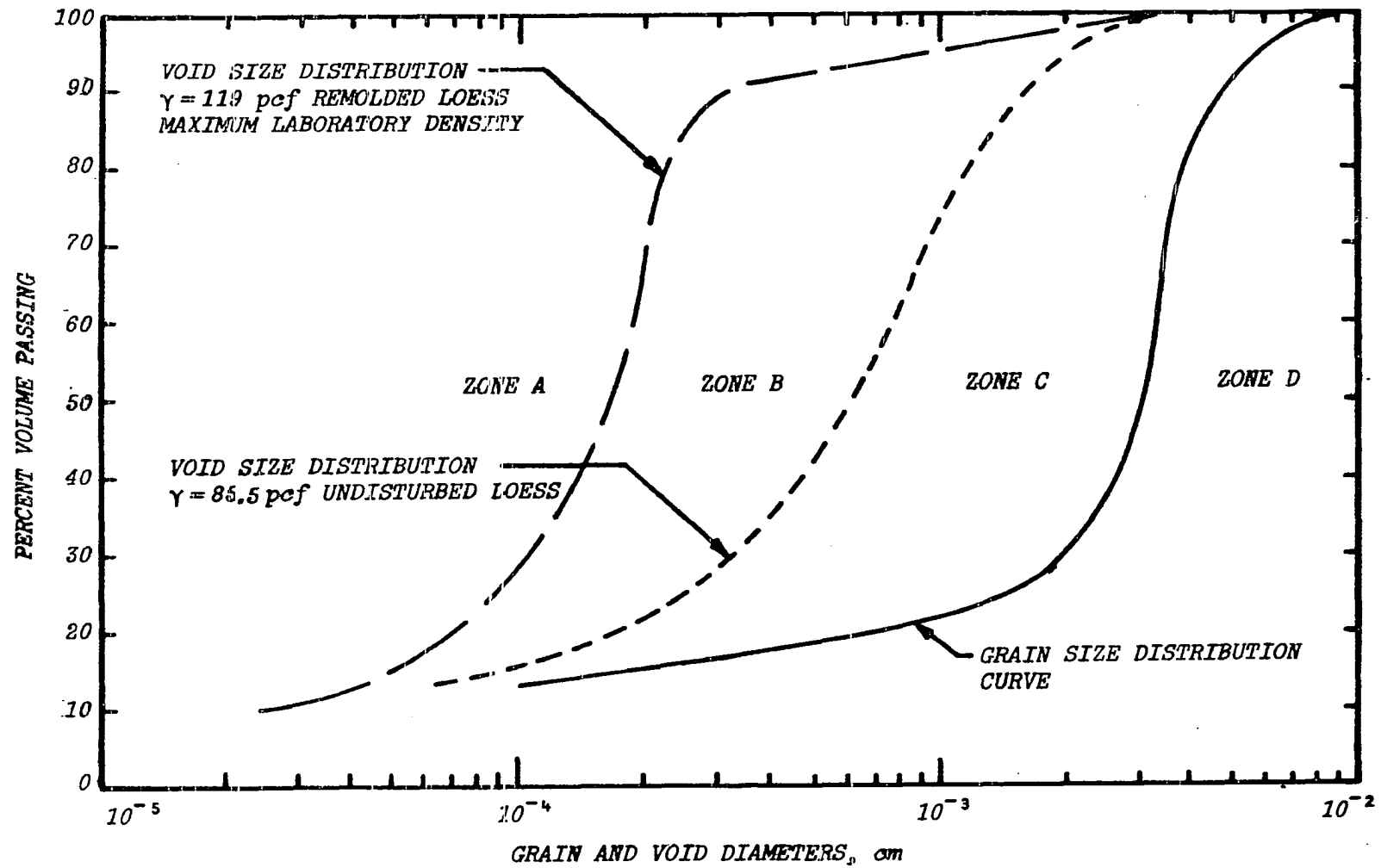
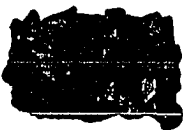


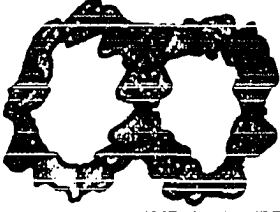


Figure 33 Void and grain size distribution zones.

Table 12. Type structure and corresponding photograph references

Zone	Type structure	Sketch	Photograph references
A	Altered particle		Figure 34 ¹
B	Particulate		Figure 35
C	Composite		Figure 36
D	Honeycomb		Figure 37

¹This photograph is actually of a structure of loess in the upper portion of Zone B, but provides the massive appearance of the type structure defined in Zone A.

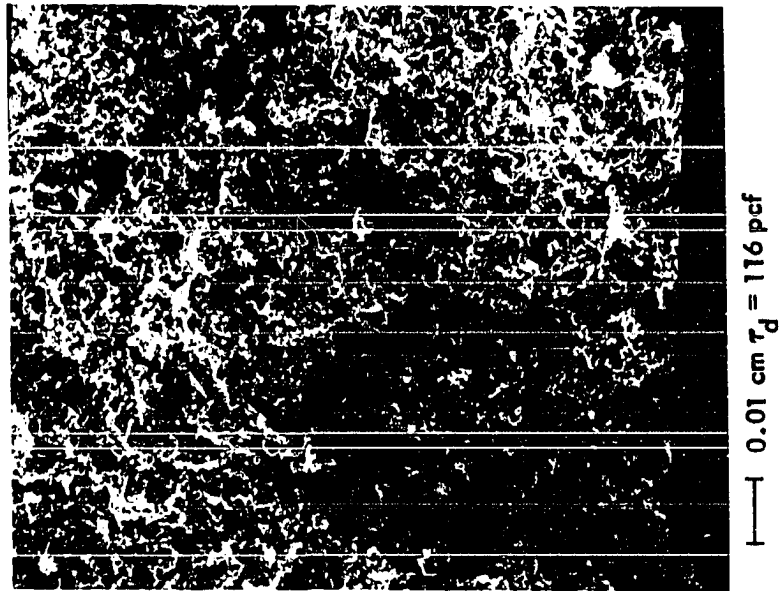


Figure 34 SEM photograph of REM loess at 116 pcf dry density and 200x magnification.

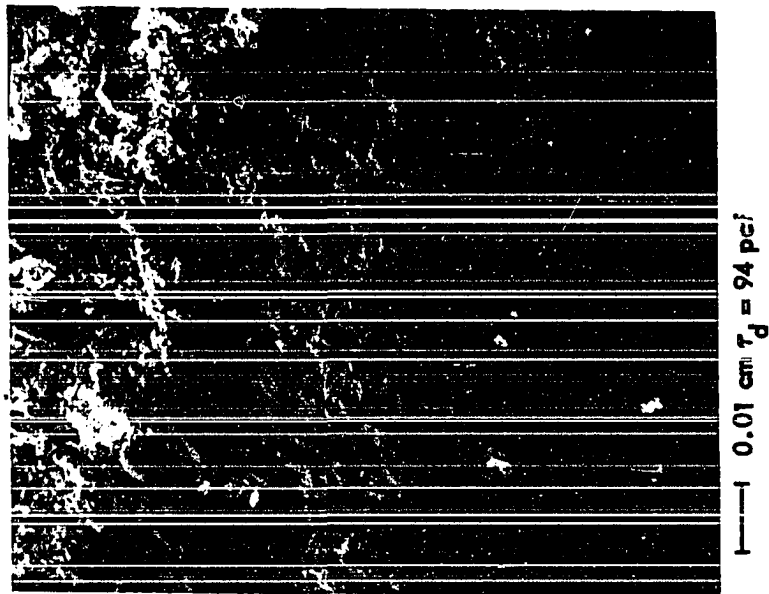


Figure 35 SEM photograph of REM loess at 94 pcf dry density and 200x magnification.

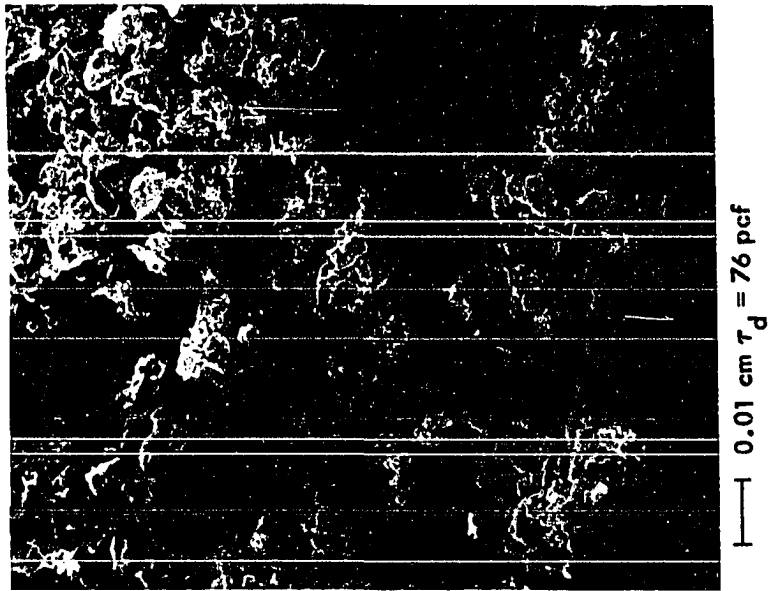


Figure 36 SEM photograph of REM loess at 76 pcf density and 200x magnification.

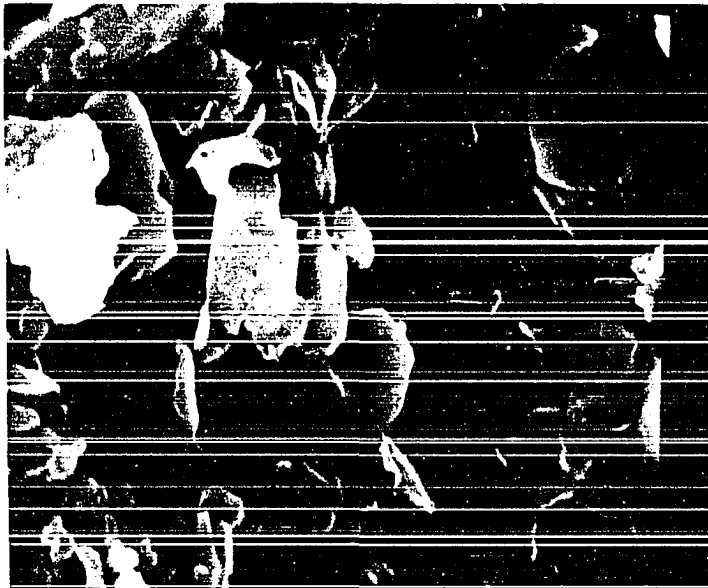


Figure 37 SEM photograph of clay from loess settled out of distilled water at 10,000x magnification.

Any void size distribution curve falling in this zone will be called a composite structure. And lastly, Zone D represents the loosest structure where the voids are larger than their adjacent grains and probably could only be formed by extreme bridging and arching of flat particles. Any void size distribution curve falling in this area will be labelled honeycomb structure.

It can be observed in the SEM photographs that remolded loess forms two distinct structures, the particulate (120-85 pcf density) and the composite (85-65 pcf density), shown in Figures 35 and 36 respectively. The other two structure classes are more theoretical or boundary-type structures and will probably never be obtained in loess.

Although the zones clearly show the structure, a method was needed to quantify the structure numerically. A grain size to void size ratio was developed for three size classes, 50, 80 and 90 percent passing respectively. This ratio is identified as "distribution ratio".

The distribution ratio was initially conceived while working on the soil classification system (Appendix A), modified while defining the types of structural zones (Table 12), and developed as an attempt to quantify the structure of loess. For example, enter Figure 32 at 50 percent passing and read across the page to the void size distribution curve for hand carved (HC) loess. Then read down to determine the

void diameter, which is 0.00062 cm. Continue across the figure at 50 percent passing to the grain size distribution curve and read down to determine the grain diameter, which is 0.0031 cm. By dividing the grain diameter 0.0031 cm by the void diameter of 0.00062 cm, the distribution ratio of 5.0 is obtained. The distribution ratio is defined as the ratio of the particle diameter at the 50 percent passing size divided by the diameter of the voids at 50 percent filled by mercury. (If mercury injection is not used to determine the void sizes, then the void diameter at which 50 percent of the voids are larger and 50 percent are smaller will be used). The particle and void size at 50 percent was selected over the 80 and 90 percent sizes because it seemed to be easier to determine and it seemed to have less scatter when plotted with the other two sizes, Figure 38.

The distribution ratio for HC loess is 5.00 compared to 3.65 for loess remolded to equivalent dry density. At this 85 pcf dry density and 10 percent saturation, the unconfined compressive strength for HC loess is 7.0 psi and for REM loess is 2.7 psi shown in Figures 10 and 11 respectively. Since the density and saturation are the same for the HC and REM loess, part of the difference in strengths may be attributed to the structure. Figure 16 shows the relationship of unconfined compressive strengths to density.

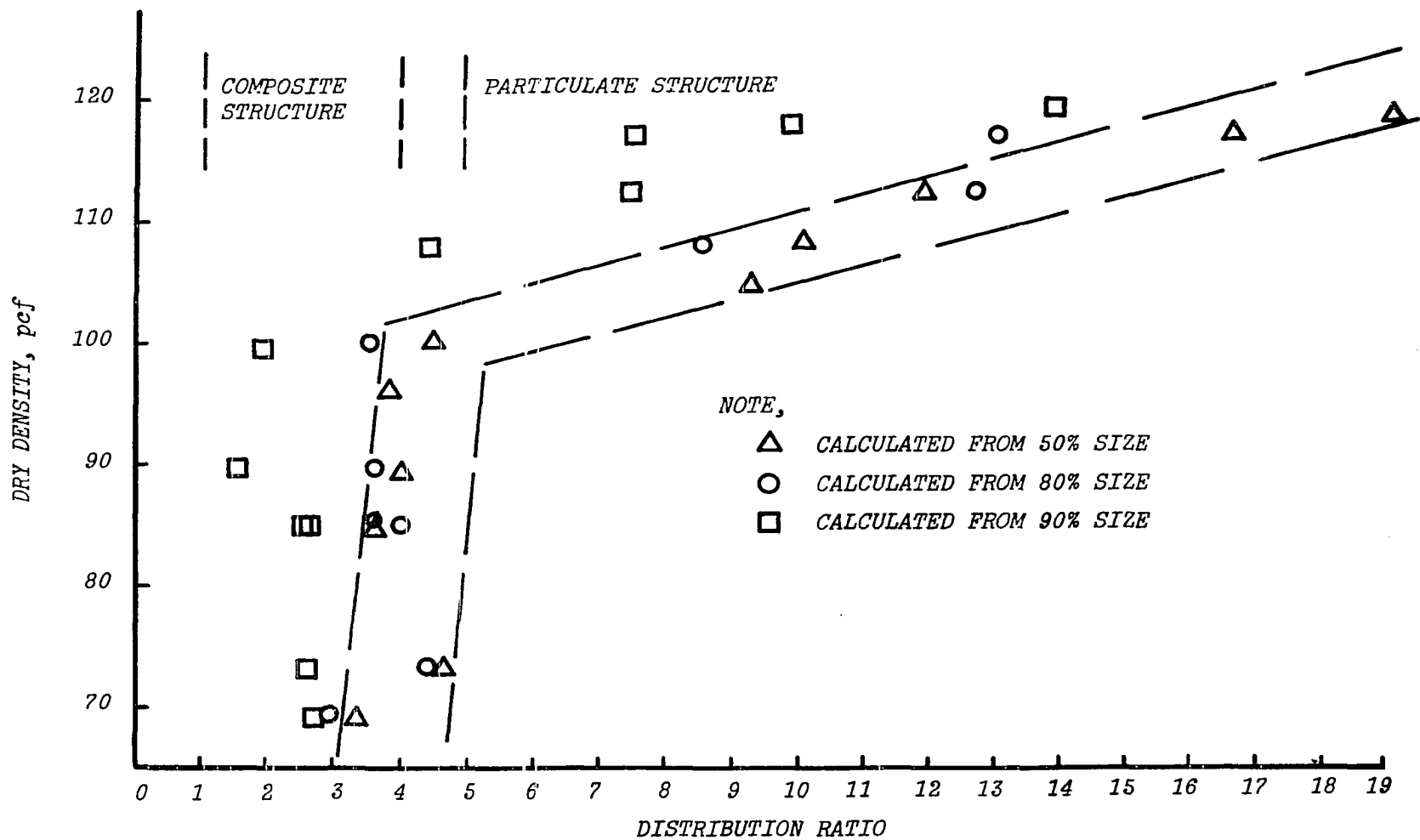


Figure 38 Distribution ratio and dry density curve.

If this is the case, then the distribution ratio may be used to correlate structure to strength.

For loess, the distribution ratio of 5 seems to be the boundary between composite structure and particulate structure, Figure 38 and 39. And all ratios higher than 5 probably indicate a type structure that would indicate an adequate foundation material. All ratios lower than 5 indicates an inadequate foundation material. The curve in Figure 38 is bipartite and differentiates between the composite and particulate structure. However, the boundary between the two type structures is at approximately 100 pcf density which is higher than the chosen 85 pcf density boundary between Zones B and C. In the particulate structure range the distribution ratio is a function of density, but in the composite structure range the ratio is independent of density. By plotting the distribution ratio versus permeability, the ratio in the particulate range is a function of permeability, whereas in the composite range, there is little correlation. The lack of mercury injection data in the macrovoid range places a significant limitation on the interpretation of the distribution ratio correlations. However, the distribution ratio concept is considered a good method of quantitatively defining the soil structure.

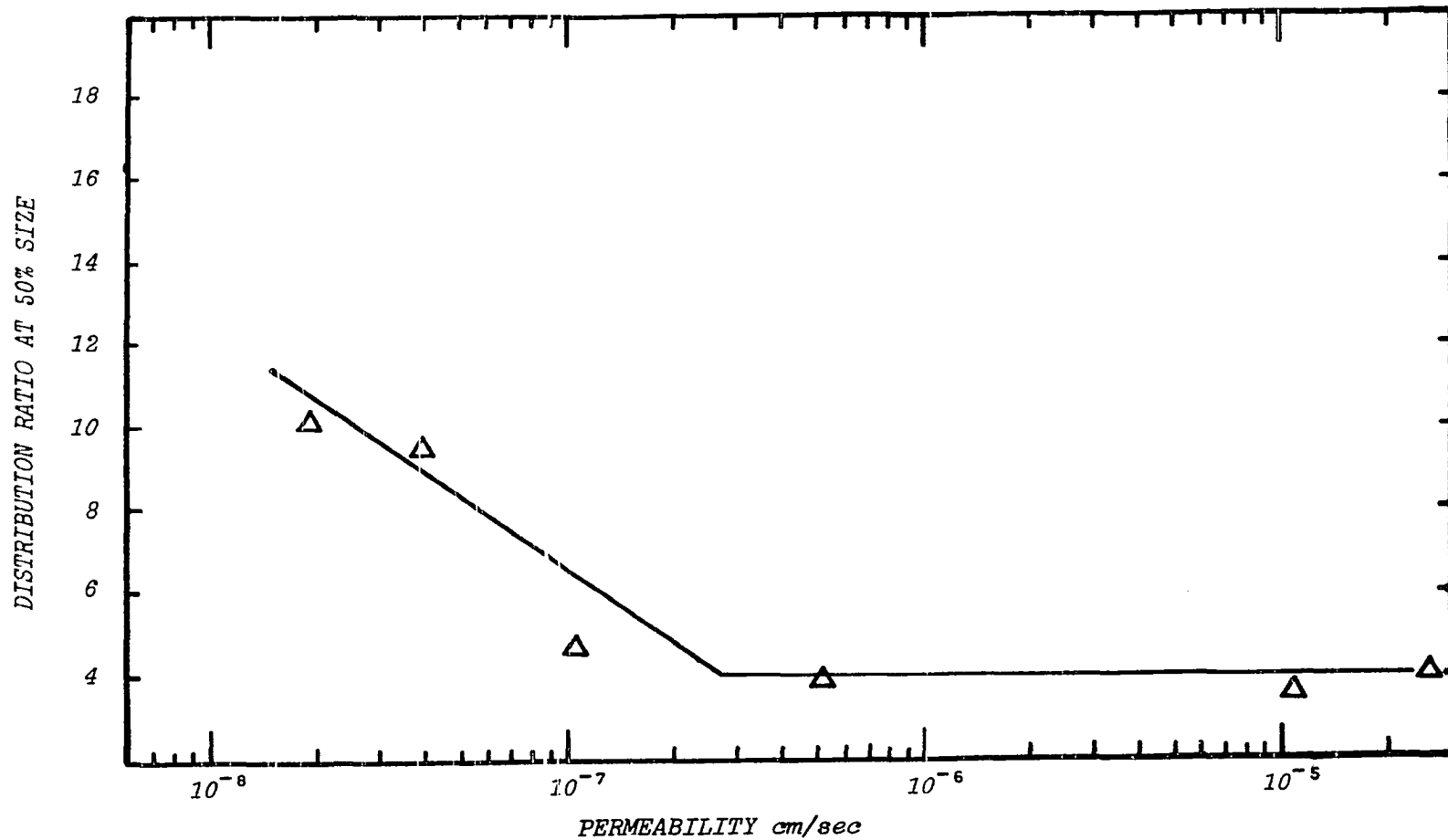


Figure 39 Distribution ratio and permeability.

When the mercury injection technique of measuring the macrovoids is improved, the correlation of density, permeability and unconfined compressive strength to distribution ratio in the composite structure range should be obtainable.

VIII. DISCUSSION

A parameter named "distribution ratio" which quantifies the soil structure was developed. For loess the distribution ratio smaller than 5 denotes poor strength values, while a ratio larger than 5 indicates good strength values. The friable Iowa loess forms two basic types of structures when remolded. First, loess forms a composite structure characterized by large variable size voids associated with composite particles. This structure which corresponds to distribution ratios less than 5 is formed in the 69-85 pcf dry density range. The scatter of the permeability and mercury injection data in this range indicates the variable nature of this type structure. Loess also shows an extreme sensitivity to any change in molding moisture. Due to the large voids and consequently high permeability, loess in the composite structure has good internal drainage, facilitating rapid intake of moisture. This increase of moisture reduces both apparent and true cohesive strengths causing this density loess to become a structurally undesirable foundation material. The second basic structure which corresponds to distribution ratios more than 5 is a particulate structure in the dry density range of 95 pcf and above. The voids of this type structure are formed between individual particles and this void size is governed by the size of the neighboring grains. This type structure is characterized by restrictive

internal drainage, by a high degree of clay bonding and by high surface tension induced strengths. Although increased moisture decreases both types of cohesion, the restrictive internal drainage nature of this structure tends to keep the moisture out of this density loess. With high strengths and minimum collapsible voids, loess with a particulate type structure is considered a good foundation material.

For clayey soil it may be possible to form three basic type structures. First, a honeycomb structure in which the distribution ratio may be less than one. That is, the voids formed may be larger than the adjacent particles. This type of structure is of significant interest because it exhibits extreme settlement characteristics. Therefore, any soil with a distribution ratio of less than one is even more undesirable as a foundation material. Secondly, a composite structure similar to the composite structure of loess may develop with characteristics like the composite structure of loessial soils. And lastly, the particulate structure is formed where the clay plates are face to face.

During remolding the voids of the loess are reduced in size in order of the largest voids first. Since the larger voids are composite type voids, the loess can be reduced in total volume by breaking minimum clay bonds; consequently, small compactive efforts are needed. It appears that clay bonding contributes significant strengths to undisturbed and

high density remolded loess but contributes little strength to the low density remolded loess. However, in the particulate structure range the smaller voids are more difficult to eliminate because of the increased number of clay bonds which have to be broken. This increases the required compactive energy. Any additional moisture decreases the clay bonding strength, reducing the needed compactive energy. However, too much moisture produces pore pressures which increase the compactive effort. This emphasizes the importance of compaction at optimum moisture content under proper compactive effort; otherwise slickensides may develop.

Moisture greatly affects the stability or strength of loess and this moisture may be categorized into three classes. The molecular moisture which is adsorbed by the clay causing a loss of true cohesive strength forms the initial class. The capillary moisture which forms the menisci at the contact points constitutes the next class. The apparent cohesive strength decreases with increased moisture up to menisci coalescence. Lastly, the gravitational water which fills the large voids adding total weight to soil mass may cause a condition where the loess may fail from its own weight. A simple test will clearly demonstrate that undisturbed loess will collapse on saturation. When a dry undisturbed sample is placed on a porous stone which is slowly wetted, the sample fails under its own

weight. Each type moisture acts on the soil mass in the priority order of molecular, capillary and gravitational water respectively, Figure 40.

For different porosities the degree of saturation that is adsorbed by the clay is shown in Table 13. These saturation values denote the boundary between the molecular moisture zone and the overlap zone shown in Figure 40.

Table 13 Moisture adsorbed by the clay

Porosity percent	Density pcf	Saturation percent
47.64	88.23	3.84
37.54	101.87	5.35
30.19	117.63	8.09
25.95	124.77	10.00

The permeability of loess is primarily a function of density and structure. The composite structure (low density) produces higher permeabilities, while the particulate structure (high densities) produces low permeabilities.

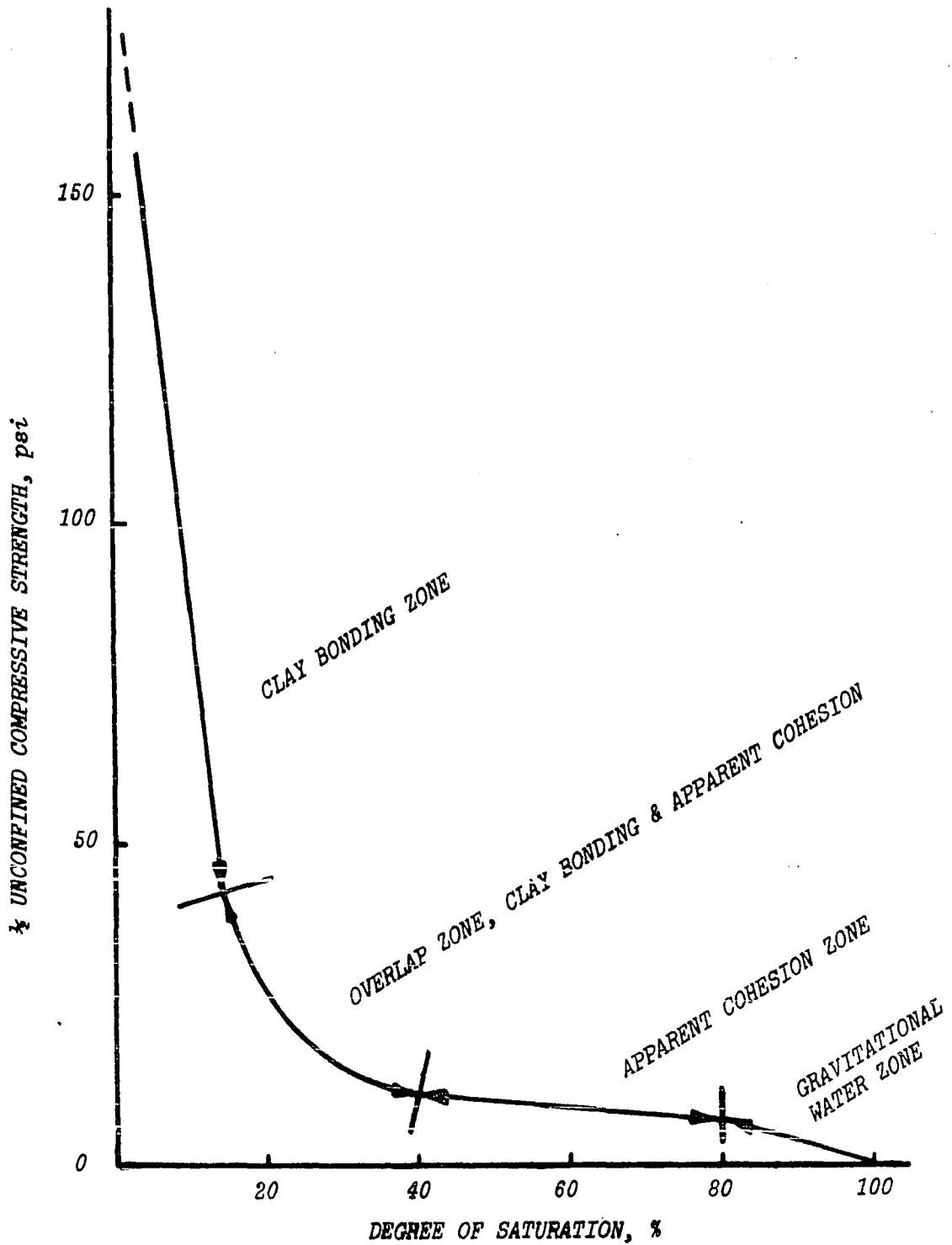


Figure 40 Theoretical moisture curve (based on the general shape of Lutton's, 1969, curve).

A small amount of moisture present at molding causes a composite (flocculated) structure, and high molding moisture causes a particulate (dispersed) structure which produces low and high permeabilities respectively. The friable Iowa loess permeability values are comparable to the Nebraska loess permeability values of Holtz and Gibbs (1951).

Although the mercury injection technique provides good comparative data in the microvoids, ultramicrovoids and cryptovoids ranges, it does not provide adequate data in the macrovoids and mesovoids ranges. The macrovoids are the most significant voids in determining permeability values and for comparing void configurations for different structures. To improve the mercury injection technique of soil in the macrovoids range will require a more sensitive pressure measuring device in the 0.1 psi to 10 psi range. A second alternative is to supplement the existing mercury injection data with macrovoids data measured from the SEM photographs. However, it was found to be extremely difficult to relate the two dimensional scaled SEM values to the mercury injection data.

The theoretical apparent cohesion equation provides a good method of predicting apparent cohesion in fine grained soils. This apparent cohesion contributes significantly to the total cohesion in silts and loess type soils. For fine soil with an effective radius of 0.0002 cm and a porosity of

26 percent, apparent cohesive values of 18-22 psi were determined in the 0-30 percent saturation range. This equation with proper adjustments may be used over a range of porosities from 26.9 to 47.5 percent.

Apparent cohesion plays an important role in the design of retaining wall and the determination of maximum slopes in stability work. The change in apparent cohesion with corresponding change in moisture content is evident; however, a simple mathematical relationship which could predict the amount of apparent cohesion in terms of saturation and porosities was needed. The apparent cohesion equation developed in Appendix C provides a simple and fairly accurate equation that can be used to calculate apparent cohesion in the zero to 80 percent saturation range for fine grained soils. Jumikis (1962) lists an increase in moisture as a primary contributing factor in slope failure because of the decrease in total cohesion due to this increased moisture. Although the apparent cohesion is only one of the elements which contributes to this total cohesion, an equation which allows the designer to predict the amount of apparent cohesion is extremely important.

IX. CONCLUSIONS

1. The distribution ratio serves as an accurate indicator of any change in structure of loess.
2. Remolded loess forms two basic types of structure, particulate at high densities/high distribution ratios and composite at low densities/low distribution ratios.
3. At 85 pcf dry density (composite structure) the q_u strength of remolded loess is approximately equal to the q_u strength of silt and the cohesion developed from clay bonding does not become a contributing factor until higher densities (particulate structure) are obtained.
4. Clay bonding is the dominant cohesive force in a particulate structured loess.
5. Apparent cohesion is the dominant cohesive force in a composite structured loess.
6. Clay bonding in loess is a function of density and moisture, increasing as density increases and decreasing as moisture increases.
7. The developed theoretical apparent cohesion equation provides a good method to predict apparent cohesion in fine grained soils. This apparent cohesion contributes significantly to the total cohesion in silts and loess type soils.
8. The larger the grains the smaller the cohesive force obtained from surface tension with 0.003 cm radius, the

boundary where the grains begin to act like flat plates.

9. The smaller the grains the more sensitive the apparent cohesive force is to moisture changes.

10. The apparent cohesive strength of loess decreases with increased moisture up to menisci coalescence at which time it becomes zero.

11. Moisture greatly affects the stability of loess slopes, and this moisture may be categorized into three classes, molecular, capillary and gravitational.

12. Low molding moisture causes a composite structure with relatively high permeability while high molding moisture causes a particulate structure of relatively low permeabilities.

13. Friable loess shows a decrease in permeability with an increase in molding moisture.

14. Permeability for low density remolded loess sample exhibits extreme scatter when plotted because of the variable nature of the composite structure.

15. At equal densities the dynamically compacted sample produces higher permeability values than the statically compacted samples.

16. The permeability of loess is primarily a function of density and structure.

17. The friable Iowa loess permeability values are comparable to the Nebraska loess permeability values of Holtz

and Gibbs (1951).

18. The qu strength of the 85 pcf density undisturbed loess was found to be greater than the 85 pcf density remolded loess.

19. Undisturbed loess has a more uniform distribution of pore volume than remolded loess which clearly indicates the effect of remolding.

20. At each increment of compactive effort, the largest void available in the soil structure is eliminated before the next smaller sizes are collapsed.

21. Although the mercury injection technique provides good comparative data in the microvoids, ultramicrovoids and cryptovoid ranges, it does not provide adequate data in the macrovoids and mesovoids range.

22. There is a need for a mercury injection apparatus which is capable of measuring macrovoids and mesovoids of soils.

X. SUGGESTION FOR FURTHER RESEARCH

A. Mercury Injection Apparatus for Soils

There is a need for a mercury injection apparatus which is capable of measuring macrovoids of soils. This new apparatus should have a pressure gage which is sensitive enough to measure low pressure in the range of 0.1 to 1.0 psia. The low psia is needed for the large composite voids of low density loessial soils. A chamber-sample holder large enough to hold a Harvard Miniature sample is recommended.

B. Soil Structure Study

The variation of soil structure may be determined by mercury injection. It is anticipated that the soil structure will differ with changing soil types, molding moisture, density and compactive effort. The structure should also vary within one soil group with density and moisture changes. Any change in soil structure should be clearly shown in a corresponding change in void size distribution. With this additional void size distribution data, a better correlation of the distribution ratio and soil parameter could be made. Therefore a variety of soils should be studied simultaneously.

C. Correlation of Pore Size Distribution Data to Permeability Values

With a complete range of pore size distribution data available, a correlation between the pores and permeabilities

should be obtainable. Marshall (1958), Millington and Quirk (1959) and Purcell (1949) developed equations where permeability could be calculated from pore size distribution data. The primary advantage of being able to determine permeabilities from pore size distribution data is that only relatively small size samples are required. Also an irregularly shaped sample can be intruded with mercury with the same accuracy as more regularly shaped samples. The mercury injection determined pore size distribution data then could be used in a Marshall type equation to calculate undisturbed permeability values.

D. Soil Classification from SEM Photographs

As the different type soils are tested in the ERI Laboratory, a 200x, 500x, 1000x and 5000x series of photographs should be taken of typical undisturbed samples at some reference depth and orientation. Probably the best reference depth would be the average footing depth for Iowa. When an adequate number of photographs and related soil parameters are obtained, a correlation between classification number and soil parameter can be made.

XI. ACKNOWLEDGMENTS

I wish to express my sincere appreciation to my major professors, Turgut Demirel and Robert A. Lohnes, for their leadership and devoted interest in my graduate program. I extend many thanks to all the members of my graduate committee for their help. This blend of talent provided the responsive support required for me to complete my task.

My appreciation and thanks to Janie for her patience, understanding and computer help.

My thanks to Colonel Ernest D. Peixotto, the Director of the Waterway Experiment Station, for the use of their Scanning Electron Microscope and the support provided by the Station's Technical Library.

The funding for the experimental work was provided by the United States Army Research Office Durham, Environmental Science Division, under Grant No. DA-ARO-D-31-124-G1141 and National Science Foundation Grant GK-26423.

Credit is also extended to my many Lieutenants who fought well in the data collection battle. Bob Hamilton on Mercury Injection Hill, John Gray on Unconfined Compression Ridge, John Hartwell on Permeability Gap and Tony Fung on Computer Run all performed outstandingly. These Laboratory technicians showed keen interest and displayed great skill in conducting our many experiments.

XII. BIBLIOGRAPHY

- Bally, R. L., Antonescy, I. P. and Perlea, V. D. 1965. Loess as Foundation Soil for Irrigation Systems. Proceedings of the Sixth International Conference on Soil Mechanics and Foundation Engineering, Vol II, University of Toronto Press 8-12.
- Baver, L. D. 1948. Soil Physics. 2nd. Edition. John Wiley and Sons, New York, N. Y.
- Brewer, R. 1964. Fabric and Mineral Analysis of Soils. John Wiley & Son, New York, N. Y.
- Childs, E. C. and Collis-George, N. 1950. The Permeability of Porous Materials. Royal Society Proceedings A, 201: 392-405.
- Davidson, D. T., Handy, R. L. and Chu, T. L. 1953. Depth Studies of Wisconsin Loess in South-Western Iowa: Particle Size and in-place Density. Iowa Academy of Science Proceedings 60: 333-353.
- Diamond, S. 1970. Pore Size Distribution in Clays. Clays and Clay Minerals 18: 7-23.
- Fisher, R. A. 1926. On the Capillary Forces in an Ideal Soil; Correction of Formula Given By W. B. Haines. The Journal of Agriculture Science 16: 492-505.
- Gibbs, H. J., and Holland, W. Y. 1960. Petrographic and Engineering Properties of Loess. U.S. Bureau of Reclamation, Engineering Monograph No. 28.
- Graton, C. and Fraser, H. I. 1935. Systematic Packing of Spheres with Particular Relation to Porosity and Permeability. The Journal of Geology 43, No. 8, Part 1.
- Haines, H. B. 1925. Studies in the Physical Properties of Soils. A Note on the Cohesion Developed by Capillary Forces

in an Ideal Soil. The Journal of Agriculture Science 15: 529-535.

Haines, W. B. 1927. Studies in the Physical Properties of Soil. IV. A Further Contribution to the Theory of Capillary Phenomena in Soil. The Journal of Agriculture Science 17: 264-290.

Handy, R. L., Lyon, C. A. and Davidson, D. T. 1955. Comparisons of Petrographic and Engineering Properties of Loess on Southwest, East-Central and Northeast Iowa. Iowa Academy of Science Proceedings 62: 279-297.

Handy, R. L. 1956. Stabilization of Iowa Loess with Portland Cement. Unpublished Ph.D. Thesis. Library, Iowa State University, Ames, Iowa.

Holtz, W. G., and Gibbs, H. J. 1951. Consolidation and Related Properties of Loessial Soils. American Society for Testing Materials 126: 9-33.

Jenny, H. 1941. Factors of Soil Formation. McGraw-Hill, New York, N. Y.

Jumikis, A. R. 1962. Soil Mechanics. D. Van Nostrand Company, Inc., New York, N. Y.

Kane, H. 1969. Consolidation of Two Loessial Soils. National Research Council, Highway Research Record 284: 26-37.

Kellogg, C. G. 1972. Residual and Time-Dependent Strengths of Two Lateritic Soils. Unpublished M.S. Thesis. Library, Iowa State University, Ames, Iowa.

Keen, B. A. 1924. On the Moisture Relationships in Ideal Soil. The Journal of Agriculture Science 14: 170-177.

Klock, G. O., Boersma, L. and DeBacker, L. W. 1969. Pore

Size Distributions as Measured by the Mercury Intrusion Method and Their Use in Prediction Permeability. Soil Science Society of America Proceedings 33: 12-15.

Krinitzski, E. L. and Turnbull, W. J. 1967. Loess Deposits of Mississippi. The Geological Society of America special GSA paper number 94.

Lambe, T. W. 1951. Soil Testing for Engineers. John Wiley & Son, Inc., New York, N. Y.

Lambe, T. W. 1954. The Permeability of Fine-Grained Soils. ASTM Special Technical Publication 163.

Lambe, T. W. and Whitman, R. V. 1969. Soil Mechanics. John Wiley & Son, Inc., New York, N. Y.

Larionov, A. K. 1965. Structure Characteristics of Loess Soils for Evaluating their Constructional Properties. Proceedings of the Sixth International Conference on Soil Mechanics and Foundation Engineering, Vol 1, University of Toronto Press 64-68.

Lutton, R. J. 1969. Fractures and Failure Mechanics in Loess and Applications to Rock Mechanics. U. S. Army Engineer Waterways Experiment Station Research Report S-69-1.

Mayer, R. P. and Stowe, R. A. 1966. Mercury Porosimetry-Breakthrough Pressure for Penetration Between Packed Spheres. Journal of Colloid Science 20: 893-911.

Parcher, J. V. and Means, R. E. 1963. Physical Properties of Soils. Charles E. Merrill Book Inc., Columbus, Ohio.

Purcell, W. R. 1949. Capillary Pressures--Their Measurement Using Mercury and the Calculation of Permeability Therefrom. J. Petrol. Technology 1:39-48.

Ritter, H. L., and Drake, L. C. 1945. Pore-Size Distribu-

tion in Porous Materials; Pressure Porosimeter and Determinations of Complete Macropore-Size Distribution. Ind. Eng. Chem. Anal. Ed. 17:782-786.

Rootare, H. M. 1968. A Short Literature Review of Mercury Porosimetry as a Method of Measuring Pore-Size Distributions in Porous Materials, and a Discussion of Possible Sources of Errors in This Method. American Instrument Company Aminco Reprint 439.

Scheidig, A. 1934. Der Loess. Theodor Steinkopff, Dresden, Germany.

Sheeler, J. B. 1968. Summarization and Comparison of Engineering Properties of Loess in the United States. National Research Council, Highway Research Record 212: 1-9.

Spangler, M. G. 1960. Soil Engineering. 2nd. Edition. International Text Book Company, Scranton, Pa.

Smith, W. O., and Sayre, A. N. and McKinney, J. R. 1963. New Concept of Water Retension in Sand. The Johnson Drillers' Journal May-June 1963.

Sridharan, A. M., Altschaeffl, A. G. and Diamond, S. 1971. Pore Size Distribution Studies. Journal of the Proceedings of the American Society of Civil Engineers. SM5: 771-787.

Terzaghi, K. and Peck, R. B. 1962. Soil Mechanics in Engineering Practice. John Wiley & Son. Inc., New York, N. Y.

Terzaghi, K. 1951. Discussion on Loessial Soils. Symposium on Consolidation Testing of Soils. ASTM Special Technical Publication 126.

The U.S. Dept. Agriculture. 1951. Soil Survey Staff. The U.S.D.A. Soil Survey Manual Handbook. U. S. Dept Agric, Washington, D.C.

Washburn, E. W. 1921. Note on a Method of Determining the Distribution of Pore Sizes in a Porous Material. Nat. Acad. Sci. Proc. 7: 115-116.

Warnke, D. F. 1971. The Shape and Surface Texture of Loess Particles: Discussion. Geological Society of America Bulletin 81: 2357-2360.

Winslow, N. M., and Shapiro, J. J. 1959. An Instrument for the the Measurement of Pore-Size Distribution by Mercury Penetration. ASTM Bull. TP 49:39-44.

XIII. APPENDIX A: SOIL FABRIC CLASSIFICATION

A. Purpose

The purpose for including the soil classification study in this paper is two-fold. First, it shows the initial steps in the development of the concepts of structure treated in the thesis. And secondly, this classification concept exhibits adequate promise to be recorded. The initial phase of development emphasized the classification and reproducibility of the classification number. The last phase of the study was to have related the classification number to the physical properties of the soil; however, because of a lack of data a satisfactory correlation was not achieved.

B. Apparatus

The Scanning Electron Microscope is an instrument used primarily for studying the surface phenomenon of specimens with a clarity and depth which surpass the conventional light optical microscope ten to one. Image formation is produced using a scanning electron beam of less than 100 angstroms in diameter. The secondary electron emissions from the specimen are used to modulate a picture tube which is simultaneously scanned along with the specimen. Photographs of the picture tube are made to record the configuration of the relatively undisturbed sample surface. Two different SEM'S were used, the Phillip's AMR, Advance Metal Research Corporation. Burlington, Massachusetts, Serial Number 000E-1 (courtesy of

the United State Army Corps of Engineers, Waterways Experiment Station) and the JSM-U3, Japan Electron Optics Laboratory Co, LTD, Serial Number xm15116-73 (courtesy, Iowa State University).

C. Procedure

All samples were air dried and broken to proper size, see Chapter III and Table 6. With the silver paint "GC Electronic" the sample was secured to the SEM specimen stub. After the paint was dry, the samples were placed in the evaporator and a 10^{-5} torr vacuum obtained. The samples were then coated with carbon which was evaporated under a potential of 90 volts and a current of 1.0 amp for 10 seconds at a distance of 8 cm from the specimen and 200 angstroms of 60 percent gold and 40 percent palladium (8 mil wire, Ladd Research Industries, Burlington, Vermont). Upon removal from the evaporator the samples were stored in a zero humidity desiccator.

D. General

While attempting to analyze a large group of SEM photographs it became apparent that some system of controls and limits were required. The initial approach to analyzing SEM photographs was to develop a check-list of properties which were marked if observed. However, just a yes or no check did not provide adequate means for comparing soil types.

To quote from Lord Kelvin (1824-1907), "I often say that when you can measure what you are speaking about, and express it in numbers, you know something about it; but when you cannot express it in numbers, your knowledge is of a meager and unsatisfactory kind; it may be the beginning of knowledge, but you have scarcely, in your thoughts, advanced to the stage of Science, whatever the matter may be." The next developmental step was to measure grain sizes, to describe shapes, and to designate magnifications. After many trials, errors and corrections, a Soil Fabric Classification System using the SEM photographs was developed. It is identified in this report as the Soil Fabric Classification, and in short form, as the SFC.

The SFC is subdivided into eight groupings, each discussed in order:

1 Magnification. The magnifications of 200x, 500x, 1000x and 5000x seem to be the best magnification levels to study soil properties. These magnifications give sizes as follows:

1 cm at 200x represents 0.005 cm (50 microns) on the sample.

1 cm at 500x represents 0.002 cm (20 microns) on the sample.

1 cm at 1000x represents 0.001 cm (10 microns) on the sample.

1 cm at 5000x represents 0.0002 cm (2 microns) on the sample.

200x magnification seems to be the best magnification to study soil structure of loess while 1000x and 5000x magnification seems best for clays.

2 Structure. Descriptive and distinctive terms were needed to classify the soil structure. Parcher and Means (1963) used terms like slickensided, fissured, friable, crumbly, marly and vared. The Soil Survey Manual (1951) used terms like ped, clod, fragment and concretion. Terzaghi and Peck (1962) used terms like loose or dense single-grain, honey-combed, skeleton, clustered, transverse isotropy and transverse anisotropy. Although, these terms were descriptive and distinctive, they applied to soils on a macroscopic scale. What was needed for SFC analysis were terms which would describe two dimensional black and white photographs in terms meaningful for both macroscopic and microscopic scales. The following structural terms were selected:

a. Massive A soil structure which appears to be continuous, all one large massive particle, Figure 34.

b. Particulate A soil structure which appears to be composed of many individual grains, Figure 35.

c. Composite A soil structure which appears to have grouping of primary particles clustered into larger composite particles, Figure 36.

d. Additional descriptive words to describe the above structure groups are:

- (1) Fissured--denoting cracks
- (2) Non-interlocking--no grain interplay.
- (3) Interlocking--grains so stacked as to influence each other when stressed.
- (4) Cemented--Other substances holding grains together.
- (5) Oriented--showing grains in some pattern.

(A combination of terms may be used to describe the structure).

3 Grain shape. Initially only geometrical terms were used. Emphasis was placed on two-dimensional figures, then on three dimensional models. This provided so many different terms to choose from that reproducibility in selecting shapes was impossible. This necessitated a reduction to the following shape terms:

- a. Spherical Any grain which appears round or ellipsoidal.
- b. Cubic Any grain which appears blocky.
- c. Wedge-shaped Any grain which appears angular.
- d. Rod-shaped Any grain which appears long in one dimension and rounded in the other two dimensions.
- e. Platy Any grain which appears flat, could have round or square shape.

4 Grain size. Initial attempts at measuring grains and calculating the actual size were too time consuming to be useful. A more expeditious method of determining grain size was needed. The use of a transparent plastic one centimeter grid technique was developed. By the relatively simple method of determining the average number of grains per grid square, and taking the reciprocal of that number, the average area of the grains is determined. However, when there are five to ten grains per square just the designation B is used, and when there are more than ten grains per square, just the designation C is used.

5 Grain size distribution. This distribution is determined by inspection using the classification from Parcher and Means (1963):

U - Uniform, All grains approximately the same size.

P - Poorly graded, Two or more sizes predominate.

W - Well graded, All sizes present from coarsest to finest.

6 Void opening shape. A lack of reproducibility resulted when two dimensional shapes or three dimensional models were used to describe the void openings. Therefore, just the two groupings of angular and rounded were finally selected.

7 Void opening size. For ease of classification, the same grid technique used in determining grain size is used

for determining void opening size. An estimate of the average void opening area per grid square for the ten largest openings on a single photograph is made, and the average area in percent of one grid square is recorded.

8 Void opening distribution. The same classification as used in grain size distribution is used, uniform, poorly graded and well graded.

An example of how to use the SFC on loess is presented below:

1. Magnification, A photograph of 200x magnification is selected because the photograph is clear and distinct. The magnification number becomes 200x, Figure 2.
2. Structure, Examination shows particulate structure which is classed as 2, and interlocking which is B. Then the structure number is 2B.
3. Grain Shape, Examination shows an angular wedge-shaped grain. The shape letter is W.
4. Grain Size, When the photograph is covered with the plastic grid sheet it is evident that each grain fills approximately one grid square. A 1 cm distance on a 200x magnification photograph is 0.005 cm. Therefore the grain size is listed as 0.005 cm, or 50 microns.
5. Grain Size Distribution, Examination shows that all grains are approximately the same size. Then the distribution factor is uniform, U.

6. Void Opening Shape, Examination shows that the void openings are angular.

Then the shape description is angular, A.

7. Void Opening Size, Again cover the photograph with the grid and determine the average opening size in percent for a typical grid square for the ten largest openings. This estimate is approximately 30 %.

8. Void Opening Distribution, Examination shows that the void opening appears well graded, WG.

Then the combined number becomes the soil fabric classification number for loess, (200x2BW50UA30WG).

This initial soil classification technique has many shortcomings, some of which are discussed below:

a. Lacks complete reproducibility. Even at 1000x magnification the soils vary so greatly that it is difficult to neatly place the soil into subgroupings. Most clay appears massive in structure which complicates the procedure of determining grain size and shape. One solution would be to establish a SFC system for loess and a different SFC system for clays. The current SFC system allows the classifier too much subjectivity. A revised SFC system which is more objective is desired. To obtain this objectivity will require identification and analysis of just how subjectivity is introduced in the present classification, and the elimination of this subjectivity in a revised SFC system.

b. Eliminate research prejudices. The natural tendency is to photograph differences, not typical sections. Usually the photographer will take photographs of some special grain shape or void opening. This treatment of the specific case and not the general case makes classification tendentious. The requirement for random selection of where a photograph will be taken may be necessary.

c. Subgroupings have no direct connection with physical properties of the soil. The terms used in the subgroupings were selected because of their descriptiveness and not because of any relationship to the physical properties of soils. Another approach would be to start with the physical properties and select soil property terms to describe the SEM photographs.

d. Create a classification technique based on simplicity. The present SFC has eight sub-groupings which gives a SFC number of approximately 15 characters. The size of this classification number is much too large. One method of reducing the number of groupings is to keep usage factors for each grouping and eliminate any category not being used. Currently, the data base is inadequate to properly check the groupings for usage.

e. Sample preparation technique not perfected. Without careful study of what effect the evaporating and coating process has on the soil samples, it is difficult to determine

if what appears to be a cementing agent is really an agent or just the coating. Also without viewing some freeze-dried samples, it is difficult to determine the structural change which may take place during the evaporation process.

The soil fabric classification system should reflect the engineering characteristics of a soil. Therefore a correlation chart could be developed, i.e. after the SFC number is obtained the engineer should be able to go to the chart and find out what his soil really is - e.g. friction angle, cohesion, permeability, consolidation coefficient, frost susceptibility and etc. Establishment of such a correlation is a major project by itself. However, such an undertaking may be significant and fruitful.

Table A1. Soil fabric classification guidelines

-
- I. MAGNIFICATION: (200x, 5000x, 1000x or 5000x)
- II. STRUCTURE:
- 1-MASSIVE (If soil is classified massive go to next higher magnification)
 - 2-PARTICULATE
 - 3-COMPOSITE
(Additional descriptive words)
 - A-FISSURED
 - B-INTERLOCKING
 - C-NON-INTERLOCKING
 - D-CEMENTED
 - E-ORIENTED
- III. GRAIN SHAPE:
- S-SPHERICAL
 - C-CUBIC (Blocky)
 - W-WEDGE-SHAPED (Angular)
 - R-ROD-SHAPED (Angular)
 - P-PLATY
- IV. GRAIN SIZE:
- Group A - 1 to 5 grains per grid square calculated and list the size.
 - Group B - 5 to 10 grains per grid square list as B.
 - Group C - More than 10 grains per grid list as C.
- V. GRAIN SIZE DISTRIBUTION:
- U-UNIFORM
 - P-POORLY GRADED
 - W-WELL GRADED
- VI. VOID OPENING SHAPE:
- A-ANGULAR
 - R-ROUNDED
- VII. VOID OPENING SIZE:
(Average void opening area per 1 square cm grid)
- VIII. VOID OPENING DISTRIBUTION:
- P-POORLY GRADED
 - W-WELL GRADED
-

XIV. APPENDIX B: DEVELOPMENT OF THE EQUATION FOR
THE VOLUME OF CONTACT WATER

To calculate the volume of contact water between spheres, the water was subdivided into shapes with known volume equations. Shape CHFD represents the frustum of a cone. Shape HOFL represents the segment of a sphere. And shape CHG is the sector of a circle and when rotated around axis AOB forms a modified torus. The actual shape of contact water is represented by shape GHOEF.

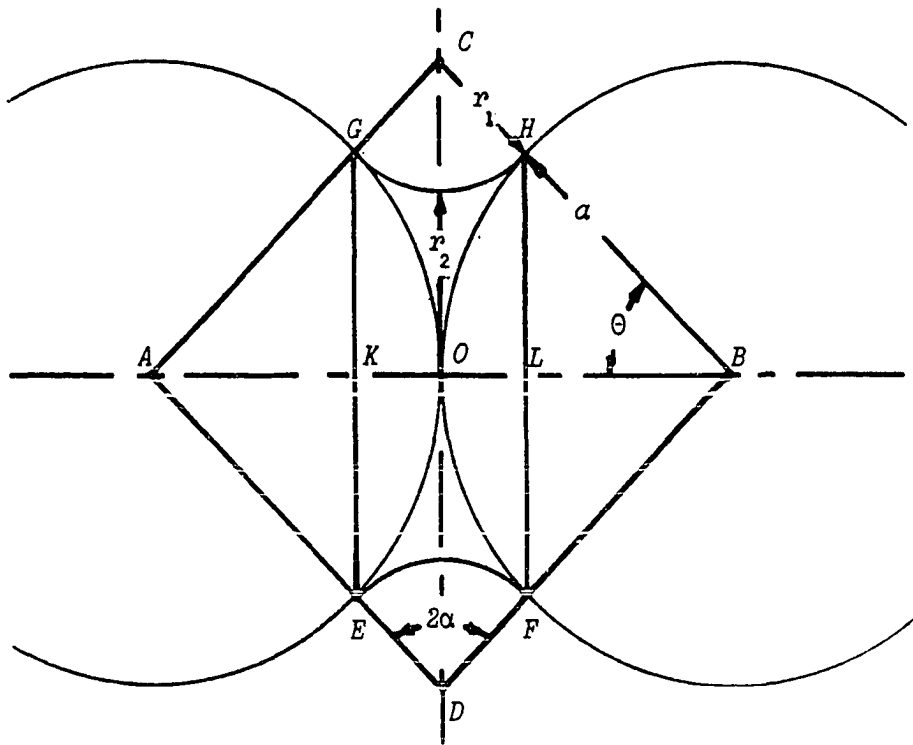


Figure B.1. Volume water at contact point

From Figure B.1, the following relationships were obtained:

$$r_1 + r_2 = a \tan \theta$$

$$r_1 = \frac{a}{\cos \theta} - a = (a \sec \theta - a)$$

$$BO = BH = BF = AO = AG = AE = a$$

$$LB = KA = a \cos \theta$$

$$OL = OK = a - a \cos \theta$$

$$LH = LF = KG = KE = a \sin \theta$$

From Figure B.1, the equation for the total volume of water at one contact point can be written as:

$$V_T = 2V_{fc} - 2V_{seg} - V_{TOR} \quad B.1$$

The standard equation for the frustum of a cone is:

$$V_{fc} = \frac{1}{3}[A_1 + A_2 + (A_1 \times A_2)^{\frac{1}{2}}]h \quad B.2$$

The areas and height are shown in terms of a and θ from Figure B.1

$$A_1 = \text{Area HF} = \pi(LH)^2 = \pi(a \sin \theta)^2$$

$$A_2 = \text{Area CD} = \pi(OC)^2 = \pi(r_1 + r_2)^2 = \pi(a \tan \theta)^2$$

$$h = OL = (a - a \cos \theta)$$

And after substituting and reducing, Equation B.2 becomes:

$$V_{fc} = \frac{1}{3}\pi a^3 (1 - \cos \theta) [\sin^2 \theta + \tan^2 \theta + \sin \theta \tan \theta] \quad B.2A$$

The standard equation for the volume of a segment of a sphere is:

$$V_{seg} = \frac{1}{3}\pi h^2 (3R - h) \quad B.3$$

The radius and height are shown in terms of a and θ from Figure 1B.

$$R = a$$

$$h = (OL) = (a - a \cos\theta)$$

$$h^2 = (OL)^2 = (a - a \cos\theta)^2$$

And after substituting and reducing, Equation B.3 becomes:

$$V_{seg} = \frac{1}{3}\pi a^3 [(1 - \cos\theta)^2 (2 + \cos\theta)]$$

$$V_{seg} = \frac{1}{3}\pi a^3 (1 - \cos\theta) [(1 - \cos\theta)(2 + \cos\theta)] \quad B.3A$$

Lastly, the equation for the modified torus was generated by rotating a sector of a circle 2π radians.

$$V_{TOR} = (2\pi)(Area\ Sector)(r_1 + r_2 - Centroid\ of\ Sector) \quad B.4$$

$$Area\ Sector = \frac{1}{2}R^2(2\alpha)$$

$$Centroid\ of\ Sector = \frac{2R \sin\alpha}{3\alpha}$$

And the radius and centroid are shown in terms of a and θ from Figure 1B.

$$R = r_1 = \left(\frac{a}{\cos\theta} - a\right)$$

$$r_1 + r_2 = a \tan\theta$$

$$\alpha = 90^\circ - \theta = \left(\frac{\pi}{2} - \theta\right) \text{ radians}$$

And after substituting and reducing, Equation B.4 becomes:

$$V_{TOR} = (2\pi) \left(\frac{1}{2} \left[\frac{a}{\cos\theta} - a \right]^2 \times 2 \left(\frac{\pi}{2} - \theta \right) \right) \left(a \tan\theta - 2 \left(\frac{a}{\cos\theta} - a \right) \frac{\sin\left(\frac{\pi}{2} - \theta\right)}{3\left(\frac{\pi}{2} - \theta\right)} \right)$$

Note, $\sin(\frac{\pi}{2} - \theta) = \cos\theta$

$$V_{TOR} = 2\pi a^3 \left[\left(\frac{1}{\cos\theta} - 1 \right)^2 \left(\frac{\pi}{2} - \theta \right) \left(\tan\theta - 2 \left(\frac{1}{\cos\theta} - 1 \right) \frac{\cos\theta}{3 \left(\frac{\pi}{2} - \theta \right)} \right) \right]$$

$$V_{TOR} = 2\pi a^3 \left[\frac{3(1-\cos\theta)^2}{\cos^2\theta} \left(\left(\frac{\pi}{2} - \theta \right) \tan\theta - \frac{2}{3}(1-\cos\theta) \right) \right]$$

$$V_{TOR} = -\frac{2}{3}\pi a^3 (1-\cos\theta) \left[\frac{3(1-\cos\theta)}{\cos^2\theta} \left(\frac{2}{3}(1-\cos\theta) - \left(\frac{\pi}{2} - \theta \right) \tan\theta \right) \right] \quad B.4A$$

Finally, combine Equations B.1, B.2A, B.3A and B.4A to obtain volume of water at a point in terms of a and θ :

$$V_T = \frac{2}{3}\pi a^3 (1-\cos\theta) \left[(\sin^2\theta + \tan^2\theta + \sin\theta \tan\theta) - (1-\cos\theta)(2+\cos\theta) + \frac{3(1-\cos\theta)}{\cos^2\theta} \left(\frac{2}{3}(1-\cos\theta) - \left(\frac{\pi}{2} - \theta \right) \tan\theta \right) \right] \quad B.5$$

Simplified form as :

$$V_T = \frac{2}{3}\pi a^3 f(\theta) \quad B.5A$$

The above developed volume of contact water Equation B.5 proved to be equivalent to the Keen (1924) and Fisher (1926) equations. Volume of water values calculated for particles of 0.003 cm and 0.0001 cm and a Theta angle of 40° for each of the three equations gave the same values, 4.2367×10^{-9} and 1.5691×10^{-13} cc respectively.

XV. APPENDIX C: APPARENT COHESION EQUATION DEVELOPMENT

Fisher (1926) corrected the Haines (1925) force equation by adding a second term after the plus sign:

$$F = \pi r_2^2 T \left(\frac{1}{r_1} - \frac{1}{r_2} \right) + 2\pi r_2 T \quad C.1$$

This equation may be rearranged in terms of surface tension (T), particle radius (a) and meniscus angle by substituting relationships from Figure B.1 into Equation C.1:

$$\begin{aligned} r_1 + r_2 &= a \tan \theta \\ r_1 &= \left(\frac{a}{\cos \theta} - a \right) = (a \sec \theta - a) \\ r_2 &= a \tan \theta - r_1 \\ r_2 &= a \tan \theta - (a \sec \theta - a) \\ r_2 &= a(1 + \tan \theta - \sec \theta) \end{aligned}$$

By rearranging Equation C.1:

$$\begin{aligned} F &= \pi r_2 T \left[r_2 \left(\frac{r_2 - r_1}{r_2 r_1} \right) + 2 \right] \\ F &= \pi r_2 T \left[\frac{r_2^2 - r_1 r_2 + 2r_1 r_2}{r_1 r_2} \right] \\ F &= \pi r_2 T \left[\frac{r_2^2 + r_1 r_2}{r_1 r_2} \right] \\ F &= \pi r_2 T \left[\frac{r_2 + r_1}{r_1} \right] \end{aligned}$$

By substituting a & θ values for r_1 and r_2 in the above equa-

tion, the force equation becomes:

$$F = \pi T \left[a(1 + \tan\theta - \sec\theta) \right] \left[\frac{a \tan\theta}{a(\sec\theta - 1)} \right]$$

$$F = \pi a T \frac{(1 + \tan\theta - \sec\theta)(\tan\theta)}{\sec\theta - 1}$$

$$F = \pi a T \frac{\left(1 + \frac{\sin\theta}{\cos\theta} - \frac{1}{\cos\theta}\right) \left(\frac{\sin\theta}{\cos\theta}\right)}{\frac{1}{\cos\theta} - 1}$$

$$F = \pi a T \frac{\sin\theta(\cos\theta + \sin\theta - 1)}{\cos\theta(1 - \cos\theta)}$$

since:

$$(1 - \cos\theta)(1 + \cos\theta) = 1 - \cos^2\theta = \sin^2\theta$$

and:

$$\begin{aligned} & (\cos\theta + \sin\theta - 1)(\cos\theta + \sin\theta + 1) \\ &= (\cos\theta + \sin\theta)^2 - 1 \\ &= \cos^2\theta + \sin^2\theta + 2\sin\theta\cos\theta - 1 \\ &= 1 + 2\sin\theta\cos\theta - 1 = 2\sin\theta\cos\theta \end{aligned}$$

and:

$$\frac{(1 + \cos\theta)(1 + \cos\theta + \sin\theta)}{(1 + \cos\theta)(1 + \cos\theta + \sin\theta)} = 1$$

By multiplying the force equation by the last trigonometric functions and substituting two preceding trigonometric relationships:

$$F = \pi a T \frac{\sin \theta}{\cos \theta} \frac{2 \sin \theta \cos \theta}{\sin^2 \theta} \frac{(1 + \cos \theta)}{(1 + \cos \theta + \sin \theta)}$$

$$F = \pi a T \frac{2(1 + \cos \theta)}{(1 + \cos \theta + \sin \theta)}$$

$$F = 2\pi a T \frac{1}{\frac{(1 + \cos \theta + \sin \theta)}{(1 + \cos \theta)}}$$

$$F = 2\pi a T \frac{1}{1 + \frac{\sin \theta}{1 + \cos \theta}}$$

since;

$$\tan \frac{1}{2} \theta = \frac{\sin \theta}{1 + \cos \theta}$$

The force equation is:

$$F = \frac{2\pi a T}{1 + \tan \frac{1}{2} \theta} \quad C.1A$$

The above equation is Fisher's force equation in terms of the surface tension, radius of sphere and the meniscus angle. To develop the apparent cohesion equation an "ideal soil" of uniform spheres packed in an open cubic arrangement as defined by Graton and Fraser (1935) was selected. The simplest complete unit cell is a cube composed of 1/8 of each of 8 spheres formed by passing three pairs of parallel planes through the centers of the 8 spheres whose corners are located at the 8 corners of a cube of edge length 2a. The following relationships were derived from this geometrical

arrangement:

$$\text{Total Volume, } V_t = 2a \times 2a \times 2a = 8a^3 \quad C.2$$

$$\text{Volume Solids, } V_s = 8(1/8)4/3\pi a^3 = \frac{4}{3}\pi a^3 \quad C.3$$

$$\text{Volume Voids, } V_v = V_t - V_s = 8a^3 - \frac{4}{3}\pi a^3 = \frac{4}{3}(6 - \pi)a^3 \quad C.4$$

$$\text{Side Surface Area, } A_s = 2a \times 2a = 4a^2 \quad C.5$$

In the unit cell, cube arrangement, there is a total of three complete contact points. The numbers in Figure C.1 represent 1/4 contact point per number.

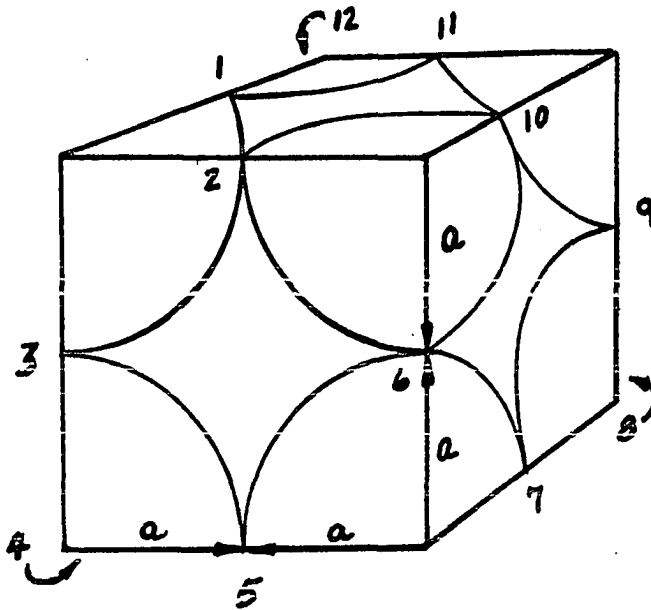


Figure C.1 Unit cell with contact point numbers.

From Appendix B the equation for the volume of water for each contact point was obtained. By multiplying Equation B.5A by three, the number of contact points per unit cell for open packing, the volume of contact water per unit cell becomes:

$$V_{wuc} = (3)\frac{2}{3}\pi a^3 f(\theta) = 2\pi a^3 f(\theta) \quad C.6$$

The degree of saturation, S , expressed as a percent is defined as the volume of water divided by the volume of voids and multiplied by 100. By substituting the amount of water per unit cell (Equation C.6) and the volume of voids per unit cell (Equation C.4) the degree of saturation is expressed in terms of a constant and a function of meniscus angles.

$$S = \frac{V_{wuc}}{V_v} \times 100 = \frac{2\pi a^3 100 \cdot f(\theta)}{\frac{4}{3}(\theta - \pi)a^3} = 164.85 \cdot f(\theta) \quad C.7$$

$$\theta = 164.85 f^{-1}(S) \quad C.7A$$

The particle radius cancels and consequently has no influence on the curve of the relationship between the degree of saturation and the meniscus angles, Figure 8, curve 1. The following explicit expressions for Equation C.7A were developed by least squares curve fitting (curve 1 of Figure 8).

$$\frac{1}{2}\theta = 2.3 \ln S + 10.59 \quad \text{For } S = 10\% \quad C.8A$$

$$\frac{1}{2}\theta = 7.8 \ln S - 0.11 \quad \text{For } S = 10 \text{ to } 90\% \quad C.8B$$

To obtain the cohesion equation, the Fisher force Equation C.1A was divided by the surface area of one side of the unit cell, Equation C.5.

$$C = \frac{F_F}{A_s} = \frac{2\pi aT}{4a^2(1 + \tan\frac{1}{2}\theta)} = \frac{\pi T}{2a(1 + \tan\frac{1}{2}\theta)} \quad C.9$$

Equations C.8A & B were substituted into Equation C.9 providing the desired apparent cohesion equations:

$$C = \frac{\pi T}{2a[1 + \tan(2.3 \ln S + 10.59)]} \quad \text{For } S = 0 \text{ to } 10\% \quad C.10A$$

$$C = \frac{\pi T}{2a[1 + \tan(7.8 \ln S - 0.11)]} \quad \text{For } S = 10 \text{ to } 90\% \quad C.10B$$

For temperatures of 25° C the surface tension of water is 71.97 dynes per cm. By assuming a constant temperature of 25° C, the apparent cohesion equation becomes:

$$C = \frac{16.4 \times 10^{-4}}{a[1 + \tan(2.3 \ln S + 10.59)]} \quad \text{For } S = 0 \text{ to } 10\% \quad C.11A$$

$$C = \frac{16.4 \times 10^{-4}}{a[1 + \tan(7.8 \ln S - 0.11)]} \quad \text{For } S = 10 \text{ to } 90\% \quad C.11B$$

C is cohesion in psi.

a is particle radius in cm.

S is degree of saturation in percent.

Example calculation for $S = 20\%$, $a = 0.0001$ cm and $n = 47.65\%$ is:

$$C = \frac{16.4 \times 10^{-4}}{0.0001[1 + \tan(7.8 \ln 20 - 0.21)]}$$

$$C = \frac{16.4}{1 + \tan 23.23^\circ} = \frac{16.4}{1 + 0.430}$$

$$C = 11.4 \text{ psi}$$

This apparent cohesion equation is limited to a system of spheres in open cubic arrangement with a 47.64 percent porosity obtained from equations C.2 and C.4 as follows:

$$n = \frac{V_v}{V_t} 100 = \frac{4(6 - \pi)100}{24} = 47.64$$

To expand this concept to include soil systems of varying porosities requires that additional systems be analyzed, see Table 9.

In case 1, the cubic arrangement which was treated in the first part of the appendix, there are 3 contact points per unit cell. The assumption was made that one contact point provides a force in the x-direction, another in the y-direction and the last in the z-direction. Therefore, the cohesion developed in Equation C.11 considering 3 contact points, one in each direction, is valid at 47.6 percent porosity.

Table C.1 Density factor, D_f

cases	contact points force factor	area factor	density factor
1	1	1	1
2	$\frac{4}{3}$	$\frac{2}{3}$	$\frac{8}{3\sqrt{3}}$
3	$\frac{5}{3}$	$\frac{4}{3}$	$\frac{20}{9}$
4	2	$\frac{2}{\sqrt{2}}$	$\frac{4}{\sqrt{2}}$

However, when using case 2 with 4 contact points, $4/3$ of the force acts in each direction. And in case 3 with 5 contact points, $5/3$ of the force acts in each direction. Lastly in case 4 with 6 contact points, 2 times the force acts in each direction. The contact point correction is included in Figure 9 with the decreasing side area correction for the unit cell.

The side area for the cube, case 1, was used as the standard and the side areas for each of the other cases was

divided into the standard. The contact point force factors were multiplied by the area factors to obtain a total correction or density factor, see Figure 9. In a system of uniform spheres, the maximum porosity is 47.64 percent and in any looser arrangement the spheres would not be in contact with each other. Also for uniform spheres the minimum porosity is 25.95 percent, and in any closer arrangement would cause crushing of spheres. The density factor for the desired case is multiplied times the case 1 apparent cohesion equation values.

The last adjustment is a correction for the degree of saturation. As the porosities decrease from case 1 to case 4 the degree of saturation increases, see Figure 8.

Example calculations for $S = 40\%$, $a = 0.0002$ and $n = 35\%$ are:

$$C = \frac{16.4 \times 10^{-4} D_f}{a \left[1 + \tan \frac{\theta}{2} \right]} \quad C.12A$$

Go to Figure 8 and enter at $S = 40\%$, read across to approximately $1/2$ the distance between curves 2 and 3 and read down, theta equals 43° . Go to Figure 9 and enter at $n = 35\%$ read across to the curve and read down, D_f equals 1.86.

$$C = \frac{1.86 \times 16.4 \times 20^{-4}}{0.0002[1 + \tan(\frac{43}{2})]} = 10.9 \text{ psi}$$

The last modification on Equation C.12A before it can be used on loess type soils is the replacement of the sphere radius "a" with the effective radius of loess "re". Then the apparent cohesion equation for loess becomes:

$$C = \frac{16.4 \times 10^{-4} D_f}{r_e [1 + \tan \frac{\theta}{2}]} \quad C.12B$$

With C in psi

D_f from Figure 9

water at 25°C

r_e from grain distribution chart where r_e is the radius at 90% passing in the silt range.

theta is from Figure 8 at appropriate saturation and porosity.

XVI. APPENDIX D: PERMEABILITY DATA

Test Series Number One, Static-Constant Moisture-16%

Soil	Remolded Friable Iowa Loess
Type Test	Falling Head
Size Sample	Harvard Miniature
Compaction	Static
Permeant	Distilled Water (25-29° C) not deaired
Saturation	100%, bottom to top
Head	44 inches

Dry Density pcf	Molding Moisture (%)	Permeability cm per sec
74.8	15.3	1.9 x 10 ⁻⁴
78.3	15.6	4.6 x 10 ⁻⁵
83.3	16.7	2.4 x 10 ⁻⁵
88.3	15.8	5.8 x 10 ⁻⁶
93.1	16.4	6.3 x 10 ⁻⁶
94.4	16.2	1.6 x 10 ⁻⁶
99.7	16.8	5.9 x 10 ⁻⁶
102.1	16.5	1.9 x 10 ⁻⁷
104.0	17.2	7.6 x 10 ⁻⁸
109.5	16.5	2.2 x 10 ⁻⁸
114.0	16.4	7.2 x 10 ⁻⁸

Test Series Number Two, Dynamic-Constant Moisture-16%

Soil	Remolded Friable Iowa Loess
Type Test	Falling Head
Size Sample	Harvard Miniature
Compaction	Dynamic
Permeant	Distilled Water (25-29° C) not deaired
Saturation	100%, bottom to top
Head	44 inches

pcf	(%)	cm per sec
79.6	15.1	1.2 x 10 ⁻⁴
82.5	16.4	1.1 x 10 ⁻⁴
88.9	15.6	1.8 x 10 ⁻⁵
93.1	16.7	9.4 x 10 ⁻⁶
102.5	15.6	1.4 x 10 ⁻⁶
103.1	15.7	3.7 x 10 ⁻⁷
108.1	15.5	2.4 x 10 ⁻⁷
109.3	16.4	2.0 x 10 ⁻⁷

Dynamic Compactive Effort

density pcf	layers	tamps	lbs/tamp	total load lbs
----------------	--------	-------	----------	-------------------

79.6	6	7	2.5	105
82.5	5	11	2.5	137
88.9	6	11	3.0	198
93.1	5	11	3.0	165
102.5	5	3	43.5	348
103.1	5	4	43.5	870
108.1	6	7	43.5	1383
109.3	5	15	43.5	3160

Test Series Number Three, Constant Density-75

Soil	Remolded Friable Iowa Loess
Type Test	Falling Head
Size Sample	Harvard Miniature
Compaction	Static
Permeant	Distilled Water (25-29° C) not deaired
Saturation	100%, bottom to top
Head	56 inches

Dry Density pcf	Molding Moisture (%)	Permeability cm per sec
77.9	6.8	8.5 x 10 ⁻⁵
74.2	8.1	9.9 x 10 ⁻⁵
79.1	8.2	3.2 x 10 ⁻⁵
79.5	13.1	3.8 x 10 ⁻⁵
78.0	14.5	3.8 x 10 ⁻⁵
79.0	14.6	1.0 x 10 ⁻⁵
78.5	14.9	1.3 x 10 ⁻⁵
77.1	18.0	4.8 x 10 ⁻⁶
78.4	18.5	7.1 x 10 ⁻⁶
75.5	18.6	6.1 x 10 ⁻⁶
75.8	19.3	1.9 x 10 ⁻⁵
74.5	20.8	1.2 x 10 ⁻⁵

Test Series Number Four, Constant Density-85

Soil	Remolded Friable Iowa Loess
Type Test	Falling Head
Size Sample	Harvard Miniature
Compaction	Static
Permeant	Distilled Water (25-29° C) not deaired
Saturation	100%, bottom to top
Head	56 +1, -1, inches

Dry Density pcf	Molding Moisture (%)	Permeability cm per sec
87.7	3.1	2.5 x 10 ⁻⁵
87.7	3.3	2.3 x 10 ⁻⁵
85.5	5.6	1.9 x 10 ⁻⁵
84.0	6.5	4.2 x 10 ⁻⁵
84.1	6.9	1.6 x 10 ⁻⁵
84.4	6.9	2.0 x 10 ⁻⁵
82.8	7.0	3.6 x 10 ⁻⁵
86.8	7.2	1.9 x 10 ⁻⁵
89.6	7.4	1.9 x 10 ⁻⁵
84.1	7.4	3.3 x 10 ⁻⁵
82.4	8.3	1.2 x 10 ⁻⁵
82.3	8.5	3.6 x 10 ⁻⁵
81.6	9.0	3.5 x 10 ⁻⁵
82.2	9.7	3.6 x 10 ⁻⁵
85.7	10.5	9.5 x 10 ⁻⁶
81.0	11.4	2.0 x 10 ⁻⁵
80.1	11.6	8.7 x 10 ⁻⁶
85.6	12.9	1.1 x 10 ⁻⁵
84.9	15.6	4.9 x 10 ⁻⁶
84.9	17.1	4.0 x 10 ⁻⁶
86.1	18.8	7.8 x 10 ⁻⁷
85.7	20.8	1.1 x 10 ⁻⁶

Test Series Number Five, Constant Moisture-7%

Soil	Remolded Friable Iowa Loess
Type Test	Falling Head
Size Sample	Harvard Miniature
Compaction	Static
Permeant	Distilled Water (25-29° C) not deaired
Saturation	100%, bottom to top
Head	56 +1, -1, inches

Dry Density pcf		Molding Moisture (%)	Permeability cm per sec
74.2	(3)	8.1	9.9 x 10 ⁻⁵
77.9	(3)	6.8	8.5 x 10 ⁻⁵
79.1	(3)	8.2	3.2 x 10 ⁻⁵
82.8	(4)	7.0	3.6 x 10 ⁻⁵
86.8	(4)	7.2	1.9 x 10 ⁻⁵
89.6	(4)	7.4	1.9 x 10 ⁻⁵
94.0		5.7	1.1 x 10 ⁻⁵
94.6		6.9	4.0 x 10 ⁻⁶
100.3		7.6	5.9 x 10 ⁻⁷
100.4		6.4	1.7 x 10 ⁻⁶
109.2		7.6	2.6 x 10 ⁻⁷

(3) & (4) denotes test which appear in other test series

Test Series Number Six, Washed Silt

Soil	Washed Silt
Type Test	Falling Head
Size Sample	Harvard Miniature
Compaction	Static
Permeant	Distilled Water (25-29° C) not deaired
Saturation	100%, bottom to top
Head	56 +1, -1, inches

Dry Density pcf	Molding Moisture %	Permeability cm per sec
74.8	11.6	9.9×10^{-4}
79.8	11.0	5.8×10^{-5}
85.5	11.1	5.8×10^{-6}
89.8	11.2	9.4×10^{-7}
94.8	11.2	4.3×10^{-6}

Test Series Number Seven, Triaxial Samples

Soil	Undisturbed & Remolded Loess
Type Test	Falling Head
Size Sample	(Dia. = 2.8 inches & Len. = 5.6 inches)
Compaction	Static
Permeant	Distilled Water (25-29° C) not deaired
Saturation	100%, bottom to top
Head	54 +2, -2, inches

Density pcf	Moisture (%)	Type Sample	Permeability cm per sec
87.3 (tot)		undisturbed	1.0×10^{-4}
93.2 (tot)		undisturbed	5.4×10^{-5}
85.3 (dry)	4.6	undisturbed	7.0×10^{-5}
86.0 (dry)		hand carved	7.0×10^{-5}
85.0 (dry)	11.3	remolded	7.8×10^{-5}
85.0 (dry)	11.3	remolded	1.2×10^{-5}